N84-28279

HIGH PRECISION MEASUREMENTS IN CRUSTAL DYNAMIC STUDIES

Frank Wyatt and Jon Berger

Institute of Geophysics and Planetary Physics
University of California, San Diego
La Jolla, California 92093

FINAL REPORT
NAG 05-11
(2/80-9/83)

NATIONAL AERONAUTICS AND SPACE ADMINISTRATION
GODDARD SPACE FLIGHT CENTER
GREENBELT, MARYLAND 20771

HIGH PRECISION MEASUREMENTS IN CRUSTAL DYNAMIC STUDIES

Frank Wyatt and Jon Berger

Institute of Geophysics and Planetary Physics
University of California, San Diego
La Jolla, California 92093

FINAL REPORT
NAG 05-11
(2/80-9/83)

NATIONAL AERONAUTICS AND SPACE ADMINISTRATION
GODDARD SPACE FLIGHT CENTER
GREENBELT, MARYLAND 20771

TABLE OF CONTENTS

Abstract

This report covers two elements of the geophysical research program at Piñon Flat Observatory conducted during the period 2/80-9/83: the development of high-precision instrumentation for monitoring benchmark stability and the evaluation of coseismic strain and tilt signals. For the former, use of an optical anchoring technique has provided surface monuments effectively tied to the rock at a depth of 25 m. Strain and tilt measurements between these monuments yield records of short term deformation (< hour) whose accuracy rivals the instrumental resolution ($\sim 4.0 \times 10^{-10}\varepsilon$). For the latter, in more than eleven years of observations we find no evidence to suggest that the earth behaves other than purely elastically in response to abrupt faulting. Data from the observatory are found to be particularly useful for quantifying the overall seismic dislocations.

Recognition of true crustal deformation signals in the period range of hours to months awaits further instrumental improvements, to both observatory-based and geodetic surveying techniques.

High Precision Measurements in Crustal Dynamic Studies

1.0 Introduction

Piñon Flat Observatory (PFO, Figure 1.1) began operation in 1971. Commencing shortly thereafter and continuing up through 1983, the Geodynamics Program of the National Aeronautics and Space Administration played a major role in sponsoring development of the facility. This commitment has led to a geophysical observatory widely recognized for its advancements in instrumentation, and its sustained observational program.

This report outlines the results of NASA sponsored research from the period February 1980 through September 1983; an earlier document, submitted for NGR 05-009-246 (J. Berger et al., 1981) covers the period November 1973 to June 1981. Because most of the instrumental details were explained in the previous report, we limit ourselves here to a description of the records produced by those sensors. Section 2.0 presents the long term strain data from all three 731 m laser strainmeters as well as the most recent observations from the Northwest-Southeast component, which has been optically "tied" to a depth of 25 m. Section 3.0 discusses observations from a similarly anchored 535 m fluid tiltmeter. The low noise of both these instruments provides unprecedented resolution of the geodynamic signals in southern California. Coseismic strains and tilts are the subject of Section 4.0. In more than eleven years of recording at PFO, we do not find any evidence for anomalous signals either immediately before, or during, seismic events although accelerated post-seismic deformation may be present. All of these observations point to the need for further refinement of instrumentation designed to monitor crustal deformation.

1.1 Motivation and Background

Much could be learned from highly accurate and continuous measurements of the earth's crustal deformation. It is generally accepted that earthquakes result from straining of crustal rocks to the point of failure, and while studies of seismic phenomena tell us much about the stress changes during an earthquake and something about the absolute level of stress--direct observation of deformations seem essential if we are to understand the total process. With continuous and accurate strain measurements we could hope to address such questions as: How do crustal strains accumulate over time, what is their normal character, and how are they released by an earthquake? How

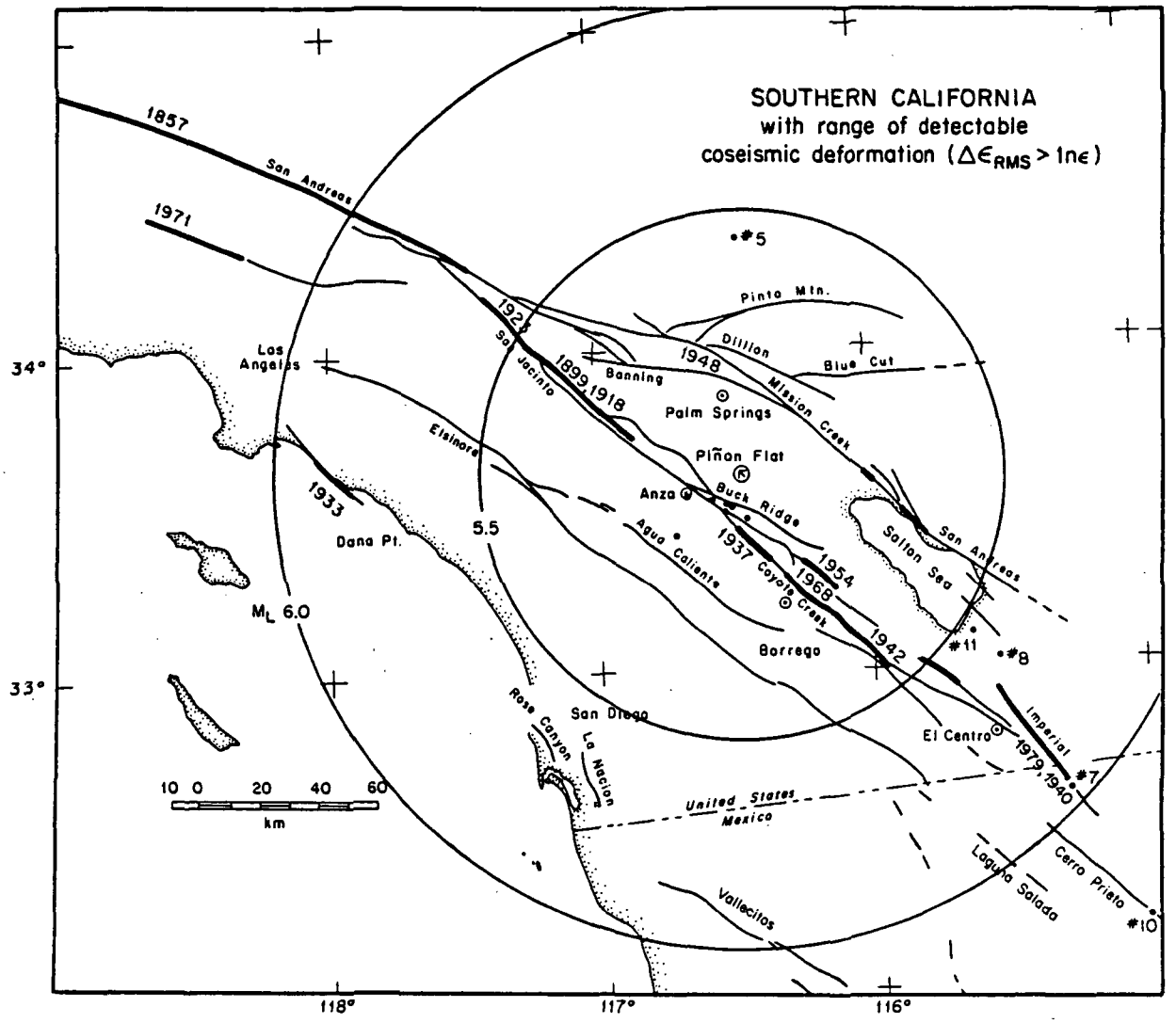
SOUTHERN CALIFORNIA
with range of detectable
coseismic deformation ($\Delta\epsilon_{RMS} > 1n\epsilon$)
1857
San Andreas
1971
1923
San Jacinto
1899, 1918
Banning
1948
Dillon
Blue Cut
Pinto Mtn.
Mission Creek
Palm Springs
Piñon Flat
Anza
Buck Ridge
1954
1968
1937
Coyote Creek
Agua Caliente
Salton Sea
San Andreas
1942
Borrego
Elsinore
1933
Dana Pt.
5.5
M_L 6.0
Los Angeles
San Diego
Rose Canyon
La Nacion
El Centro
Imperial
1979, 1940
United States
Mexico
Laguna Salada
Cerro Prieto
Vallecitos
#1
#5
#7
#8
#10
#11
10 0 20 40 60
km
34°
33°
118°
117°
116°

Figure 1.1

are earthquakes "nucleated" and what is the specific triggering mechanism? What are the details of the dynamic strain changes during an earthquake?

Unfortunately, very few observatory-based programs designed to measure these signals have produced useful results. This contrasts markedly with the results from conventional geodetic studies using trilateration, triangulation, and leveling. These surveying techniques provide coverage over large areas (typically 100 km and more) with a measurement frequency of typically once or twice per year and errors of 1-10 times 10^7 strain. Such measurements have given us almost all we know about strain changes, and together with more advanced surveying techniques, they continue to provide the best data for monitoring on-going changes. However, they lack the necessary resolution, both in time and in precision, for the detection of short- to medium- term crustal signals (seconds to months). Because strain and tilt are continuous functions of time, they, like any other environmental quantity, can be expected to fluctuate over a broad range of time scales. The power spectra of high quality tilt and strain data show that the size of strain changes decreases rapidly with increasing frequency. Shorter term changes are very small and so are much harder to measure than the larger changes which occur over "geodetic" time scales. Most efforts to build observatory-based sensors have not succeeded in measuring continuous changes simply because the signals have proven to be so small.

Consideration of the theoretical static deformation at the time of an earthquake yields an estimate for the largest short-term variations to be expected, as well as the magnitude of the long term rates. Roughly speaking, the strain change ($\Delta \varepsilon$) will be proportional to the stress drop according to:

$$\Delta\varepsilon = k \frac{\Delta\sigma}{\mu} \left(\frac{r_0}{r}\right)^3$$

where

k is a geometric constant, of order unity
$\Delta\sigma$ is the stress drop, typically 10 bars (10^6 N/m^2)
μ is the rigidity, usually assumed to be 3×10^{10} N/m^2
r_0 is the earthquake source dimension
r is the hypocentral distance

As the stress drop is roughly independent of seismic moment, bigger earthquakes do not necessarily involve bigger strain changes--only the area affected is larger. As an example, for a moderate earthquake in California the pertinent dimension is 10 km to 15 km, the depth of faulting. Further away than this the strains will be smaller than $10^{-5}\,\varepsilon$. If the total inter-event deformation (strain accumulation) is of the same order as the coseismic deformation, the corresponding strain rates between major events turn out to be quite small. Indeed, this is what has been found generally in

California (Savage et al., 1981b) and specifically in the neighborhood of PFO (King and Savage, 1983, and Sections 2.0 and 3.0).

While very little sensitivity may be necessary to accomplish one very important goal—the detection of precursors to earthquakes—the accumulated evidence indicates that this is not so. Certainly, having a continuous record of crustal deformation would enhance our understanding of tectonics over hourly to decadal time scales (the ones of interest in understanding the earthquake cycle). A seismological analogy may make the point clearer: Understanding of earthquake dangers could not progress past a fairly simple level so long as only data on large earthquakes (from felt reports) were available. The advances in instrumentation which allowed monitoring of small earthquakes and later microearthquakes have greatly increased our knowledge of seismic geography and seismicity patterns. To monitor deformations, as closely as we now do seismicity, would be an immense gain.

Given the recent advances in optical and electronic measurement techniques applicable to observatory-based sensors, there is one fundamental question still to be addressed: Will any small volume of the earth's near-surface faithfully indicate the state of strain in the underlying crust? Our progress in reducing the noise in crustal deformation records at PFO suggests that it may, as do the many observations of coseismic signals (Section 4.0) and the measurements of similar tidal signals at different locations across the site (Wyatt et al., 1983). But to really answer this question will require longer-term high-quality observations in order to monitor the deformational signals at periods far beyond a day—along with refinement of the existing instruments to remove the known sources of noise.

1.2 Observatory-based measurements and the Geodynamics Program

It is worthwhile reviewing the relevance of the research underway at PFO to NASA's goals in crustal dynamics and related studies. NASA's involvement in this subject arises from the advanced techniques they have developed to measure the position of points on the earth's surface relative to earth satellites and extragalactic sources. The research goals of these studies relate to seismic and tectonic activity, polar motion and rotation rate.

Our goals, at PFO, are directed towards the understanding of both seismic and tectonic motions and their interconnections. We are pursuing an observation program that involves the development and testing of new instrumentation and measurement techniques: observing strain, tilt and gravity continuously with what we believe are the most sensitive and stable instruments currently available. This program has, over the past few years, provided consistent upper limits to the spectrum of crustal deformations occurring in the area of the observatory. This area is an area of high tectonic activity, high seismic risk, and is very likely typical of most active fault zones.

While our measurements are made over rather short baselines, by NASA standards, the sensitivity and stability is exceptionally high. Further, the measurements are taken at sample intervals of no more than a few minutes (limited, primarily, by our present recording capabilities). In contrast, geodetic techniques used to study crustal deformations make measurements infrequently, over baselines of tens to hundreds of kilometers and can be subject to both temporal and spatial aliasing. In the case of the USGS trilateration networks (e.g., Savage et al., 1981b), the survey areas are irregular figures with large dimensions when compared to moderate faulting. (The Palmdale net is a notable exception.) The time taken to survey completely a single network is typically many weeks or even months. Data are reduced under the assumption of spatially uniform strain and constant strain rate (Prescott et al., 1979). Whether the tectonic strain fields approximate the assumptions of spatial uniformity and temporal rate constancy has yet to be determined, but the impact of these assumptions to NASA's crustal dynamics observational program is considerable.

We believe that an essential element of the overall study of crustal dynamics must be high precision measurements of deformation, much higher than is possible with terrestrial or extraterrestrial qeodetic techniques. There are three fundamental aspects of this approach that bear examination:

1. Are such precise and accurate measurements truly necessary to monitor crustal deformation?

2. Need these observations be made continuously?

3. Is Piñon Flat Observatory a reasonable location for this effort?

Briefly, our justifications would be that we need both precise and continuous measurements to begin to understand crustal strain changes adequately, and that these measurements ought to be made in an area of tectonic and seismic interest. The area surrounding PFO is such a locale.

To explain these at greater length:

1. In the NAS report (1981) it was noted that:

"Data from repeated geodetic surveys, both horizontal and vertical, have been analyzed to determine tectonic deformation. The present body of geodetic data related to horizontal crustal deformation shows that the long-term deformation rates in seismic zones (such as the San Andreas Fault) are less than 3 parts in 10^7 per year, which might be considered a threshold level for studies of long-term horizontal crustal deformation rates. Much of the interesting and anomalous horizontal deformation will be smaller than this, and only in the near field of earthquakes will the rates occasionally exceed it.

"Figure [1.2] illustrates the strain magnitudes to be expected as a function of earthquake moment (and hence magnitude) and hypocentral distance. This figure refers to coseismic deformation, and it is reasonable to assume that most preseismic or post seismic deformations that may occur will be smaller than this. From this figure we can clearly see that only in the near field (i.e., within a fault rupture dimension) will the strains be much larger than 1 part in 10^6 ."

Thus, much of the pertinent crustal deformation will occur at strain levels less than 10^{-7} . For this reason most of our current and past effort at PFO has been directed towards developing instrumentation capable of such performance. Indeed, if this premise is correct, then:

1. Extraterrestrial geodetic techniques with an accuracy goal of 1 cm will be most productive in measurements of the strain field related to the faulting process over baselines of 100 km and greater. This applies to existing Very Long Baseline Interferometry (VLBI) and Satellite Laser Ranging (SLR) techniques, as well as the new Global Positioning System (GPS) which utilizes an array of navigation satellites.

2. Terrestrial EDM (Electronic Distance Measurement) techniques currently limited to statistical errors of a few parts in 10^{-7} (in the case of trilateration nets, or two-color ranging devices) must be improved in order to resolve strains at least an order of magnitude smaller. Further, it is possible that the spatial averaging and infrequent sampling of the trilateration nets may obscure many tectonic signals. If this is so, then densification and more frequent re-surveys of the networks are needed.

3. Observatory based instrumentation must be improved to provide lower noise levels at long periods--primarily to distinguish environmental signals from tectonic signals.

2. The spectrum of tectonic deformation is usually "red," but one of the most important activities, both from a scientific and social point of view, happens discontinuously--the earthquake process. It is, in a manner of speaking, the culmination of geological processes in an instantaneous rock failure. If we are to understand it, we must understand crustal deformation over widely differing time scales. While we know much about the Earth at very short periods (1 hour and less) from seismology, and also at very long periods (1 ae and longer) from geologic mapping, in between we know very little about either the constitutive relations or the forces at work. This is, of course, just the period range of interest in the earthquake process. It is the role of geodetic measurements, rebound studies, and crustal deformation monitoring to begin to fill this gap in our understanding.

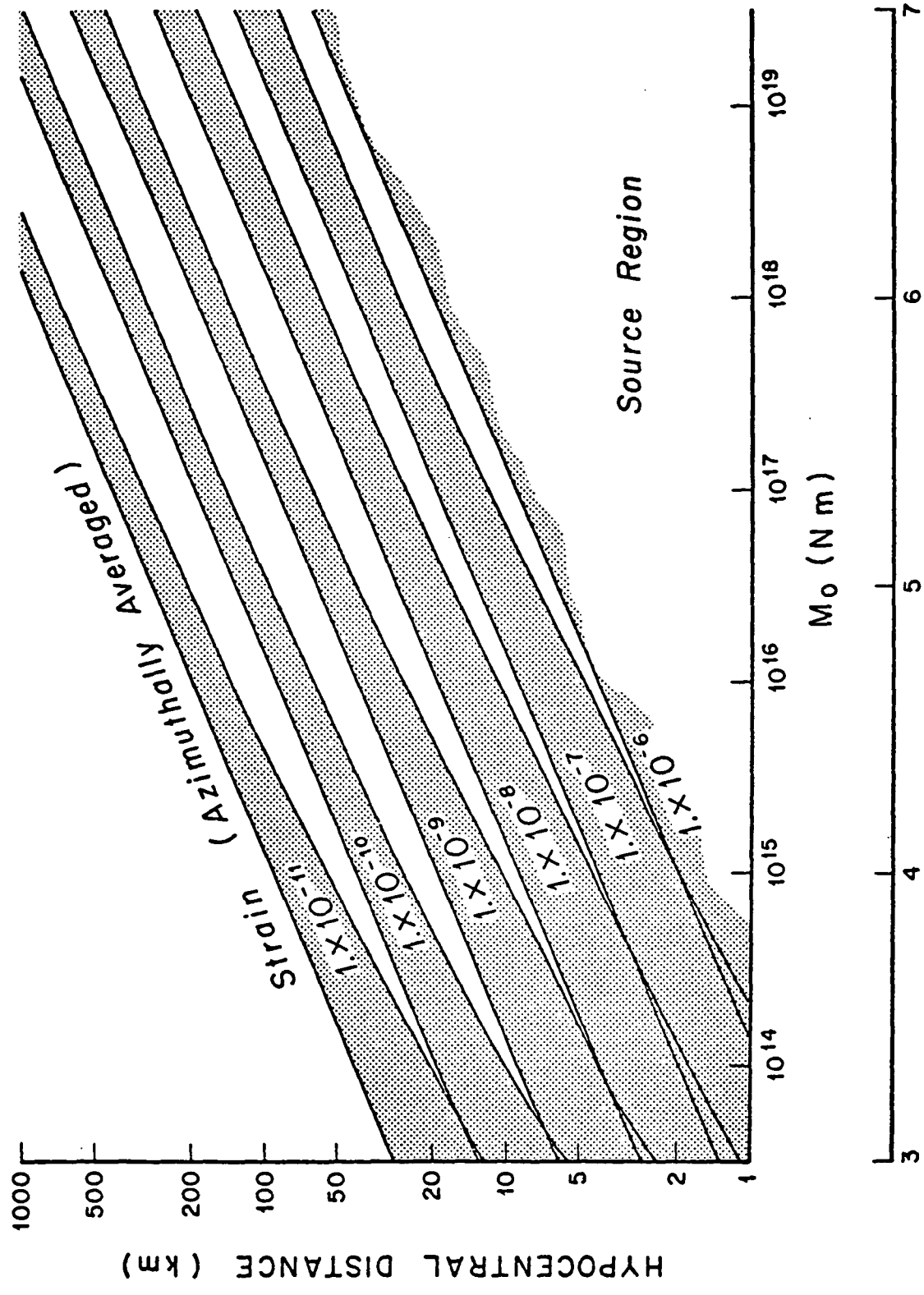

Figure 2.2 Azimuthally averaged (root mean square) strains from a buried strike slip dislocation for a given moment and distance. The width of the shaded area indicates the range of the various components of strain and tilt. The magnitude scale was determined using the moment-magnitude relation of Thatcher and Hanks (1973).

Figure [1.2]

While geodetic means of monitoring crustal deformations over a wide area have proven very effective (Savage et al., 1981b), the temporal resolution of once or twice per year severely limits our ability to study the "dynamics" of the earthquake process. Deformation precursors, if indeed they commonly exist, may be of considerably shorter duration - perhaps minutes or hours. Coseismic deformations provide valuable constraints on the moment tensor of the earthquake and postseismic deformations may be expected to occur with time constants considerably less than the normal geodetic survey repeat interval. Further, we have at least one well documented example (Savage et al., 1981a) of an aseismic deformation "event" that considerably altered the regional strain field and that occurred so rapidly that it would have been missed with normal geodetic sample rates. At this stage of our knowledge of the physics of the earthquake process, it would be myopic indeed to ignore that part of the deformational spectrum above a semiannual frequency.

3. Given the importance, then, of measuring crustal deformation as precisely as possible and on a continuous basis, the final issue that needs to be addressed is whether Piñon Flat Observatory is a representative location? Located some 20 km south of Palm Springs, California (Figure 1.1), it is situated between the San Andreas and the San Jacinto fault zones in an area of considerable tectonic interest. The actual site (Pinyon Flat) is a large flat area of Mezozoic granodiorite.

There is general agreement that in central California most of the movement between the Pacific and North American plates is accommodated on the San Andreas fault zone, which appears as one of the great transform faults of the world. What is puzzling is that the San Andreas retains this character only as far south as San Bernardino, but then cannot be traced as a single throughgoing fault until just south of the Imperial Valley. This southernmost part of the San Andreas fault zone has certainly been active in Holocene times but has not experienced a great earthquake in the last 500 years (Sieh, 1981). How then, is fault motion absorbed in the San Gorgonio Pass area (the region between the two well-defined sections of the San Andreas), and is all the slip taking place on the San Andreas or elsewhere?

The San Jacinto fault zone may accommodate at least some of the strain accumulation. In some respects this fault seems a more likely candidate for the principal plate boundary in southern California than the San Andreas. As Sharp (1967) has pointed out, the San Jacinto fault is the only fault that cuts the Transverse Ranges and yet maintains the northwest-southeast trend that the plate boundary has on a larger scale. Further, in this century it has been the most seismically active fault in Southern California, having been ruptured by at least eight moderate earthquakes (magnitude 6 or more) since 1899 (Thatcher et al., 1975; Sanders and Kanamori, 1984). In the same time period, the southern San Andreas fault has experienced only one event over magnitude 6, the 1948 Desert Hot Springs earthquake.

The San Jacinto Fault cannot be the major plate boundary because of the smallness of the cumulative horizontal motion which has taken place across it, which Sharp (1967, 1981) has estimated at 24 km of right lateral motion,

with an average slip rate of 8-12 mm/annum in the last 700,000 years. This is considerably less than the 60 mm/a deduced as the average North American-Pacific Plate motion in this area (Jordan and Minster, 1978). In the last 6 millenia the average rate on the southern San Jacinto has been only 2 mm/a, but may have increased to 5 mm/a over the last 400 years. The earthquake record in this century gives an average rate of 8 mm/a when smoothed over the whole fault zone.

However, the seismic slip on the San Jacinto fault is irregularly distributed. Thatcher et al. (1975) have shown that basically two large sections of the fault have ruptured in the last 90 years: 1) a northern segment (Riverside to Anza) which slipped 1.35 m of slip between 1890 and 1923, and 2) a southern segment (Coyote Mountain to the Superstition Mountains) which slipped .8 m between 1942 and 1973. Two gaps apparently remain, one at the northern end of the fault, and the other near the town of Anza, which is the part of the fault nearest PFO (Figure 1.3). Recent seismicity of the area near Anza has included several magnitude 4 to 5 events and a magnitude 5.3 event. Sanders and Kanamori (1984) have analyzed the local faults and their seismicity and concluded that the regional strain pattern of predominantly north-south compression has been locally distorted in the Anza area. The narrowing of the fault zone in the Anza area has led to a greater compressional force being applied across the fault, which may cause the apparent seismic gap.

The other evidence on slip on the San Jacinto fault comes from the geodetic results of King and Savage (1983), which cover the period 1973-1981. These indicate that the local strain pattern is purely right-lateral shear, with maxima over both the San Jacinto and San Andreas faults. The shear rates are consistent with slip of about 10 mm/a at depths below 5 km, which is uniform along the fault. As there have been no major earthquakes during the survey period, this must be aseismic slip, but its depth is in direct conflict with the seismicity of the area. Microseismic records show brittle, high stress, earthquakes down to depths of 15 km along the San Jacinto Fault. Perhaps the seismic evidence is misleading and the fault zone is weaker than the surrounding material, concentrating the strain from deeper slip. Or, perhaps we are seeing a short-term fluctuation (a temporal adjustment) of the strain field along the fault. The discordance between geologic, seismic, and geodetic slip rates certainly suggest that whatever is happening is complex and deserving of study.

Finally, is PFO close enough to the faults to make useful observations of strain changes on them? If deformation is concentrated into narrow bands one might expect measurements outside them to be of little use. To judge by seismicity, such a style of deformation may be occurring in central California (perhaps related to the lack of great earthquakes) but generally not in southern California (Allen, 1981). The instruments at PFO have measured strain release from earthquakes on faults many source dimensions away; there seems to be no reason to suppose that PFO does not lie within the zone of long-term strain accumulation as well as strain release.

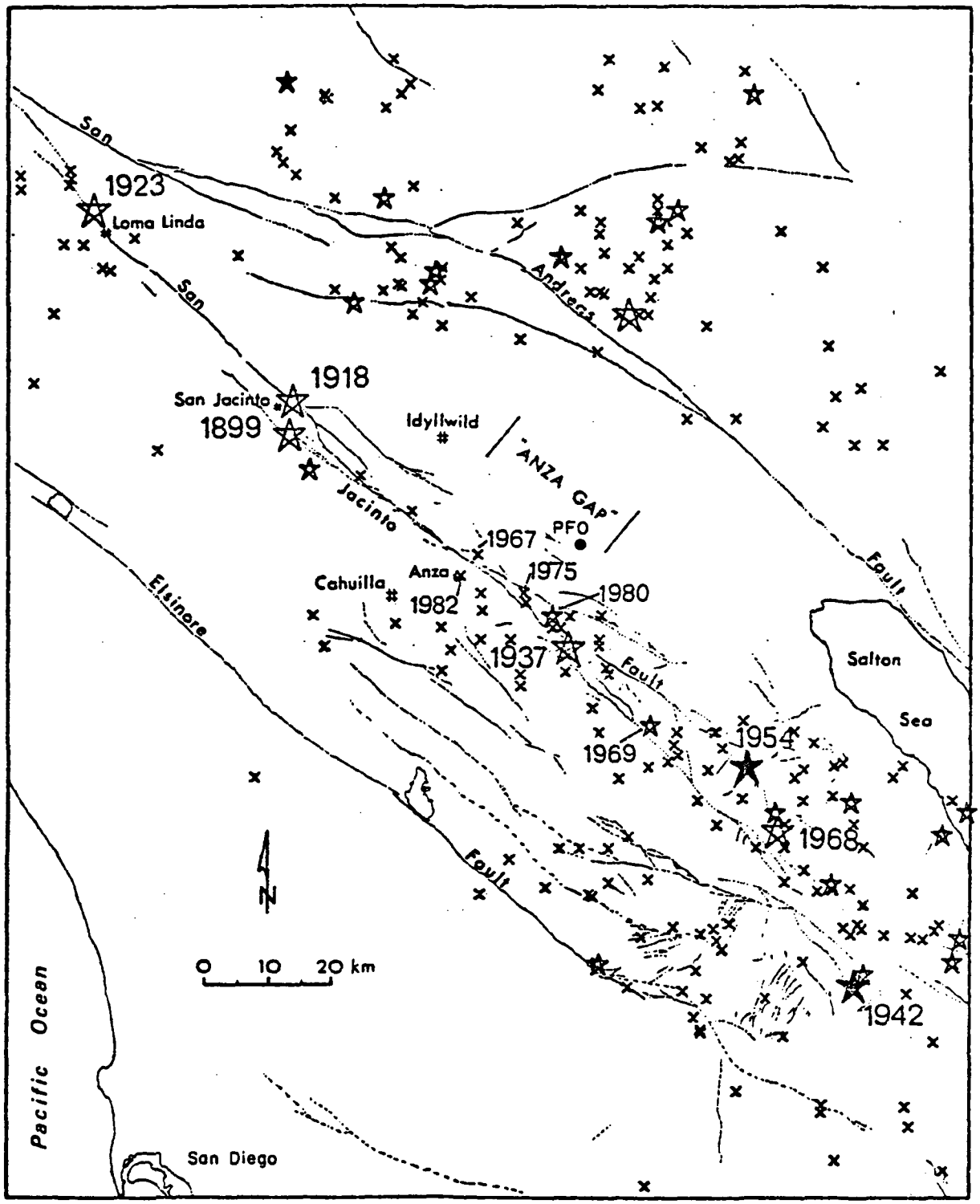

(From Sanders & Kanamori, 1984)

Figure 1.3

2.0 Laser Strainmeter Observations

The longest running instruments at Piñon Flat Observatory (PFO) are the three 732 m laser strainmeters. Figures 2.1 and 2.2 show the results from all three components since 1974 when monitoring of end-monument tilting began. Over the years these strain measurements have shown noise levels as good, or better, than those reported elsewhere. The high quality of these records has served both to establish a consistent upper limit to the level of crustal deformation in southern California and to aid in the evaluation of other techniques at the observatory. Figure 2.1 shows the components of strain measured by the three strainmeters (the continuous heavy lines), together with the geodetically determined strains measured on a subset of the USGS-Anza trilateration array surrounding PFO (data supplied by Dr. Jim Savage). (Both techniques actually measure strain changes so these two series may be shifted vertically by arbitrary amounts.) This plot also shows the rainfall measured at PFO, and the larger earthquakes nearby, labeled according to the rms coseismic deformation they could cause there.

The most obvious feature of Figure 2.1 is the large secular strain on the Northwest-Southeast (NW-SE) record through 1979. This does not agree with the geodetic measurements, and we are sure it is an instrumental artifact. While the end monuments of the North-South (NS) and East-West (EW) strainmeters are long gabbro columns sunk into pits, the end monuments of the NW-SE instrument were made from short gabbro piers installed just below floor level in underground vaults. The monument at the northwest end appears not to have been well constrained; we believe that the apparent secular strain prior to 1979 was caused by a downslope creep of this monument in response to wetting of the soil (Wyatt, 1982). In order to provide better stabilization of this, an optical anchor was installed at this end in 1979 (Wyatt *et al.* 1982b, NASA NGR 05-009-246); the results from this instrument have improved considerably since this was done. A similar anchoring scheme for the southeast end was completed in December 1983.

Particularly over the earlier part of the record, the NS and EW strain records show much less secular change. We can recombine these two records to get changes in shear strain and dilatation; the results are shown, together with the equivalent geodetic measurements, in Figure 2.2. The agreement between the two measurements of dilatation is quite good, and provides strong evidence that neither technique is significantly contaminated by changing scale errors. The two measurements of shear also agree fairly well up to the beginning of 1979. After that time both show an increase in the shear rate. However, the strainmeter record also shows a large offset not evident in the trilateration data. Because it coincides with the onset of the wet winter of 1979, and an obviously rain induced response of both the NS and EW strainmeters, we do not believe this offset is real. We should, however, note that differences of this order might be expected between the strainmeter and geodetic results because of spatial inhomogeneities in the strain field.

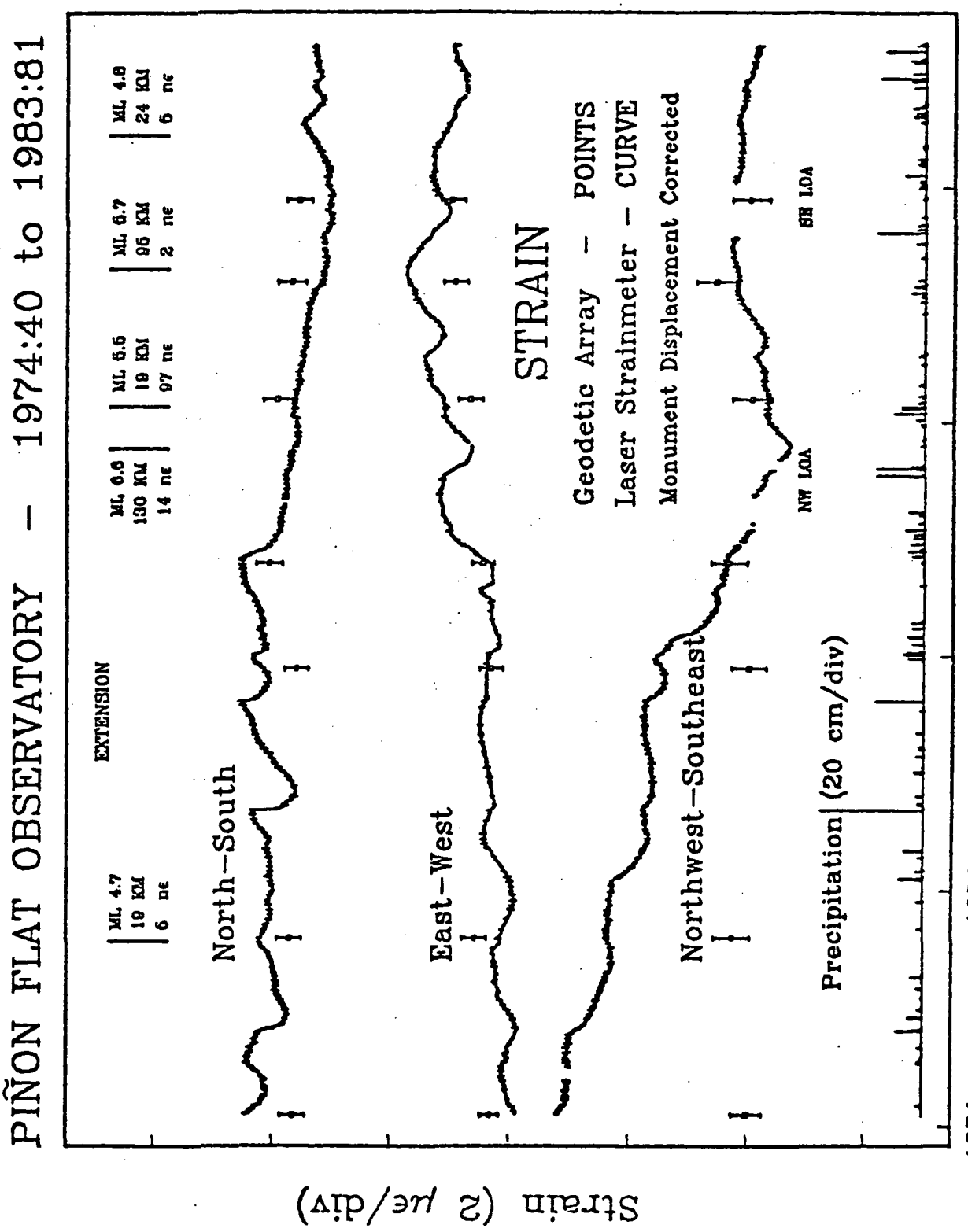
PIÑON FLAT OBSERVATORY - 1974:40 to 1983:81
EXTENSION
ML 4.7
10 KM
6 nε
ML 6.6
130 KM
14 nε
ML 6.6
10 KM
97 nε
ML 6.7
95 KM
2 nε
ML 4.8
24 KM
6 nε
North-South
East-West
Northwest-Southeast
STRAIN
Geodetic Array - POINTS
Laser Strainmeter - CURVE
Monument Displacement Corrected
NW LOA
SE LOA
Precipitation (20 cm/div)
Strain (2 με/div)
1974
1976
1978
1980
1982
Time (year)

Figure 2.1

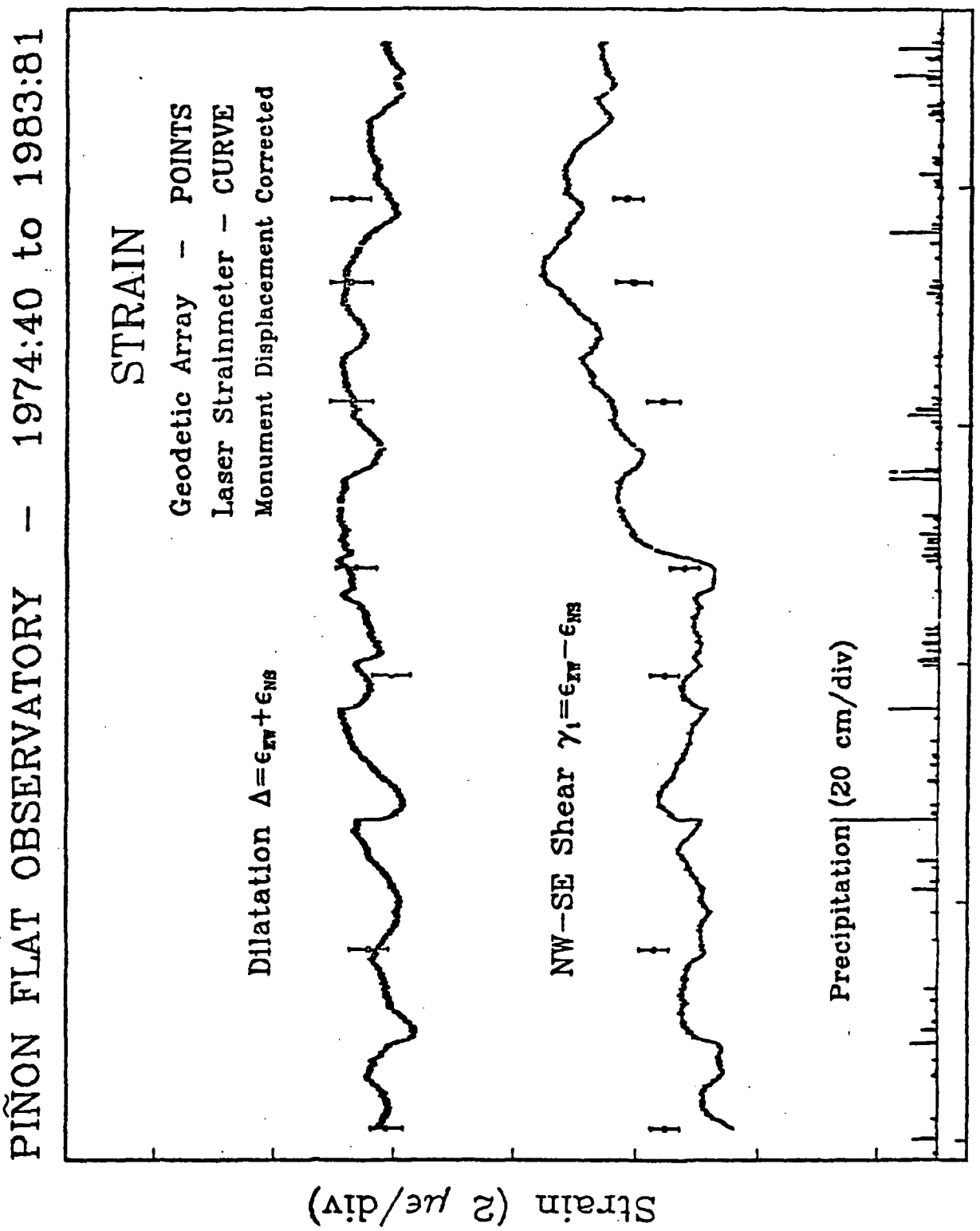
PIÑON FLAT OBSERVATORY - 1974:40 to 1983:81
STRAIN
Geodetic Array - POINTS
Laser Strainmeter - CURVE
Monument Displacement Corrected
Dilatation $\Delta=\epsilon_{EW}+\epsilon_{NS}$
NW-SE Shear $\gamma_1=\epsilon_{EW}-\epsilon_{NS}$
Precipitation (20 cm/div)
Strain (2 με/div)
1974
1976
1978
1980
1982
Time (year)

Figure 2.2

Our general conclusion from these two graphs would be that the true variations in the secular strain at PFO are unlikely to exceed a few parts in 10^7 in a year. By providing a temporal interpolation between the geodetic measurements, the PFO strainmeter records indicate that regular large fluctuations in strain (e.g., the Palmdale strain episode of 1979, reported by Savage et al., 1981a) do not occur frequently on shorter time scales than geodesy can measure. While there are fluctuations on the PFO strain records, almost all of them can be attributed to the effects of local rainfall or other changes in the instrumentation. Table 2.1 presents a comparison of the long-term strain rates derived from the two techniques. While we cannot yet match the geodetic results at these very long periods, we may use this comparison as a guide to future instrument development and improvement.

Table 2.1

PFO Secular Strain Rates

Component	Strainmeter	Geodetic Array
e_{EW} (e_{11})	+.14 με/a	+.08 ± .03 με/a
e_{NS} (e_{22})	-.11	+.01 ± .03
e_{NW-SE}*	+.12	+.01 ± .04
Δ ($e_{11} + e_{22}$)	+.03	+.08 ± .04
γ_1 ($e_{11} - e_{22}$)	+.25	+.07 ± .04

Strainmeters: 1974.1 - 1983.2 (* post 1979.3)
Geodetic: 1974.1 - 1981.9, 7 surveys

As evidence of progress in the instrument development work sponsored by NASA, Figures 2.3 and 2.4 present the records from the NW-SE stainmeter for the past year, through August 1983. This instrument, once the worst of the three at PFO, is now the best. The upper trace in Figure 2.3 shows the edited strain data, with the tides clearly visible. Below this record is the NW pier displacement record from the optical anchor and, finally, the corrected strain, adjusted for the pier motion. Near the beginning of 1983, PFO (like the rest of California) had extraordinarily bad weather, which caused the large displacement at the NW end. The corrected strain record presented in this figure and, in more detail, in Figure 2.4 still shows an obvious response to precipitation; we do not expect such behavior now that the optical anchor at the other end of the instrument has been completed. The transients around 83.2 are the result of reducing the ground-water table while drilling a nearby borehole. (A brief description of this phenomenon is presented in the next section.)

Figure 2.5 presents the most recent data from the NW-SE strainmeter, including both of the optical anchor correction series and the corrected strain. The top trace in Figure 2.5 presents the Uncorrected strain data, followed by the Residual series, created by removing the tides. Next are the NW and SE pier displacement records produced by the laser optical anchors (LOA) and converted into units of equivalent strain for the 732 m

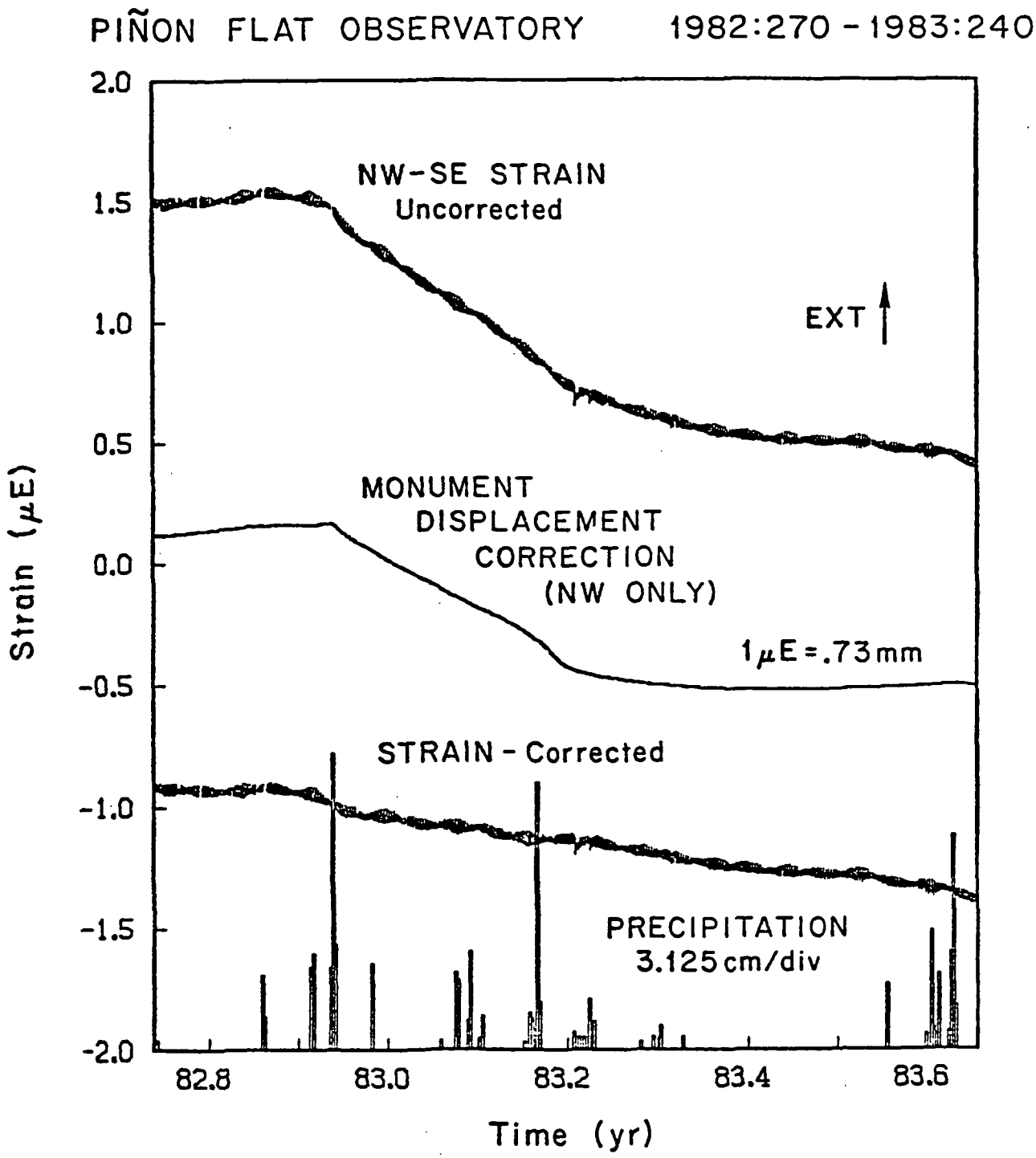
PIÑON FLAT OBSERVATORY 1982:270 - 1983:240
NW-SE STRAIN
Uncorrected
EXT
MONUMENT
DISPLACEMENT
CORRECTION
(NW ONLY)
1μE = .73mm
STRAIN - Corrected
PRECIPITATION
3.125 cm/div
Strain (μE)
Time (yr)
2.0
1.5
1.0
0.5
0.0
-0.5
-1.0
-1.5
-2.0
82.8
83.0
83.2
83.4
83.6

Figure 2.3

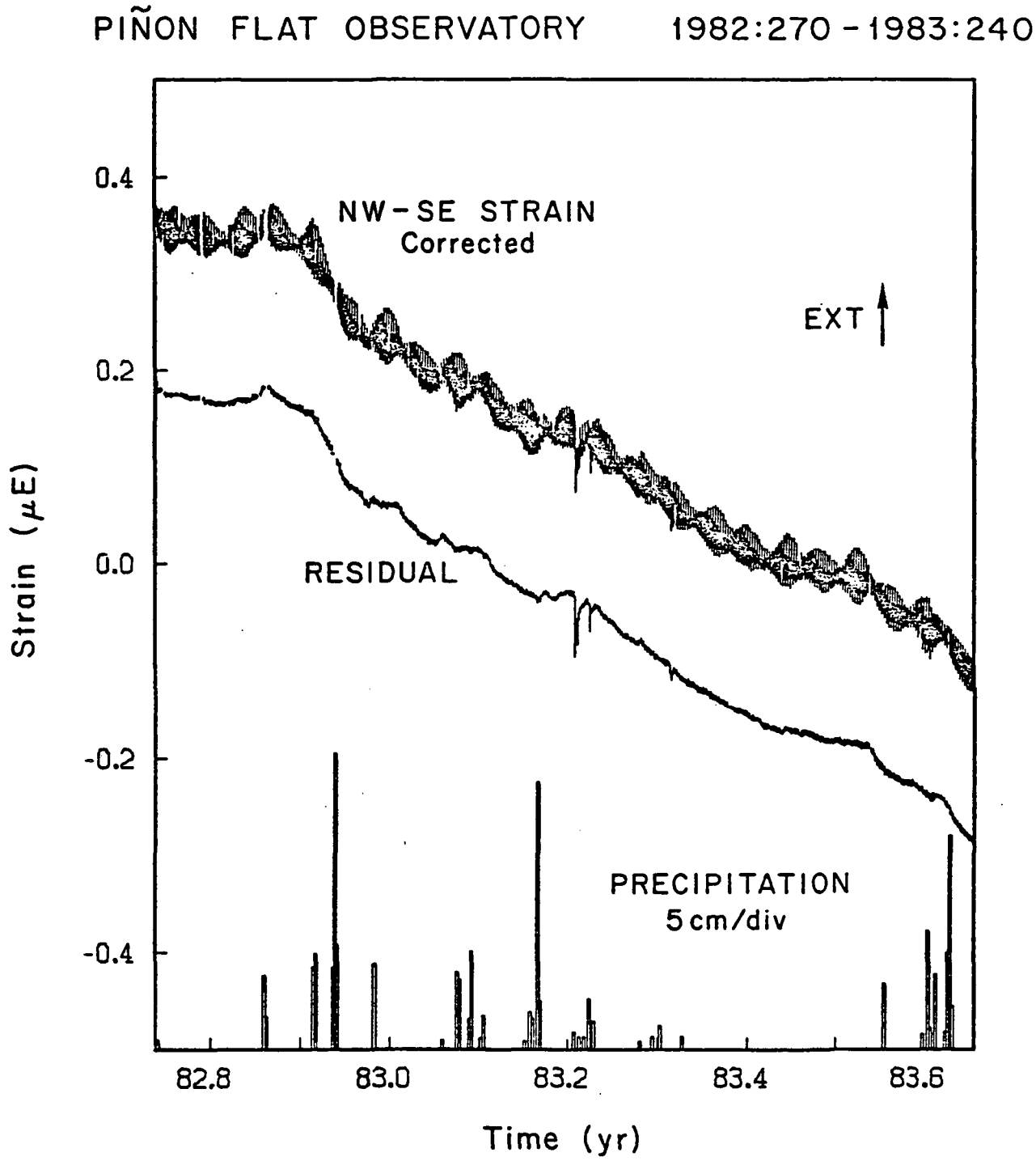
PIÑON FLAT OBSERVATORY 1982:270 - 1983:240
NW-SE STRAIN
Corrected
EXT
RESIDUAL
PRECIPITATION
5 cm/div
Strain (μE)
0.4
0.2
0.0
-0.2
-0.4
82.8
83.0
83.2
83.4
83.6
Time (yr)

Figure 2.4

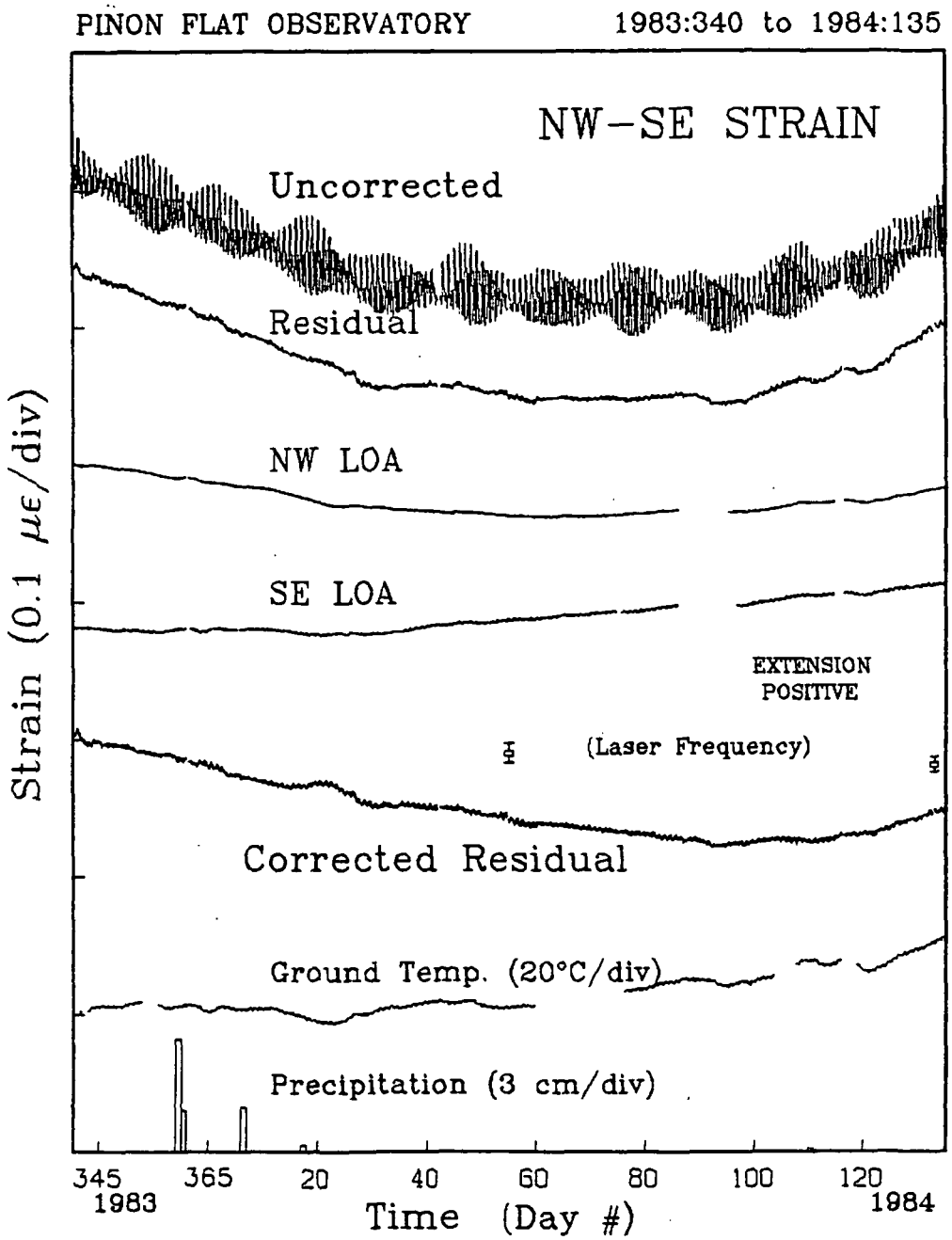
PINON FLAT OBSERVATORY
1983:340 to 1984:135
NW-SE STRAIN
Uncorrected
Residual
NW LOA
SE LOA
EXTENSION
POSITIVE
(Laser Frequency)
Corrected Residual
Ground Temp. (20°C/div)
Precipitation (3 cm/div)
Strain (0.1 με/div)
345
1983
365
20
40
60
80
100
120
1984
Time (Day #)

Figure 2.5

strainmeter. Either northwest motion of the NW LOA or southeast movement of the SE LOA will cause an apparent increase in strain in both the LOA and the Uncorrected strain series. Subtracting the LOA series yields the Corrected Residual strain. The final two curves in the figure show environmental conditions during this time period. This plot displays both the relative magnitude of the optical anchor corrections which were quite small because of the dry winter, and the low noise of the corrected signal: less than .01 με about a possibly annual cycle. If this is representative of true crustal deformation in southern California, the detection of underlying anomalous strains and tilts will be difficult indeed.

Although the record is quite short, the magnitude of both the NW and the SE LOA corrections, when extrapolated to a year, are significant; they account for nearly an order of magnitude greater long-term strain rate than that deduced geodetically for this azimuth (.01 με/a). By coincidence, they nearly cancel out in this period (at -.045 με/a and +.069 με/a, respectively). But this is certainly not generally the case; in the preceding year (Figure 2.3) we attribute as much as -1.2 με to movement of the end monuments. After correcting the most recent data (but not fitting for an annual term), a strain rate of -.13 με/a remains. We find even this rate excessive and believe we know the source, but are only now beginning to quantify it.

Within the past year and a half, we have begun to examine the stability of the optical length-standards (quartz Fabry-Perot resonators) used in the strainmeters. Earlier studies (in 1981) showed that these might drift at up to .6 με/a; in particular, for the resonator used in the NW-SE strainmeter, we found a short-term drift corresponding to a strain of -.34 με/a. Using recently acquired optics, we are beginning to monitor the frequency stability of the frequency-locked lasers at PFO relative to an atomic wavelength standard in our lab. Preliminary observations of the strain signal, caused by frequency wander of the reference resonator are shown as points with error bars in Figure 2.5. This effect is clearly large enough to explain the observed strain rate and we shall begin to apply this correction to the strain signal as soon as we commence regular measurements.

Should we realize the promise of all these corrections to the raw observations (including optical anchor measurements and monitoring of the laser frequencies), we will have advanced nearly two orders of magnitude in the quality of observatory-based strain measurements--a noteworthy accomplishment.

3.0 Long Baselength Tilt Observations

With NASA and NSF sponsorship, we have also developed a long fluid tiltmeter of caliber comparable to the laser strainmeters. We began by building a short (50 m) instrument to test our equipment and check the

vertical stability of the end monuments. These monuments were found to move by .1 mm/a, which, even over a 500 m baselength, would cause an apparent tilt of 2 μrad/a--comparable to anticipated tectonic tilts. Our long fluid tiltmeter (LFT) was therefore constructed with vertical optical anchors at each end. These devices are simply laser strainmeters which measure the vertical displacement of the surface monuments relative to the rock at depth. Shallow seismic surveys conducted at PFO (Wyatt, 1982) indicate that the material near the bottom of the optical anchors ($\sim$ 26 m in depth) is much more competent than the material near the surface. Using a combination of surface tilt and optical anchor measurements we may effectively determine the tilt at a depth of 26 m below the surface.

The first year of tiltmeter records from the LFT (1981:270 to 1982:270), uncorrected for monument displacements, are presented in Figure 3.1. The optical anchors did not become fully operational until October 1982, and so were not available for this initial data set. Nevertheless, the tilt rate for this period, .27 μrad/a, down to the ESE, was by far the lowest we had measured at PFO. Moreover, these results are in agreement with those determined geodetically. Wilson and Wood (1980) show rates of .1 to .4 μrad/a measured by leveling and lake-level measurements in the same part of California. Most of the tilts they found were, like that measured by the long fluid tiltmeter, down to the SE.

Figure 3.2 presents the second year of observation (1982:270-1983:240) beginning with the uncorrected tilt record, similar to that given in Figure 3.1, and advancing to the corrected tilt series. Fortunately, we completed the fabrication of the optical anchors before the intense rains of the winter, 1982. Up to that time the reference monuments had shown very little instability, as evidenced by the quality of the records from year one. Within a three-month period, beginning just before 1983, the east-end monument was displaced upwards some .75 mm while the west-end moved only .20 mm, causing an apparent tilt down to the WNW of 1 μrad. Correcting for the differential motion yields the bottom trace.

The corrected tilt for the second year is also shown in Figure 3.3 where it may be directly compared both with the uncorrected tilt of the previous year (Figure 3.1) and the results from the NW-SE strainmeter (Figure 2.4). Each of these figures have the same scale factors (most models of deformation in an elastic half space yield tilt and strains of similar magnitude). Apparently the change in tilt rate between these two periods is the result of failing to correct the earlier data set for monument displacements. The uncorrected tilt record for the second year begins with a continuation of the upward trend of the earlier record, while the corrected series shows a downward trend at this time. We believe that the present tilt along this axis must be predominantly down to the west with a rate of .30 μrad/a, though this estimate may be biased by an annual term.

A close examination of the tiltmeter residual series offers some clues about the source of noise in this record. At the times marked by asterisks the water table under the west end of the instrument was perturbed by

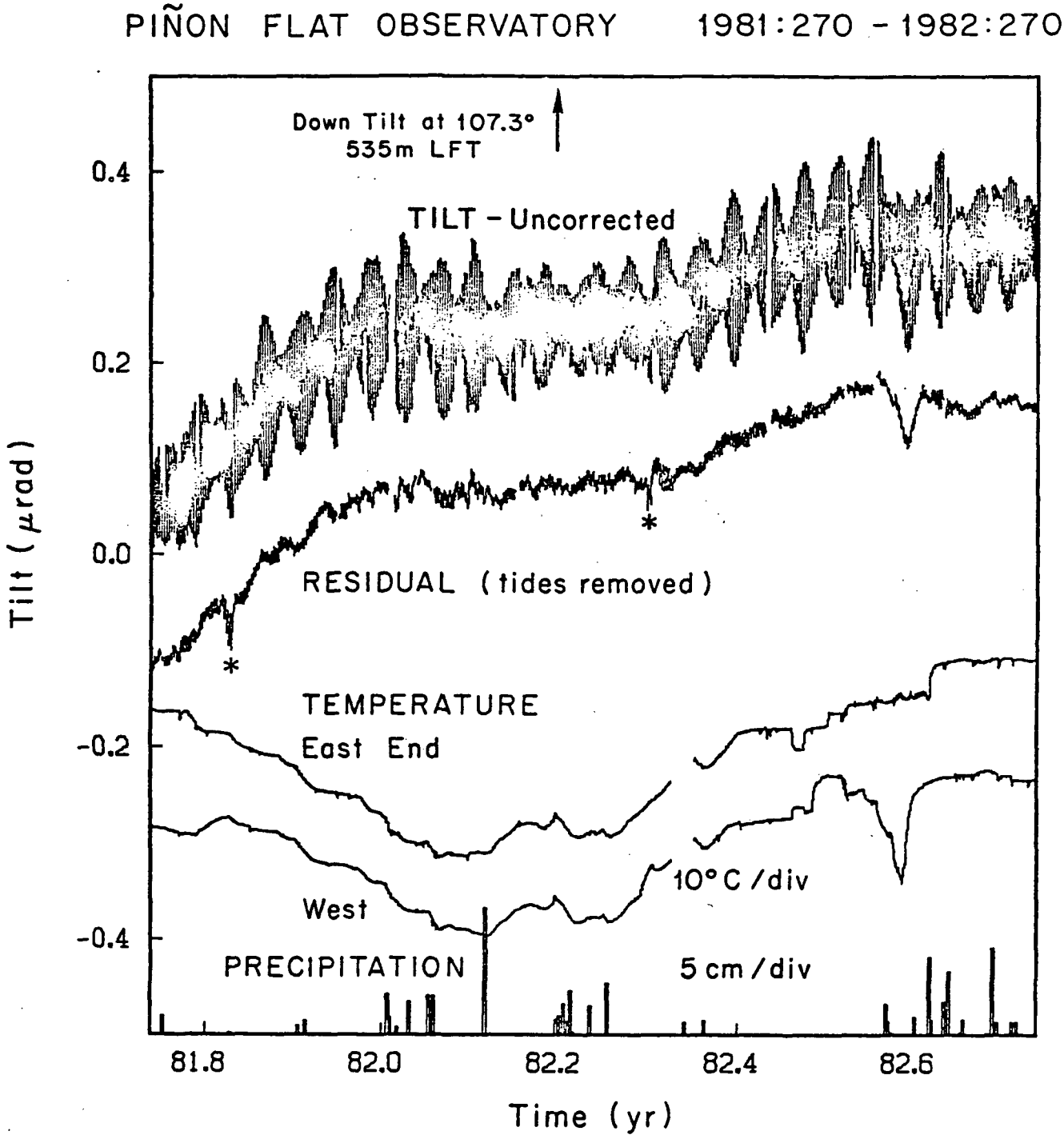
PIÑON FLAT OBSERVATORY 1981:270 - 1982:270
Down Tilt at 107.3°
535m LFT
TILT - Uncorrected
RESIDUAL (tides removed)
TEMPERATURE
East End
West
10° C /div
PRECIPITATION
5 cm /div
Tilt (μrad)
0.4
0.2
0.0
-0.2
-0.4
81.8
82.0
82.2
82.4
82.6
Time (yr)

Figure 3.1

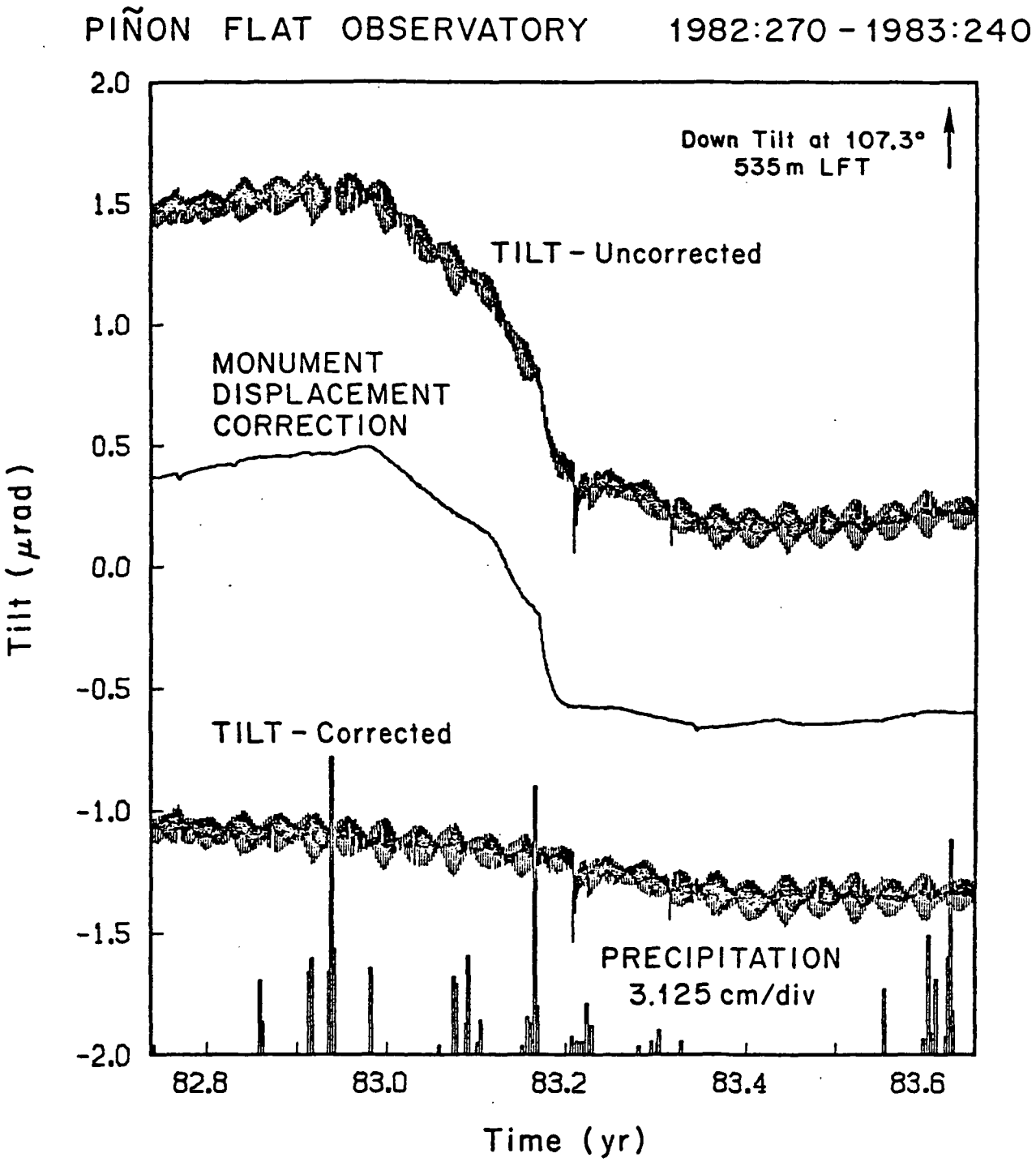
PIÑON FLAT OBSERVATORY 1982:270 - 1983:240
Down Tilt at 107.3°
535 m LFT
TILT - Uncorrected
MONUMENT
DISPLACEMENT
CORRECTION
TILT - Corrected
PRECIPITATION
3.125 cm/div
Tilt (μrad)
Time (yr)
2.0
1.5
1.0
0.5
0.0
-0.5
-1.0
-1.5
-2.0
82.8
83.0
83.2
83.4
83.6

Figure 3.2

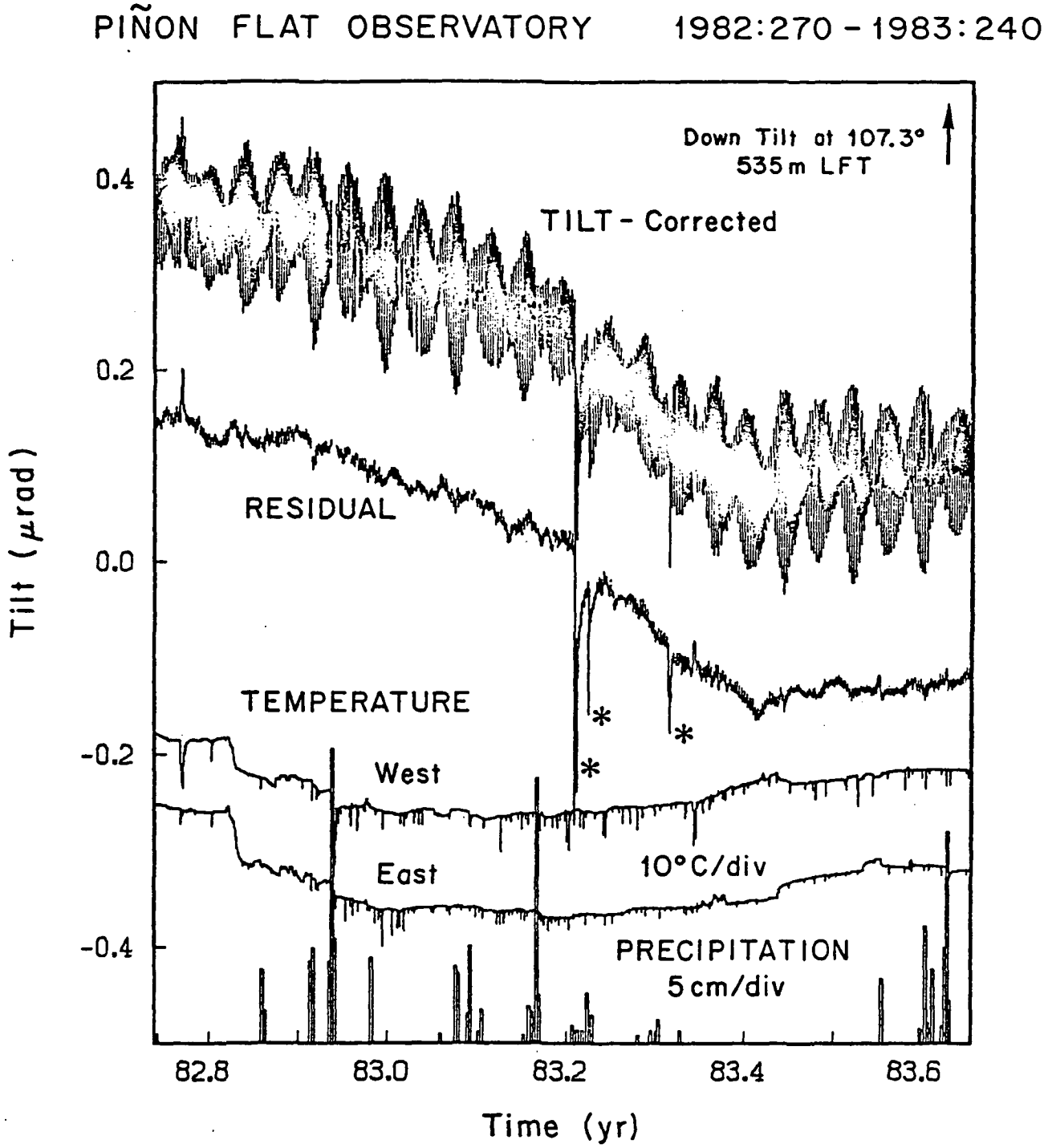
PIÑON FLAT OBSERVATORY 1982:270 - 1983:240
Down Tilt at 107.3°
535m LFT
TILT - Corrected
RESIDUAL
TEMPERATURE
West
East
10°C/div
PRECIPITATION
5cm/div
Tilt (μrad)
0.4
0.2
0.0
-0.2
-0.4
82.8
83.0
83.2
83.4
83.6
Time (yr)

Figure 3.3

drilling operations (Evans and Wyatt, 1984). Of the events shown, the response around time 1981.8 is easiest to describe; it was caused by water being purged from a borehole about 30 m distant from the end of the tiltmeter on four successive days. This resulted in the ground subsiding nearly 25 μm, for an apparent tilt of .05 μrad. If we assume 64 m as the water level change causing this effect (the height of the water column above the hypothesized fracture zone, before perturbing the hole) the tilt water level sensitivity is .7 nrad/m, a very small but significant value. The actual coefficient may be much larger than this because our estimate is biased towards the short period (a few hours) response of the hydrological system, before the pressure effects can propagate far from the hole: a permanent water level decrease should cause a greater subsidence. Fortunately the natural water level fluctuations over the past year have been less than 5 m, which should be small enough not to cause an appreciable error signal.

However, substantial changes have been caused by temperature. In particular, a deliberate temperature change at the west end of the tiltmeter around date 1982.6 produced a very large tilt signal. The thermal coefficient derived from this event is .02 μrad/°C (10 μm/°C). We believe this response to be the result of the thermal contraction of the 1 m high cement platform, which supports the tiltmeter sensor (1 m * 10 με/°C = 10 μm/°C). One approach to reducing this sort of problem would be to allow the temperature of the two ends of the tiltmeter to track one another, following the mean air temperature, as was done throughout the first year of the records presented here. Another approach, which we are now pursuing, is to keep both vaults at a constant temperature. This provides us with data largely free of thermally induced noise as well as giving us the means to establish the thermal coefficients. In any event, now that the laser optical anchors are operating, displacements of the end monuments, whether thermally induced or otherwise, should not affect the corrected tilt record.

4.0 Measurements of Coseismic Deformation

4.1 Introduction

The simple model of an earthquake as a dislocation in an otherwise isotropic elastic medium shows that quasi-static deformation of the earth's crust should be observable at distances far from the region of faulting. However, very few instruments are capable of resolving this deformation beyond the range of two or three fault dimensions because the size of the strain offsets scale roughly in inverse proportion to cube of the distance from the fault and the amplitude of strain is limited to 10**-4 e near the rupture. Continuously recording strainmeters and tiltmeters are such sensors, with resolutions often exceeding 10**-9 e for short term signals. This threshold allows the detection of static deformation for earthquakes of magnitude 7 at distances as remote as 500 km. Figure 4.1 presents the relationship between the size of events versus the radius of detection for Piñon Flat Observatory in southern California.

The history of coseismic measurements is, however, not so easily described. Very often reports of static deformation produced by continuously recording instruments greatly exceed the levels predicted by this one element of the elastic rebound theory. Press (1965) and Wideman and Major (1967) were some of the first to popularize the study of strain-steps, though both reported signals much larger than expected; the list of those who found similar results is quite long. (The term strain will be used throughout, to indicate the deformation measurable by both strainmeters and tiltmeters.) More recently, an awareness has grown that near-surface observatory-based instrumentation is particularly prone to minor adjustments of the ground nearby the sensor, or simple instrumental hysteresis. Sacks et al., (1971), for example, ran a pair of volumetric borehole strainmeters at a location not far from a 100 m quartz-bar extensometer in Japan and discovered that all of the strain-steps from the extensometer were either spurious or at least a magnitude larger than those seen on the borehole instrument. Others who have reached this same conclusion include: Stacey and Ryan (1970), Alewine and Heaton (1973), Mikumo (1973), McHugh and Johnston (1977), Allen (1978), and McGarr et al., (1982).

A comparison with geodetic measurement techniques makes it clear why it has proven so difficult to obtain meaningful coseismic records of deformation: while most geodetic surveys are absolute measurements, verifiable at different times with independent standards, high-resolution observatory-based techniques are, by and large, relative measurements. They depend on continuous recording for their meaning; individual readings cannot be checked for correctness by separate measurements. While geodectic results are limited primarily by the random noise introduced by the atmosphere separating the survey monuments, it is the monuments themselves which are the

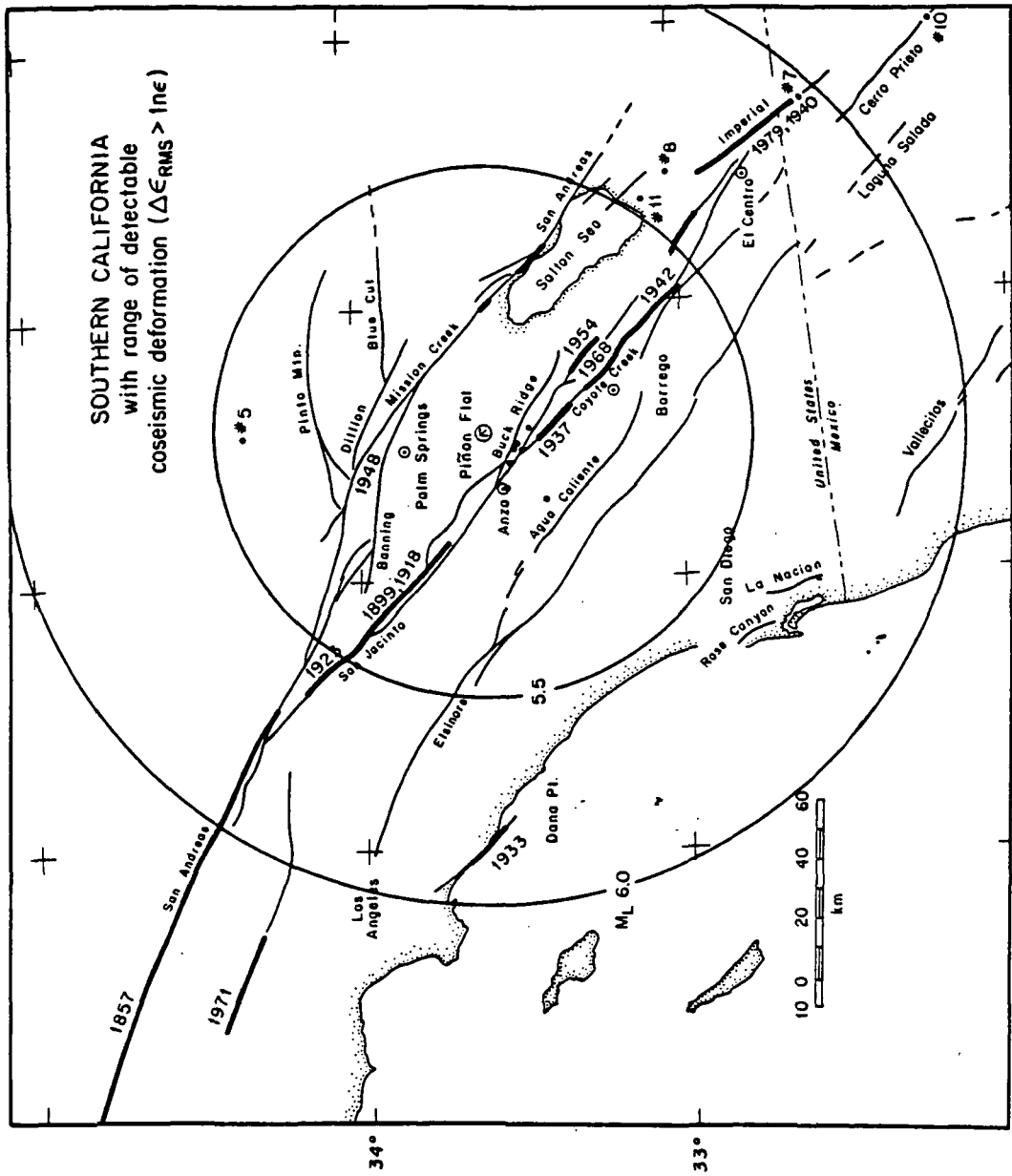

Figure 4.1. Map of southern California and northern Baja California, Mexico, showing faults (labeled), historic surface slippage (heavy lines), and location of twelve seismic events (dots) which caused measurable deformation at Piñon Flat Observatory in the period 1972-1982. Also shown is the range of earthquakes capable of producing detectable strains at the site.

biggest source of uncertainty in observatory-based records (Wyatt, 1982). The usual method of discounting anamolous tares in the record of high resolution instruments will not work here, as we anticipate just such signals shortly after the onset of appropriate seismic events.

The motivation for pursuing these signals comes from their usefulness in understanding the complete faulting process. Because most seismic records, even at periods of the earth's lowest fundamental modes, owe their existence to traveling waves they cannot provide a complete picture of the earthquake process. Throughout an event there will always be some sub-seismic component associated with gradual deformation within the source region, or, perhaps, in a zone nearby which has been agitated. These adjustments may be viewed as pre- and post seismic phenomena; but in fact they are part of the continuum of deformation. As developed by Aki (1966) and Brune (1968) the concept of seismic moments is particularly useful for characterizing the extent of fault slippage and area. The moment is defined as:

$$Mo = mu\ U\ S \qquad (1)$$

where mu is the modulus of rigidity (shear modulus), and U is the average displacement over the fault area S. Knowledge of Mo and mu, and an estimate of S, allows computation of U. Several measurements of the far-field deformation, along with a model of the earth's response, leads to an estimate of the static moment; this in turn gives us the approximation of the overall movement (U) on the fault, or an estimate of the average dislocation area if U is known.

Using this technique and the historic records Thatcher et al., (1975) identified two ~30-km-long sections of the San Jacinto fault zone in California as likely to generate moderate (ML 6-7) earthquakes within our lifetimes--a possibility emphasized more recently by Raleigh et al., (1982). The location of PFO, approximately 12 km astride one of these areas, provides an opportunity to monitor the preseismic deformation. Since 1890 the remainder of the fault, from its intersection with the San Andreas system in San Bernardino to the Imperial Valley has undergone at least 30 cm of right-lateral displacement. Studies by Sanders et al. (1981) and Sanders and Kanamori (1984) indicate that the slip deficient zone near PFO (the "Anza Seismic Gap") is presently highly stressed, evidenced by the consistently high stress-drop seismic events in the area and the number of earthquakes which have occured off the main fault trace. Long-term geodetic records (King and Savage, 1983) leave little doubt that stress is continuing to accumulate in the upper 5-10 km of crust. A high resolution record of both the gradual and abrupt (earthquake) changes of strain in the near-field of this gap could tell us much about the subsurface accomodation of these high stress levels.

Only 25 km to the northeast of PFO resides a potentially greater hazard--the dormant San Andreas vault system of the Imperial Valley. Alone, seismic slip for both the 1857 Fort Tejon earthquake (Sieh, 1978) and the 1940 Imperial Valley earthquake (Hartzell and Helmberger, 1982) indicate that

several meters of displacement could occur during the next great event. The absence of historic faulting coupled with estimates of the average relative plate motion as high as .06 m/a (Jordan and Minster, 1978) yields possible displacements up to 30 m. While the likely repeat time of such an event, and indeed even the character of earthquakes along the unbroken 180 km long segment, are the subject of some debate (Allen, 1981), the proximity of PFO should allow for the detection of small displacements at depth over a portion of this fault.

Common to all measurements of coseismic strain-steps is the sparse nature of the data sets; there are simply very few high-resolution instruments, or frequently-sampled small geodetic nets, in the world. Because of this, and because many of the recordings are contaminated by site/instrument instabilities, there have been relatively few successful applications of interpreting coseismic strain data. Recent examples of inverting geodetic data are: Dunbar et al., (1980), King et al., (1981), and Stein and Lisowski (1983) and for observatory-based instrumental data: Canitez and Toksoz (1972), Mikumo (1973), Jovanovich (1975), and Sacks (1981). Despite the low number of length-change observations involved (~10), each of these studies was quite valuable in resolving the subsurface displacements.

In the twelve year history of Piñon Flat Observatory (PFO) we have never found any consistent signals which were either indicative of extraordinary coseismic deformation, or clearly precursory to, strike-slip earthquakes which range from 12 to 200 km. Neither have we noticed any evidence for silent earthquakes, as discussed recently by Bonafede et al., (1983) for a number of deep dip-slip events. Many of the events near PFO have produced permanent deformation and one, the Imperial Valley earthquake of 1979 shows possible postseismic deformation, perhaps related to postseismic slippage on the Imperial Valley fault or subsidiary ones. Unfortunately the existing data fail to identify either the time history or the magnitude of sympathetic displacements which were observed along secondary faults following the larger events in the the Imperial Valley. Of the twelve earthquakes discussed here, the coseismic observations from six of these yield useful estimates of the seismic moment and the fault orientation, three are compatible with the observations and three were poorly recorded. Overall these data seem to generate more questions than they answer; but they are important ones and ones that should yield to closer examination. The high probability for future events in this area, as discussed, for example, by Liu and Chang (1979), further emphasizes the value of continued recording at this location.

4.2 Instrumentation

The sensors used in this study are not free from the defects inherent in observatory-based instrumentation; they react erroneously to sufficiently high accelerations, as will be discussed. Figure 4.1 should be amended to include the fact that a sizeable earthquake too close to the observatory will also not be recorded reliably. Thus for a given magnitude event there is a limited range over which it will be possible to deduce the static moment. Improvements to two of the long baselength instruments at the site (Wyatt et al., 1982a, 1982b) promise to reduce their sensitivity to local site effects caused by the radiating seismic energy. In addition, the recent installation of four permanent borehole strainmeters (Linde et al., 1982, and Gladwin, 1984) should further increase both the range and the reliability with which it will be possible to record coseismic events.

We shall consider here the results from two classes of instruments: long baselength strainmeters and tiltmeters, and short baselength near-surface tiltmeters. The general principles of the three 731 m laser strainmeters at PFO were described by Berger and Lovberg (1970). Basically they consist of an unequal-arm Michelson interferometer which measures the distance between two 3-4 m long end-monuments with a resolution of half a wavelength of He-Ne laser light (4.33 x 10**-10 e). The wavelength of the laser is stabilized by reference to a secondary mechanical length standard, and the 731 m optical pathway is environmentally controlled by maintaining a low pressure (1 Pa) inside a fixed-length aluminum pipe. While there are sources of noise associated with each of these servoed systems, the largest problem for high frequency studies is erroneous displacement of the end-monuments. Wyatt (1982) found that only for accelerations less than .05 m/s**2 (.005 g) could the reference monuments at PFO be considered stable. To reduce this sensitivity problem, an issue primarily for secular studies, special purpose tiltmeters were added to the sides of all the columnar end-monuments, allowing a simple correction in the event of end-monument tilting. Because this technique could not correct for translations at the base of the monuments, eventually a more sophisticated approach was applied to the most error-prone instrument. An optical anchor (Wyatt et al., 1982b) was added to the NW end of the NW-SE strainmeter in 1979, while the SE end was anchored in 1983. These devices measure directly the horizontal motion of near-surface monuments relative to the underlying material at a depth of ~25 m. From at least one of these three strainmeters then, we should expect a more reliable measurement of future seismic events.

A long baselength tiltmeter of similar construction is described briefly by Wyatt et al., (1982). Here the equipotential fluid level in a half-filled buried pipe is monitored for vertical displacements relative to two end-monuments separated by 535 m. The difference in apparent motion of the fluid at the two ends, when divided by the baselength, is interpreted as tilt. Optical anchors again are employed to correct for unwanted movements of the near-surface monuments. These interferometers are, however, simple vertical strainmeters capable of detecting only the vertical motions with

respect to the rocks below. The resolution of the tiltmeter is 3.89 x 10**-10 rad but it is much noiser than the strainmeter at the higher frequencies because of its reliance on water as the communicating medium rather than light in a vacuum, as is the case for the strainmeters. The fluid is the source of another drawback, namely a limited frequency response, which may be modeled as an overdamped system with a period of 1500 s. The current instrument was completed in January 1981; an earlier version of this tiltmeter, only 50 m in length and without the optical anchors, was in operation from June 1979 until the start of 1981.

The longest running short baselength instruments in the period 1972-1983 were the tiltmeters integral to the end-monuments of the laser strainmeters, and four shallow borehole tiltmeters buried at a depth of ~4.5 m (Wyatt and Berger, 1980). Because the monument tiltmeters were designed to record the rather large tilts found on gabbro columns cemented-in near the surface (e.g., 10**-5 - 10**-6 rad, which is typical for small scale structures at the ground surface), the sensitivity of these instruments was rather poor, 10**-8 rad. Nevertheless the magnitude of the coseismic offset signals from these instruments was not much different from those produced by the buried tiltmeters, with a sensitivity of 10**-9 rad. The monument tiltmeters were installed in 1974, and the shallow borehole sensors in early 1977; both have been in continuous operation since then.

Because the site is a testing ground for new geophysical instrumentation by a number of organizations, many other records are available for this study; this is particularly true more recently. While some of these records will be discussed for the individual earthquakes, our primary emphasis will be on the long baselength instruments which we operated. Over the years they have proven the most useful.

The basic recording system for most of the data presented here was a slow-speed 12-bit cassette data logger which sampled at 300 second intervals. While in almost every case higher speed records were available, ranging from sampling rates of 100 hz to .1 hz, these data sets were invariably contaminated by the limitations of the recorders or preconditioning filters: either in their sampling rate or dynamic range. Even for the more distant events a dynamic range of 16 bits is needed both to record the high-frequency dynamic signals and to resolve the underlying deformational component. The purpose of our earlier high-speed recordings was mainly to capture the frequent small seismic events as a check for instrumental artifacts. A newer system specifically designed to record the full dynamic range of the laser strainmeters over a 1 Hz bandwidth was installed in June 1984.

4.3 Model

Inspired by the self-consistency of the observations, a simple faulting model was selected to test their validity. Following the early work of Chinnery (1961), Maruyama (1964), and Press (1965), the earthquakes are modeled as a uniform strike-slip dislocation (U) in a homogeneous isotropic elastic half-space with equal Lame parameters Lambda and mu (i.e., a Poisson solid, nu = .25). The fault is assumed to be rectangular and vertical with area S. Savage and Hastie (1966), Mansinha and Smylie (1971), and Iwasaki and Sato (1979), among others, extended the elastic theory of dislocations to include the response due to an inclined rectangular fault, but incorporation of this feature was not needed to fit the reliable observations. Only for the closest earthquakes, at epicentral distances commensurate with their depth (~ 12 km), does a slightly non-vertical fault significantly alter the calculated deformations; most such events were either too small to cause sensible deformations, or were so large as to disrupt the recordings. Similarly neglecting the effects of curvature of the earth (Ben-Menahem et al., 1970) and stratified layering of the crust (Jovanovich et al., 1974) is justified for intermediate (100 km) epicentral distances. Because we are assuming a homogeneous medium, it is not even necessary to know the shear modulus (mu) of the material, other than to scale the geometric moment (U S) by the modulus to form the seismic moment. (This independence, however, does lead to a difficulty in interpreting signals which originate in the adjacent alluvium-filled Imperial Valley, as we shall see.) Finally, using the local topographic and geologic distortion maxtrix calculated by Berger and Beaumont (1976), it is possible to invert the site observations of strain to determine those which were impressed on the immediately surrounding crust: that is, to correct for site effects. However, this operation can be performed only if, in the case of surface strain, at least three independent measurements are available. Even then the magnitude of the correction at PFO is typically less than 5 percent of the observed signal which is generally smaller than the uncertainty of the measurements and so will be ignored.

Selecting this model greatly reduces the number of variables we must consider. Otherwise, for an arbitrary slip on an inclined fault there are nine independent parameters to be considered: the location of the event (3) its length, width, dip and strike, and the magnitude and orientation of the dislocation vector. This is an insurmountable problem with, as we have in this study, at most four reliable observations from a single observation point. The oft employed remedy is to rely on independent sesimic evidence to justify our choice of the earthquake location, verification of the vertical fault plane surface (peculiar to our study), and the direction of slip. This leaves us with only the fault area (length times width), the average displacement, and, if we choose, the strike of the fault to determine. Characterization of the problem in these terms suggest a least-square approach to finding the model which best fits the data. Only for two of the events which we shall discuss is such an effort justified. For those earthquakes we will follow the technique of solving a non-linear least-squares problem using an incremental procedure, first introduced to the

study of strain-steps by Pfluke and Stewart (1973) and refined by Jovanovich (1975). Because we have far fewer observations than were available for either of those studies, our modification to their approach will be simply to identify the best solution graphically.

Key to our use of this modeling procedure is the dependence on seismically determined parameters. While Jovanovich (1975) mainly used the seismic evidence to establish the errors associated with inverting the noisy and possibly erroneous strain data, we must accept the seismic observation to contribute any new understanding of the events. Interpretation of any aseismic displacements is even more allusive, even their time of occurrence is uncertain. For such events a small set of strain observations are relegated to confirming the plausibility of a particular model. Despite this deficiency the possibility of major creep events along faults both in the seismically quiet northern Imperial Valley and along the highly stressed San Jacinto fault zone make the strain data valuable.

In contrast to the empirical studies of Wideman and Majors (1967) and Takemoto (1970) the evidence here suggests that strain-steps fall-off very nearly as R**-3, in agreement with our model; the earlier reports of R**-1.5 and R**-2.4 were, undoubtedly, skewed by instrumental/site effects induced by the seismic waves. McGarr et al., (1982) verified the theoretical relationship avg.(log(deltaepsilonV)) = log Mo (Nm) - 3 log R (m) - 12 for volumetric strain changes, deltaepsilonV, and the seismic moment, Mo, as a function of the hypocentral distance, using observations of small seismic events (ML < 3.7) in a working gold mine. Similarly the Japanese Network of Crustal Movement Observatories (1970) found general agreement between 15 3-component strain measurements and the R**-3 dependence for the 1969 ML 6.9 central Gifu earthquake of Honshu, Japan. Another potential factor, dependence on depth, turns out to be unimportant. Distant deformation is relatively insensitive to source depth so long as the depth remains shallow (e.g., Cohen, 1980), which is the situation in southern California.

Of course the spatial pattern of the deformation field is anything but uniform (see Press, 1965, or Figure 4.6, for examples); some sort of azimuthal averaging is necessary to establish the radial dependence. Averaging of our simple strike-slip dislocation model leads to a very pleasant result; the range of theoretical deformations at a given radius is remarkably narrow for either the root-mean-square (RMS) of several independent components of strain (with different azimuthal orientations relative to the fault) or for the RMS of any one azimuthal component of strain when averaged around a circumference (a less likely circumstance). Figure 4.2 presents the bounds on either of these measurements of the deformation as a funciton of both the seismic moment and the hypocentral distance. To create this figure numerous vault parameters were tried based on the general guidelines for fault size in southern California (Thatcher and Hanks, 1973). Only as the observation point approaches within a fault length L (labeled as the source regime in the figure) does the pattern of deformation become too variable to categorize simply. At these distances the strains are already 10**-6 e, which is not much less than the maximum

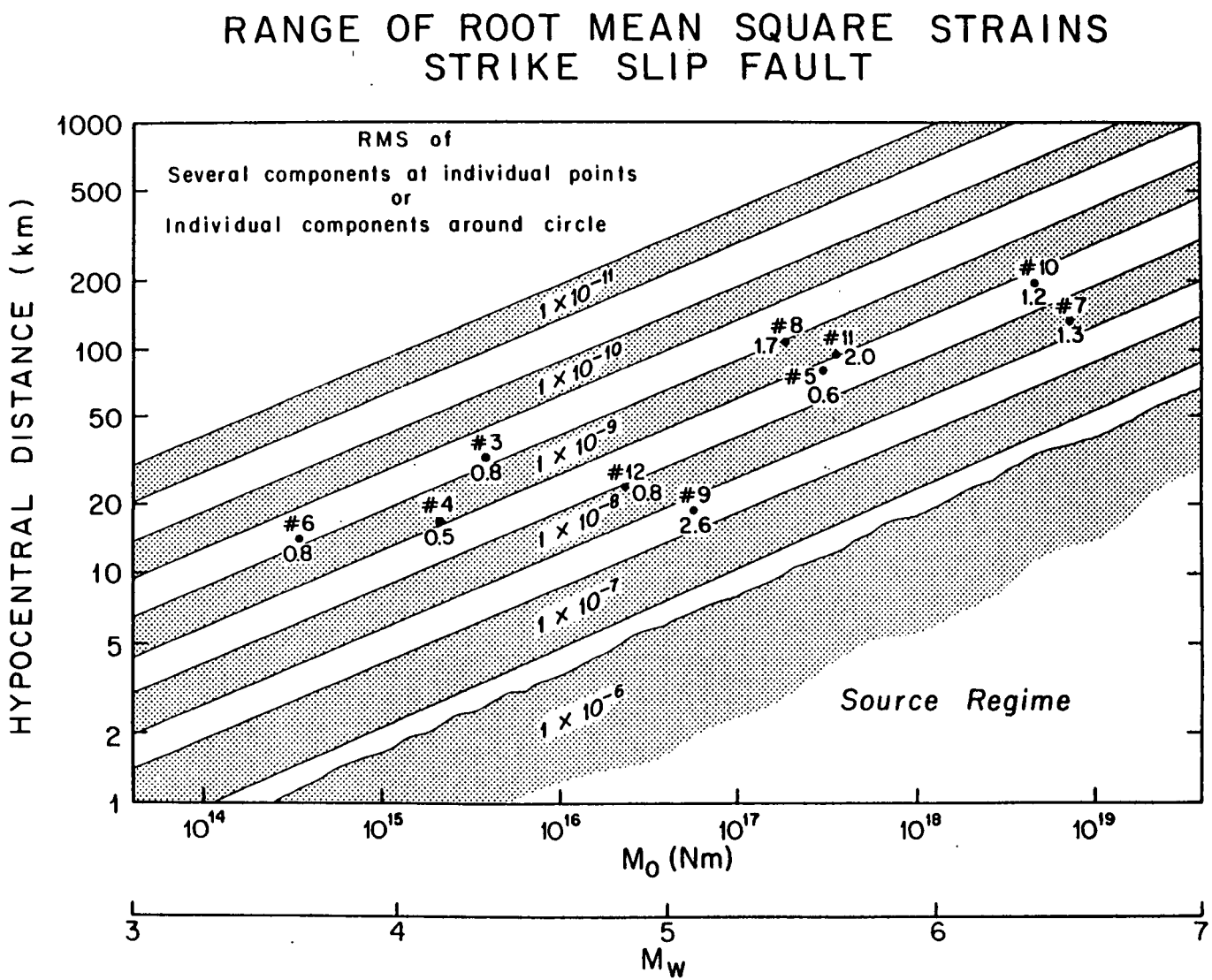

Figure 4.2. Theoretical coseismic strains (the RMS of five independent components) as a function of seismic moment and hypocentral distance. Field results, based on two or more measurements, are labeled with their event number and the ratio of observation to theory. This figure is generally applicable for estimating remote strain levels due to strike-slip faulting.

theoretical strain of 5 x 10**-5 e (deltaepsilon = deltasigma/(2 mu), where deltasigma is the nominal stress-drop). A good description of these calculations is given by

$$\log (\text{deltaepsilonRMS}) = \log \text{Mo(Nm)} - 3 \log \text{R(m)} - 11.4 \quad (+-.3) \qquad (2)$$

for deltaepsilonRMS < 10**-7.

This is a very useful result, with only a few observations from a single location a reasonable constraint may be placed on the moment of an event. Or, conversely given the seismic moment (or earthquake magnitude) the overall level of strain may be estimated. The uncertainty of a factor of two (10**+-.3) in Equation (2) is applicable for those observations from distances beyond approximately four fault lengths (i.e., in the far-field), and when three measurements of strain, and two of tilt, are used to form the RMS strain-step. Slightly less accurate estimates result from fewer records. However, because the azimuthal dependence of each of the components of strain vary quite smoothly, the RMS measure is fairly robust even with fewer observations. For those obervations nearer than 4L we may begin to exploit the details of the deformation pattern to delineate the fault surface, noteably, the nodes of distortion which radiate outward from the tips of the dislocation. Very near the ends of the fault our model breaks down, as the physically unreasonable assumption of uniform displacement results in singularities along the edge of the fault, but then again, so do the instruments.

4.4 Observations

Using the definition of the moment magnitude Mw introduced by Kanamori (1977)

$$\log \text{Mo(Nm)} = 1.5\ \text{Mw} + 9.1 \qquad (3)$$

we may convert expression (2) from dependence on the seismic moment to one of earthquake magnitude

$$\log (\text{deltaepsilonRMS}) = 1.5\ \text{Mw} - 3 \log \text{R(m)} - 2.3 \qquad (4)$$

The moment magnitude is chosen because of its similarity to the local magnitude ML (Mw ~= ML - .1, 3.5 ~< M ~< 5.5), its agreement with surface-wave scale Ms (Mw = Ms, 5 ~< Ms ~< 7.5) and its connection with a physical interpretation of faulting (Hanks and Kanamori, 1979; Kanamori, 1983). Based on this equation and seismic data from the U.S. Geological Survey - California Institute of Technology, southern California network, SCARLET (data supplied by L.K. Hutton, 1984) all the events from the period

1971:103 through 1983:187 were assigned an estimate of the coseismic deformation for Piñon Flat Observatory. Results of this calculation are plotted in Figure 4.3. As can be seen only twelve events in this time would be expected to produce detectable signals (deltaepsilon > 4.3 x 10**-10 e) at the observatory; these are listed in Table 4.1. Details of this table will be reviewed in the course of discussing the individual events.

While the permanent deformation associated with each of these events should be detectable, most of them are so small that they barely exceed the resolution of the instrumentation under normal circumstances. The effect of the transient accelerations on the sensors means that the records are less reliable than their resolution. Indeed, because the full wave form for these events was not recorded, even the length of time between the two estimates of the static strain level (before and after the seismic coda) limits the accuracy of our observations. Provisionally, we considered only those earthquakes for which the theoretical RMS deformation exceeds 1.3 ne (3 deltaepsilon) as candidates likely to yield reliable data; in fact we were able to do much better. Following is a description of the observations from all twelve of these earthquakes, roughly in the order of their contributions to our understanding of the phenomenon.

4.4.1 Imperial Valley - 1979 (#7) -

Best known of all the events is the Imperial Valley earthquake which occurred on October 15, 1979. So much has been written about this earthquake, including a wide-ranging collection of articles in the Geological Survey Professional Papers 1254 (1982), that only a brief description is required here. Initiating at a depth of 8 km just south of the U.S.-Mexican border, the ML 6.6 event ruptured towards the northwest along the pre-existing trace of the Imperial Vault and also northerly along the Brawley fault (Archuleta, 1982a). (The role of the Brawley fault will be discussed in a later section.) Very roughly, the length of the ruptured fault surface, from hypocenter to the furthest surface expression, was 40 km; Figure 4.4 shows both the location of the epicenter and the surface faulting. A maximum right-lateral displacement of 60 cm was measured during the first day after the event about 10.5 km northwest of the epicenter (Sharp et al., 1982b). Subsequently the lateral surface displacement, which tapered off to zero at the NW end, was observed to increase almost everywhere along the fault by approximately 30 percent in 160 days, though this ratio varied considerably.

The observatory, also displayed in Figure 4.4, is located some 132 km from the midpoint of the assumed dislocation surface at an approximate azimuth of -8 degrees relative to the strike of the fault. Figure 4.5 presents the records from the North-South (NS) and Northwest-Southeast (NW-SE) laser strainmeters, sampled at an interval of two seconds, much too slow to avoid aliasing contamination. The third 731 m laser strainmeter, oriented east-west, began to operate erratically several hours before the event due to a faulty laser and was not deemed reliable for this study.

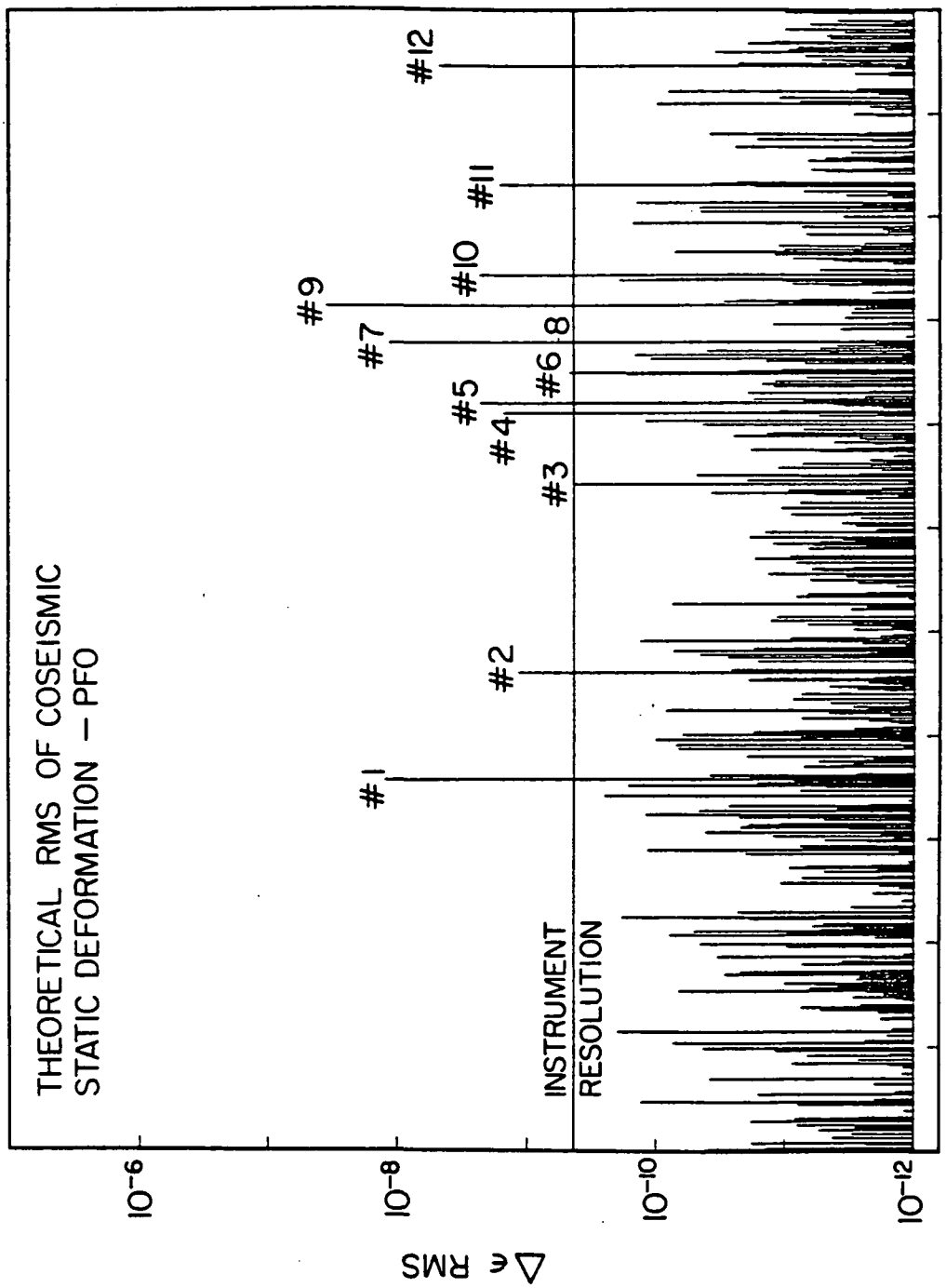

Figure 4.3. History of coseismic strain release at Piñon Flat Observatory. Earthquakes which exceed the laser strainmeter detection threshold (deltaepsilon > 4.3 ne) are identified by event number.

Table 4.1

Detectable Coseismic Events 1972-1982 - PFO

#	Earthquake Lat, Long	M_L Time	R(km)	M_0(Nm)† M_W	$\Delta\varepsilon_{RMS}{}^T$	M_0(Nm)^O M_W	$\Delta\varepsilon_{RMS}{}^O$	A_H(m/s^2)†	$\Delta\varepsilon_{RMS}{}^S$
1.	Horse Canyon 33.52°, -116.56°	4.8 1975:214:00:14	18	1.9×10^{16} [a] 4.8	13.0	-- --	--	.78 [a]	1600
2.	Lower Buck Ridge 33.48°, -116.51°	4.3 1976:224:15:24	21	2.8×10^{15}	1.2	-- --	0.5	.18	300
3.	Chihuahua Valley 33.42°, -116.70°	4.4 1978:156:16:03	33	3.9×10^{15}	0.4	3.3×10^{15} 4.3	0.3	.07	60
4.	SE Buck Ridge 33.46°, -116.43°	4.2 1979:043:04:48	17	2.0×10^{15}	1.5	4.0×10^{14} 3.7	0.7	.13	56
5.	Homestead Valley 34.33°, -116.44°	5.2 1979:074:21:07	79	3.0×10^{17} [b] 5.6	2.4	-- --	1.4	.04	32
6.	Upper Buck Ridge 33.49°, -116.50°	3.7 1979:183:11:51	14	3.5×10^{14}	0.5	-- --	0.4	.05	66
7.	Imperial Valley 32.61°, -115.32°	6.6 1979:288:23:16	132	7.0×10^{18} [c] 6.5	12.0	9.0×10^{18} 6.6	15.0	∿.10	81
8.	Brawley 33.01°, -115.56°	5.5 1979:289:06:58	107	1.8×10^{17}	0.6	2.3×10^{17} 5.5	1.0	.03	20
9.	Buck Ridge 33.50°, -116.51°	5.5 1980:056:10:47	19	5.6×10^{16} [d] 5.1	33.0	-- --	87.0	1.4 [d]	1700
10.	Mexicali Valley 32.19°, -115.08°	6.1 1980:161:03:28	192	4.5×10^{18} [e] 6.4	2.5	6.1×10^{18} 6.5	3.0	.02	20
11.	Westmorland 33.10°, -115.63°	5.7 1981:116:12:09	95	3.5×10^{17}	1.6	5.3×10^{17} 5.7	3.2	.06	32
12.	Anza 33.56°, -116.67°	4.8 1982:166:23:49	24	2.3×10^{16} [d] 4.8	7.0	-- --	5.4	.53 [d]	340

All strain in nε

T - Theoretical RMS strains
O - Observed long baselength strains
S - Short baselength strains

R - Hypocentral distance
A_H - Peak horizontal acceleration
† - Except where noted, based on M_L

a - Hartzell and Brune, 1979
b - Stein and Lisowski, 1983 (M_S)
c - Archuleta, 1984
d - Frankel, 1984
e - Munguia-Orozco, 1983

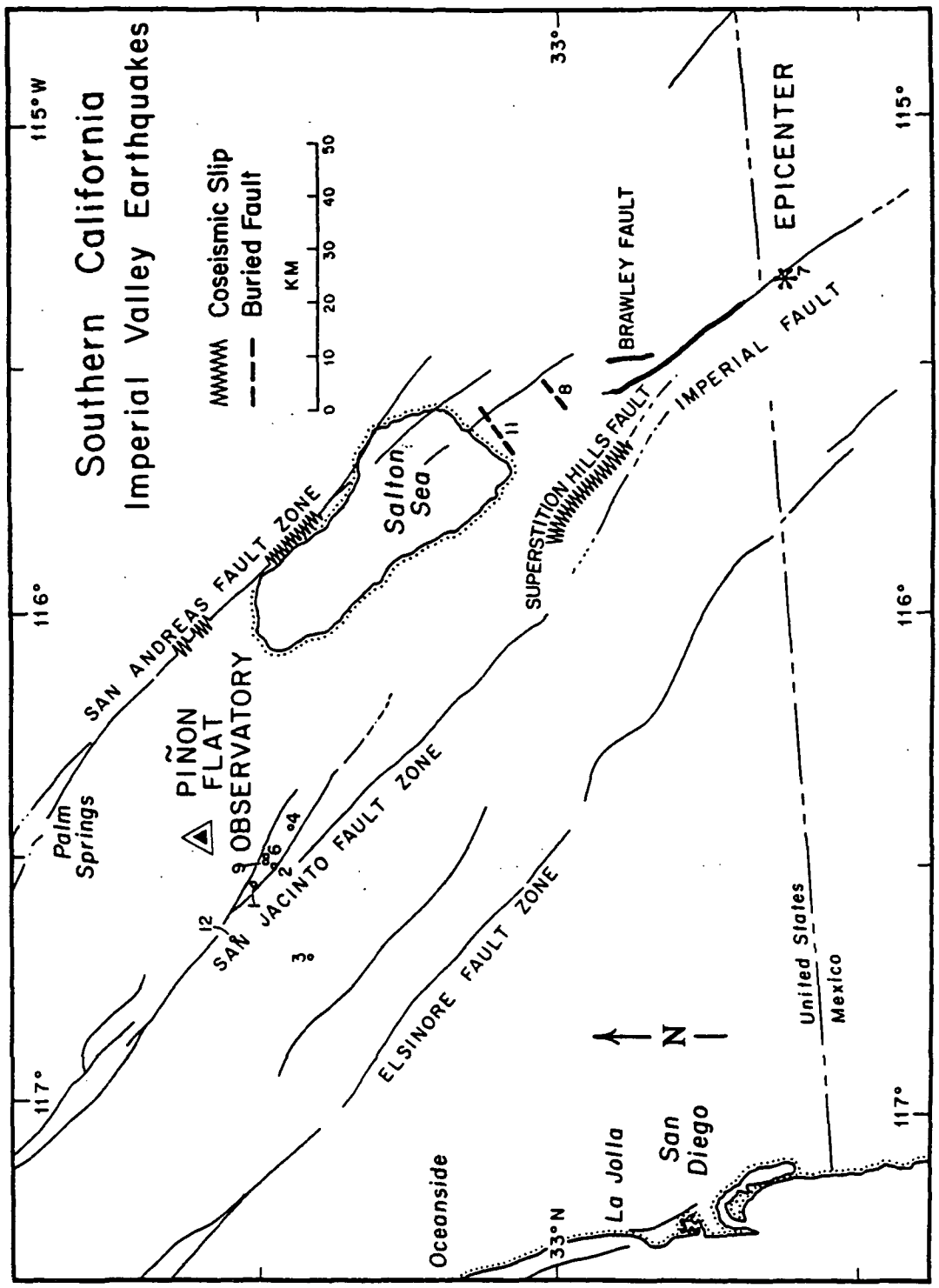

Figure 4.4. Detailed map of southern California showing location of surface rupturing (heavy line) and distant surface slip (jagged line) for the 1979 Imperial Valley earthquake (#7). Dashed lines show the modeled extent of the buried 1979 Brawley (#8) and 1981 Westmorland (# 11) dislocations. Other nearby events are labeled with their event number.

Clearly visible in the figure are the strain offsets (~10 ne) at the time of the main shock as are the many aftershocks, all superimposed on the tidal signals. Based on a triggered high-speed recording of these signals (deltaT = .01 seconds) the dynamic strains are estimated to be nearly 200 times the size of the offset. (Unfortunately the data files from this recording system were found to be full of timing errors.) On a much shorter instrument, the 50 m fluid tiltmeter aligned at an azimuth of 95.6 degrees, the strain-step was also resolved though barely above the noise. Table 4.2 lists the observed offsets along with an estimate of their uncertainty for the laser strainmeters and the 50 m fluid tiltmeter.

In addition to the records from the instruments with extended baselengths, measurements were obtained from eight short baselength tiltmeters; Table 4.3 summarizes these observations. Considered as a whole, the observed offsets are neither in agreement with the magnitude of the long baselength instruments nor are they internally consistent. Apparently the upper layers of the ground, at least at PFO , and quite probably in most locations (Wyatt, 1982), are not sufficiently stable to allow meaningful short baselength measurement of the crustal deformation in the presence of even small accelerations. Based on the empirical relationship for peak horizontal accelerations developed by Espinosa (1979):

$$Ah = 7.41*10^{**}-10\ 10^{**}ML\ Delta^{**}(2.89-.5\ logDelta) \qquad (5)$$

with Ah in m/s**2 and Delta (the epicentral distance, over the range of 5-300 km) in m, we calculate the maximum site accleration to have been 0.15 m/s**2. This very course estimate is augmented by the evidence that the U.S. Geological Survey strong-motion recorder at the site, with a threshold of 0.1 m/s**2, did not trigger (R. Porcella, personal communication, 1980).

In order to calculate the theoretical deformaton field several parameters must be selected. The length of the faulting is the least subjective element, choosen here to be 40 km. Archuleta (1982b) suggests approximating the fault profile as extending from the surface to a depth of 10 km, the depth of historic seismicity along the fault. He then breaks this down further into a sedimentary regime 0-5 km with rigidity (mu) of 7.4 GPa and a basement layer 5-10 km, mu = 26 GPa. The detailed seismic-refraction work of Fuis et al., (1984) substantiates this distinction throughout the middle of the Imperial Valley; unfortunately our simple model cannot. Proceeding with the assumption of uniform rigidity through-out (30 GPa) will unduly weight the moment generated by the sedimentary rocks, but this may be reconciled. The distribution of slip vs. depth is the most difficult factor to select, although for this variable, the model is equipped to handle any distribution by the linear superposition of solutions for patches of uniform slip. In this manner we could, for example, attempt to scale down the moment contribution of the near-surface layer to account for its lesser strength. The average horizontal surface displacement of the Imperial fault grew logarithmically with time, from 0.29 m four days after the event to about 0.43 m 160 days later (Sharp et al., 1982b). Harsh (1982), in the context of the Imperial Valley earthquake, discusses the mechanism of delayed surficial

Table 4.2

Observed vs. Theoretical Deformation

#	Earthquake	Strain			Tilt			Model			
		NS	EW	NW	Long-base (A&B)	Short-base NS	Short-base EW	Strike	L(km)	W(km)	$\bar{u}$(m)
1.	Horse Canyon	F	F	F	N	750	2100				
	1975	-10.0	12.0	.3		12	- 11	53°	1.5	1.5	.28
2.	Lower Buck Ridge	.5±0.5	F	F	N	80	400				
	1976	- .8	.6	- .9		.5	-1.6	-65°	1.0	1.0	.093
3.	Chihuahua	- .4±0.4	.4±0.5	.0±0.4	N	65	50				
	1978	- .5	.4	.1		.2	- .1	-50°	1.0	1.0	.11
4.	SE Buck Ridge	.8±0.5	- .4±0.6	.8±0.7	N	65	45				
	1979	1.0	- .3	.5		-.2	0	-52°	.75	.75	.024
5.	Homestead Valley	2.0±0.5	- .4±0.4	N	N	20	40				
	1979	2.1	- .4			-.6	2.6	- 6°	6.0	4.0	.42
6.	Upper Buck Ridge	.0±0.4	- .6±0.5	.0±0.4	N	25	90				
	1979	.6	0	- .4		-.4	- .3	-45°	0.5	0.5	.047
7.	Imperial Valley	-21.0±2.0	N	-12.0±2.0	- 9±5.0[A]	90	70				
	1979	(- 6.0) P		(- 4.0) P							
		-19.0		-15.0	- 8.0	-15	- 9	-37°	40	10	.75
8.	Brawley	- .8±0.4	N	- 1.2±0.5	0±4.0[A]	20	20				
	1979	- .9		- 1.2	.1	.6	.2	51°	5.0	5.0	-.30
9.	Buck Ridge	F	52.0±200	F	-112±5.0[A]	750	2300				
	1980	-58.0	33.0	-51.0	- 95.0	31	-93	-53°	2.0	2.0	.94
10.	Mexicali Valley	- 4.0±2.0	2.5±2.0	- 2.0±2.0	0±4.0[A]	20	20				
	1980	- 3.9	2.1	- 1.7	- 2.0	- 3	-2	-35°	30	10	.68
11.	Westmorland	- 2.8±0.5	-1.3±0.5	- 5.7±1.0	0±0.5[B]	20	40				
	1981	- 2.9	-1.3	- 5.5	- .3	1.9	.3	54°	10	5	-.35
12.	Anza	F	F	7.0±1.0	-3.2±1.0[B]	60	480				
	1982	- 2.0	1.2	7.8	- .8	7.7	1.5	-28°	1.6	1.6	.30

Observations - First line of figures
Theoretical - Second line of figures

All strains in nε, tilts in nrad

N - Not in operation
F - Failed during event
A - Azimuth 95.6°, length 50 m
B - Azimuth 107.3°, length 535 m
P - Post-seismic

Table 4.3. Observed Deformations
Short Baselength Instruments
1979 Imperial Valley Earthquake

North-South Tilt Components

Instruments	Depth	Coseismic Offset	
Alpha NS	4.5 m	20	±20
Beta NS	4.5 m	- 7	±20
Gamma NS	4.5 m	- 70	±20
Delta NS	4.5 m	- 80	±20
N Pier	2.7 m	0	±30
S Pier	1.8 m	-190	±50
Calculated tilt		- 15	

East-West Tilt Components

Instrument	Depth	Coseismic Offset	
Alpha EW	4.5 m	10	±30
Beta EW	4.5 m	- 40	±20
Gamma EW	4.5 m	60	±30
Delta EW	4.5 m	40	±20
W Pier	3.2 m	40	±50
E Pier	2.5 m	-140	±70
Calculated tilt		- 9	

Units of tilt are nrad
Positive tilt, down to the north and east

fault slip usually prescribed to postseismic strain adjustment occuring in a thick alluvium layer, though he conjectures that part of the slippage for this event might be the result of afterslip in the 5-10 km seismogenic zone. It seems likely that .4 m represents a lower limit for the fault slippage over most of the deeper fault surface. Olson and Apsel (1982) deduced a quite different picture of the subsurface motion. Using observations from 26 three-component accelerometers located in the near field, and a stabilized inversion scheme, their perferred solution consists of a peak right-lateral dislocation of 1.6 m near the middle, and in the lower half, of a 50 km-long vertical fault plane. The average displacement in the 5-10 km zone is .68 m, which is equivalent to .85 m over the 40 km-long fault zone we have supposed. Both the inverse solution and the surface observations show the offset nearer the surface (0-5 km) to be concentrated at a location between 10 and 35 km north of the epicenter, though the average slip of the theoretical model (.77 m) is nearly double that observed, after it is normalized to the 30 km zone of recorded surface rupture. A reasonable upper bound for the average slip on the overall fault plane is .75 m.

Using, in all cases, the larger estimate of the fault parameters (S = 10 km x 40 km, U = .75 m), we calculated the theoretical deformations given in Tables 1, 2, and 3, and shown in Figures 4.5, 4.6, and 4.7. The latter two figures are intended to indicate the sensitivity of the solution to the assumed fault strike and the geometric moment US, which is the seismic moment (Mo) when this factor is scaled by the assumed crustal rigidity of 30 GPa. Figure 4.6 shows the theoretical deformation pattern for the orientation of the three instruments at PFO. Clearly the NS strain measurement is well suited for establishing the moment, while the NW-SE measurement provides the better constraint on the relative fault strike; Figure 4.7a makes these same points in another manner. In this figure we consider scaling the theoretical value (shown as a heavy line) to adjust the moment, at the same time sliding along within the stippled areas (the field observations) to select the fault strike. From these two plots we find that an average strike of -37 degrees (i.e., 37 degrees W of N, all azumuths measured clockwise from north) and moment of 9.0 x 10**18 Nm are in good agreement with the observations.

4.4.2 Brawley - 1979 (#8) and Westmorland - 1982 (#11) -

These two events are discussed in parallel because of their close proximity to one another at the north end of the Imperial Valley fault zone, and their assumed sinistral fault movement. The Brawley event is actually the largest aftershock (ML 5.5) of the Imperial Valley earthquake, occurring near midnight (local time) October 15, 1979, some eight hours after the main shock, on a conjugate fault propogating from the northwest end of the Imperial Valley fault toward the northeast (Johnson and Hutton, 1982). The ML 5.7 Westmorland earthquake of April 26, 1981 occurred only 13 km to the NNE of the Brawley earthquake. Although no tectonic surface faulting of either of these ruptures was observed (Sharp et al., 1982a; Heaton et al., 1983), based on the seismic observations and the history of previous events

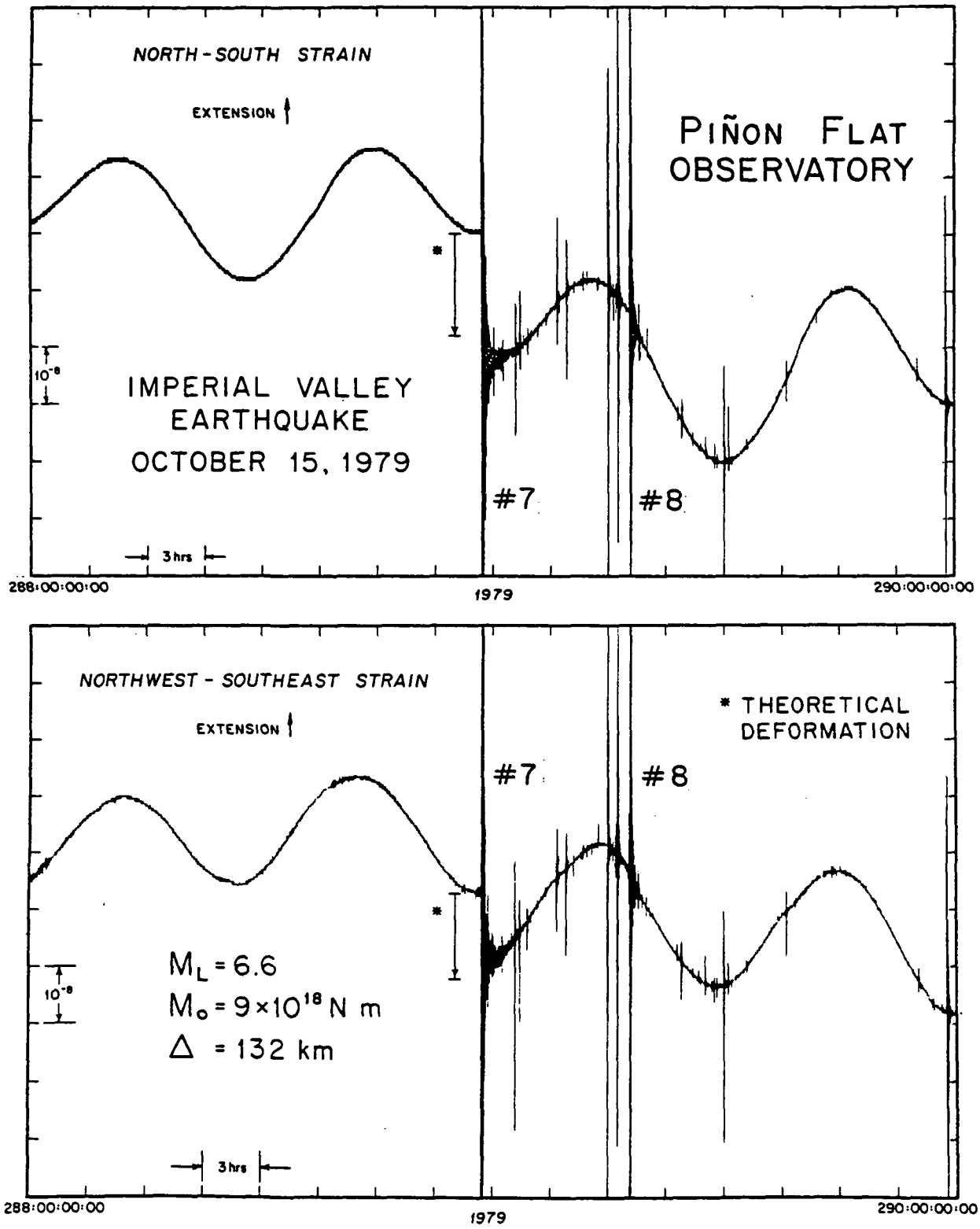

Figure 4.5. Laser strainmeter records of the 1979 Imperial Valley (#7) and Brawley (#8) earthquakes, sampled at a 2 s interval. Model values, based on the observed fault strike and location, are shown as offset arrows, indicating a seismic moment of 9.0 x 10**18 Nm for event #7.

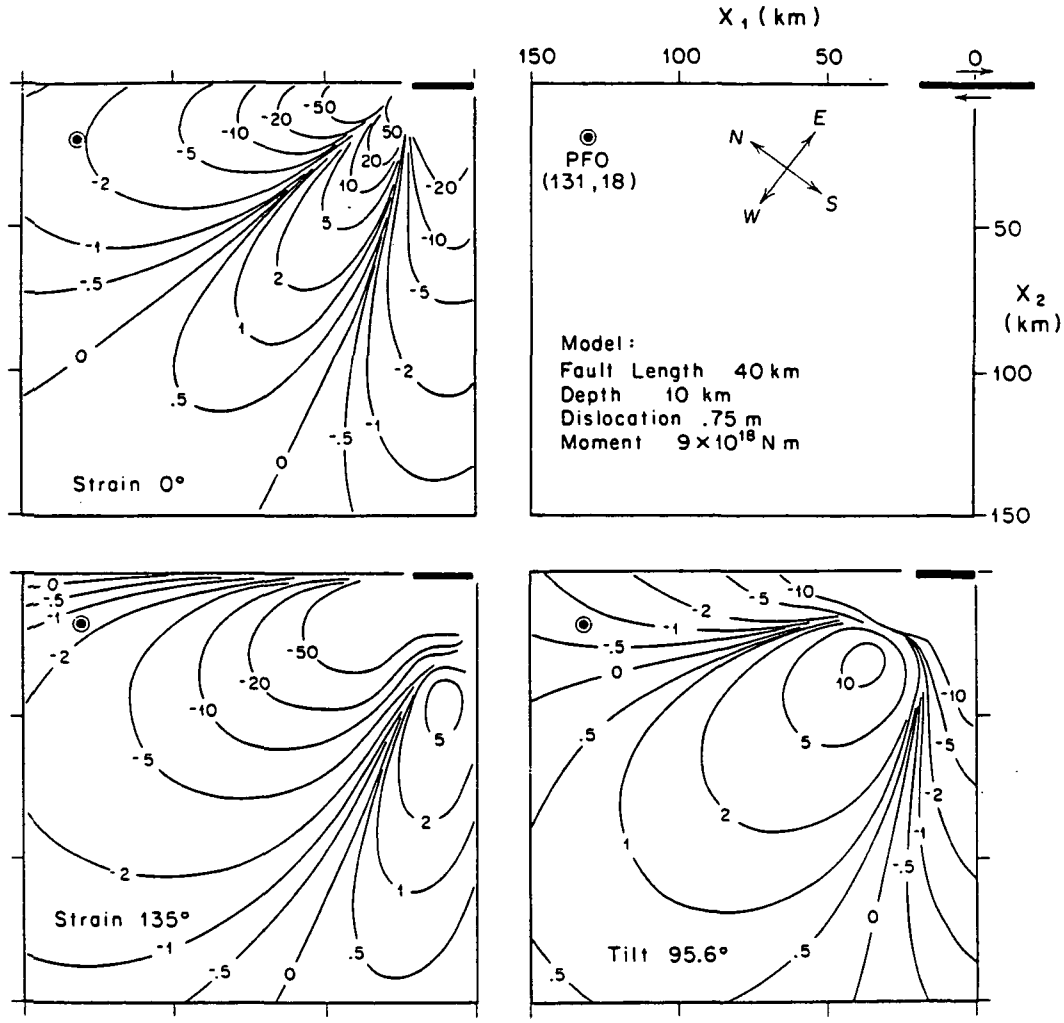

Figure 4.6. Theoretical patterns of static deformation for two components of strain and one of tilt following the Imperial Valley earthquake 1979. The circled mark shows the location of PFO.

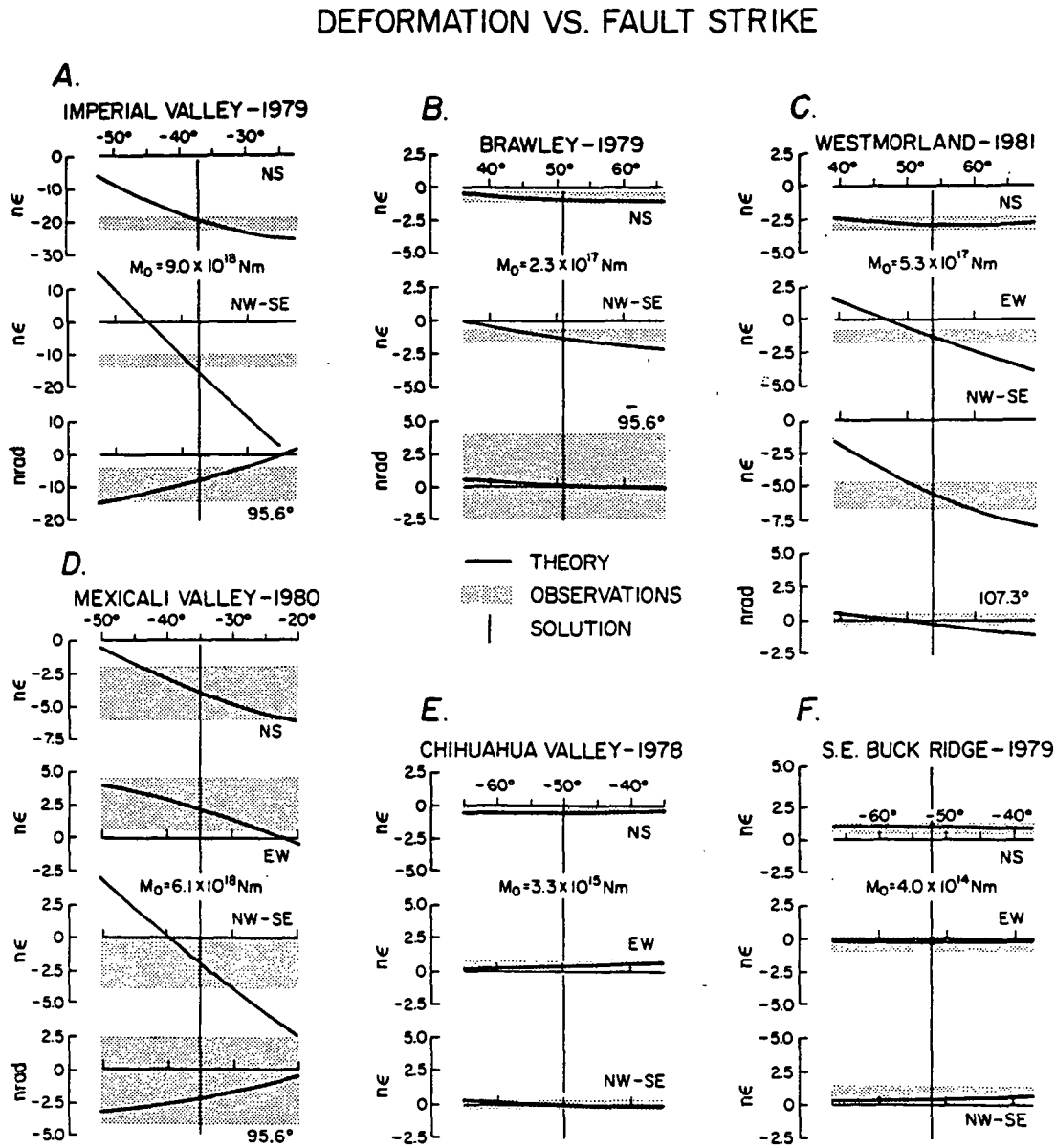

Figure 4.7. Relationship between theoretical coseismic strain-steps and the observations for the six best resolved earthquakes near PFO. Uncertainties of less than 20 percent in the theoretical seismic moment are exceptional, while the fault strike (whose dependence is shown here) is usually better constrained.

in this regime (Johnson, 1979), Johnson (personal communication, 1981) believes the faulting motion to be left-lateral with strikes of 51 degrees (Brawley) and 60 degrees (Westmorland) +-10 degrees, along nearly vertical fault planes. Right-lateral motion on conjugate faults is of course an alternate possiblility; at distances of 107 km and 95 km from these dislocations the PFO data cannot distinguish between the two models.

Although initially credited by Johnson and Hutton (1982) as a ML 5.8, the static observations of the Brawley earthquake indicate it was actually somewhat smaller than the Westmorland event; the USGS-CalTech catalog now lists the event at ML 5.5 (L.K. Hutton, personal communication, 1984). The strain signals evident in the later portion of Figure 4.5, NS -0.8 ne (compression given as negative strain) and NW-SE -1.2 ne are just resolvable above the measurement uncertainty (+-.5 ne) while the 50 m long fluid tiltmeter observation 0.0 +-4.0 nrad is not. Using Equation (4) and tentatively accepting the larger estimate of the local magnitude we fine deltaepsilonRMS = 1.6 ne, whereas the observations give deltaepsilonRMS = 1.0 ne. This relationship, of the theoretical value, based on the local magnitude, exceeding the measurements is quite unusual in this data set. All the more so when compared with the Westmorland earthquake records where this imbalance is reversed. The nearly identical pattern of deformation observed during the Westmorland event lends credence to the interpretation of these very small signals.

Only 12 km (~12 percent) closer to PFO than the Brawley earthquake, the Westmorland event induced sizeable static strains at the site. Figures 4.8 and 4.9 show the heavily filtered (~600 s) strainmeter and tiltmeter records for a period of four days before and after the event. In Figure 4.9 the predictable earth tide signals have been removed to produce a record which accentuates the coseismic static offsets. The lack of any obvious offset in the tilt record produced by the 535 m fluid tiltmeter (@ 107.3 degrees) should not be considered as erroneous for, as we shall see, this result is in agreement with the theoretical calculations. Table 4.2 lists the observations both for this and the Brawley events. The difference in distances cannot alone explain the smaller deformation from the Brawley earthquake; because the strain-steps attenuate as the third power of the ratio of hypocentral distances, this parameter can account for only a factor of 0.7 between these two events. The observations differ by roughly a factor of 0.3, indicating that the moment of the Brawley earthquake is about half that of the Westmorland, not slightly greater as suggested by the initial magnitude estimate.

Most of the short baselength instruments at the site did not produce any obvious coseismic strain-steps for either of these earthquakes. For all of these instruments the expected signals were smaller than the precision of the measurement. For those that did respond, the signals greatly exceeded the calculated values. Peak horizontal accelerations were estimated to be less than .05 m/s**2.

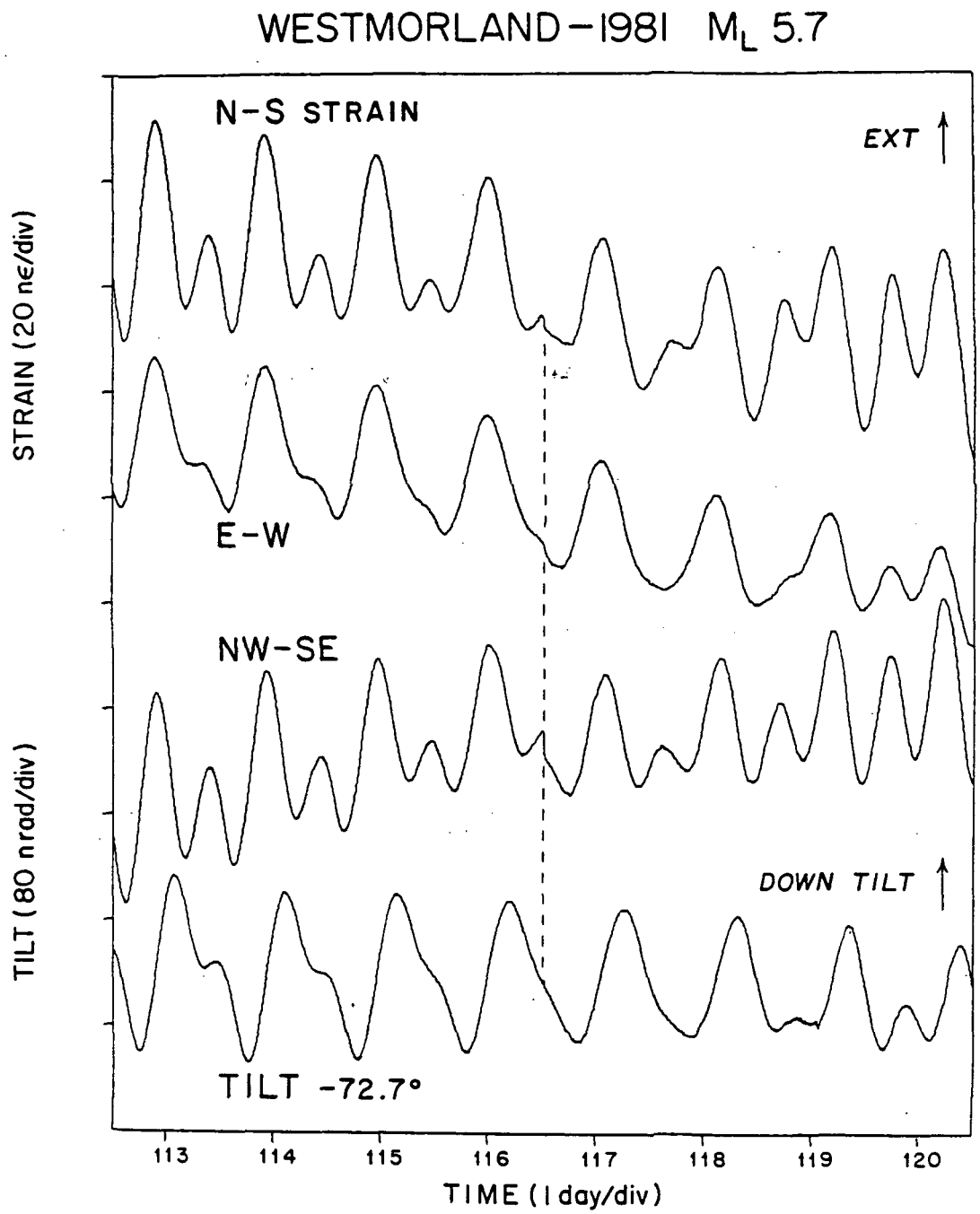

Figure 4.8. Filtered strain signals from the time of the 1981 Westmorland earthquake (#11).

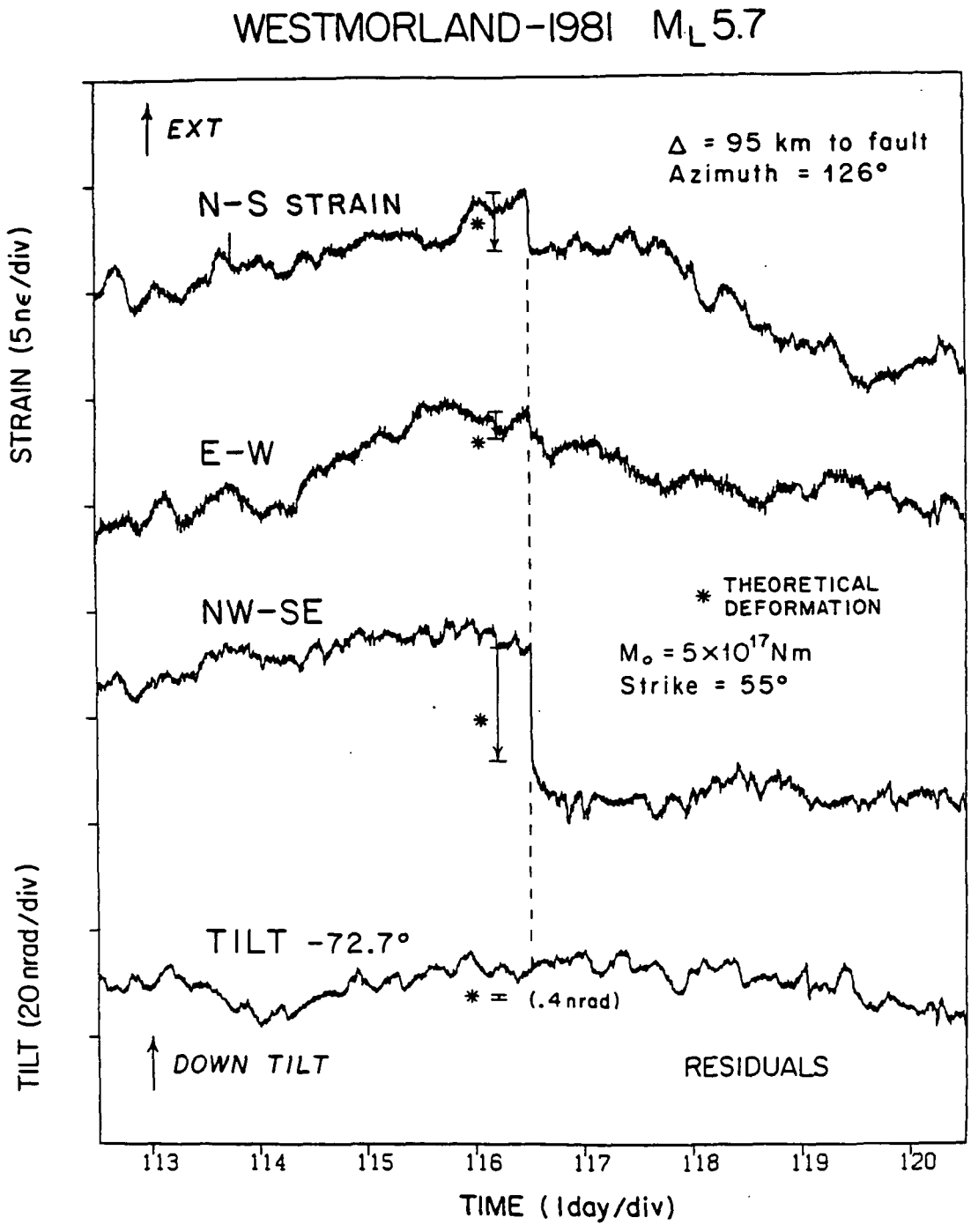

Figure 4.9. Identical to Figure 4.8, except the predictable tidal constituents have been removed and the scale changed to amplify the strain offsets. Arrows show the modeled static strains.

Selecting the subsurface fault parameter is much easier for these earthquakes because the observatory is in the far-field. For events of ML 5.7 we expect the fault length to be of the order of 10 km, while the distance to PFO is roughly 100 km. Because of this the faults may be assumed to be point source dislocations; the actual shape of the fault surface is immaterial. Using the fault strikes given earlier and relationship (3) to establish an initial estimate of the (geometric) moment, an attempt was made to fit the observations by trial and error, by systematically varying these two factors. Figures 4.9 and 4.7c and Table 4.2 present the results of this exercise for the Westmorland earthquake; the agreement between the modeled deformations and the observations is excellent. An equally good fit may be found for the Brawley earthquake (Table 4.2 and Figure 4.7b) but the small amplitude of the observations makes their interpretation less certain. The static moments determined are 2.3 x 10**17 Nm (51 degrees) for the Brawley 1979 earthquake and 5.3 x 10**17 Nm (54 degrees) for Westmorland 1981.

Missing from these estimates is an indication of how sensitive our solution is to changes in either the moment or fault strike. Once again in Figure 4.7, the observations (the dotted regions) are assumed to be fixed, while changing the calculated moment has the effect of scaling the vertical distance of the heavy solid line from the line of zero deformation, and changing the strike results in moving synchronously along those solid lines. From the figure we can judge that models of the Westmorland earthquake with either larger moments and smaller fault strike (e.g., Mo = 6.1 x 10**17 Nm, strike 51 degrees) or smaller moments with larger fault strike (e.g., Mo = 4.4 x 10**17 Nm, strike 57 degrees) would produce theoretical results compatible with our observations.

Jovanovich (1975) suggested a more formal inversion scheme, namely finding the model that minimizes the differences between the calculated and observed values in a least-squares sense:

$$\chi^2 = \sum_{i=1}^{n} \left(\frac{O_i - M_i}{E_i}\right)^2$$

where n is the number of observations, Mi the calculated model value for the i**th observation, and Oi the observations with standard error Ei. The actual inversion is complicated by the non-linear dependence of the calculated values Mi on the model parameters, particularly when the fault plane is not considered a point source (Pfluke and Stewart, 1973). Jovanovich suggested solving for some of the unknowns by non-linear least-squares and incrementally varying the rest in any combination that will reduce the misfit, as the practical solution to this problem. This we may do easily, as we have already selected for the Westmorland earthquake all but two of the model parameters (the moment and strike), so that the non-linear solution may be determined graphically. Figure 4.10 presents the values of Chi**2 for this calculation. From this we deduce that our original estimates for moment and strike are in fact the best fit to the observations.

This method should also yield a measure of the uncertainty in the model. However, in spite of the formal appearance of the results (Figure 4.10) it is

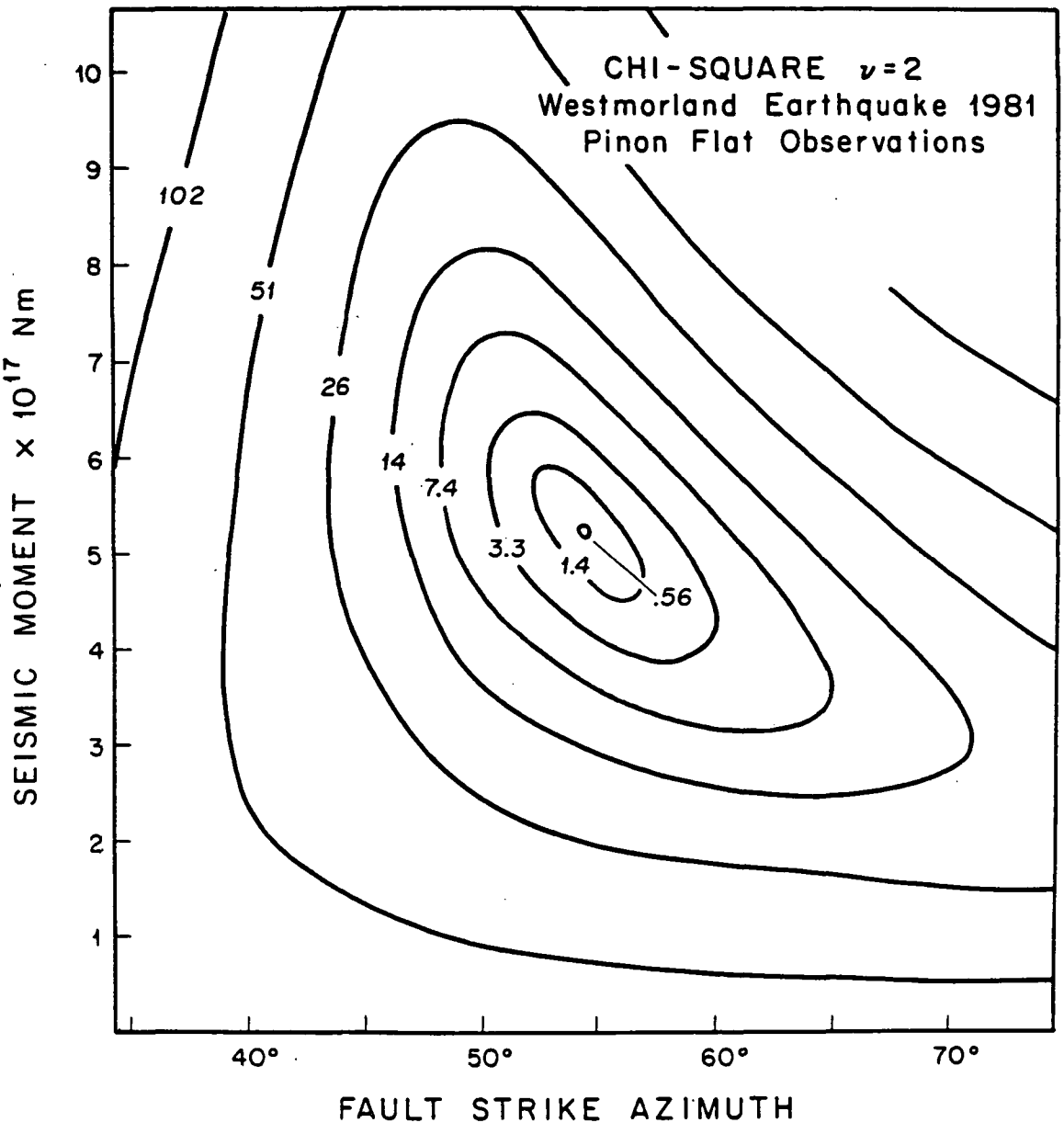

Figure 4.10. Chi-square contours of misfit between modeled fault strike and moment and the observations at PFO.

difficult to assign meaningful confidence limits to our solution. Normally we would be justified in describing the plotted distribution function as Chi-Square (Chi**2) with two degrees of freedom (nu = 4 (obs.) -2 (unknown)). In this case the 95 percent confidence limits would correspond to .05< Chi**2 < 7.4. However, the error estimates listed in Table 4.2 for the observations do not correspond to the true standard deviations associated with normal distributions: rather they are a somewhat pessimistic guess of the systemic error in the observations. This overestimate of the error Ei leads to an underestimate of Chi**2 and hence a poor constraint on the parameters. Choosing, somewhat arbitrarily, the expected value of Chi**2 for two degrees of freedom (Chi**2 < 1.4) as a more representative limit on the acceptable values in Figure 4.10 we find as our solution: Mo = 5.3 (+-0.6) x 10**17 Nm with a strike of 54.3 (+-2.) degrees

4.4.3 Mexicali Valley - 1980 (#10) -

Very similar to the Imperial Valley event, the ML 6.1 Mexicali Valley earthquake occurred on the Cerro Prieto fault in Northern Baja California, Mexico, on June 8, 1981. This 150 km long transform fault, one of a series of right stepping en-echelon faults at the south end of the San Andreas fault system, has been the site of four earthquakes greater than magnitude 6 since 1915 (Darby et al., 1984). Frez (1982) determined the focal mechanism to be right-lateral motion on a vertical fault plane with a strike of about -57 degrees. Initiating at a depth of 12 km, the rupture is generally taken to have progressed both northwestward some 25 km, nearly to the end of the mapped Cerro Prieto fault zone, and also 5 to 10 km to the southeast in the depth range of 4-14 km. This distribution is inferred from the pattern of aftershocks (Wong and Frez, 1982) and surface damage (Suarez et al., 1982), for unlike the Imperial Valley event, there is a marked absence of surface rupturing for the size and depth of the assumed fault surface (Anderson and Simons, 1982). As part of a study to synthesize the strong-motion acceleration records, Munguia-Orozco (1983) choose a fault length of 30 km, 10 km as the vertical extent, and an average strike of -44 degrees. With these parameters he obtained a seismic moment of 2.5 x 10**18 Nm, within a factor of two of the moment he estimates (4.5 x 10**18 Nm) from long-period surface-waves for both this event and the Imperial Valley earthquake. Using this latter value and Equation (3) we find the moment magnitude to be 6.4 in agreement with the surface-wave estimate (Anderson and Simons, 1982).

Figure 4.11 presents a heavily filtered version of the strain data with the tidal signal (amplitude ~20 ne) removed to accentuate the static offsets. The impulse-like response of these records was caused by saturation of the analog filters (RC = 500 sec); field charts show a simple offset in the seismic coda apparently coincident with the onset of the event. In fact for this event the field records allow a more reliable estimate of the very small steps. These values, listed in Table 4.2, are well below the resolution of the short baselength instruments. Despite the relative uncertainty in the observations the pattern of deformation can be matched quite well assuming

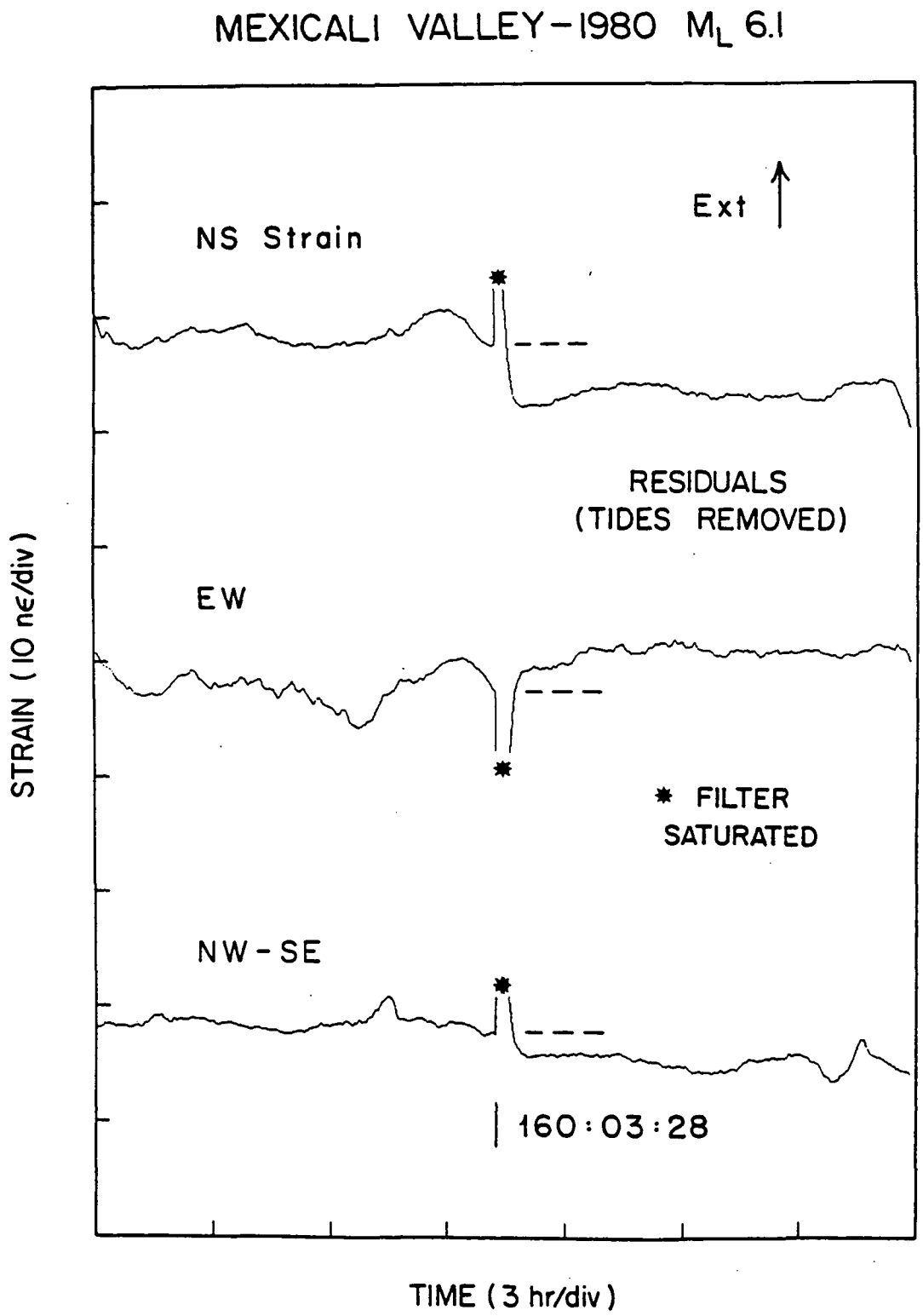

Figure 4.11. Residual strain signals (after subtracting tidal components) around the time of the 1980 Mexicali Valley earthquake (#10). The increase in uncertainty introduced by an extended time delay between estimates of the strain levels (caused here by amplifier saturation) is obvious.

.68 m of slip on a 10 x 30 km fault plane with a strike of -35 degrees. Once again taking 30 GPa as the average rigidity of the basement rocks, the seismic moment is found to be 6.1 x 10**18 Nm, or Mw = 6.5. But the unexpected result is the 9 degree difference between the Cerro Prieto fault strike and the model value. Drawing a line on the earth extending from the surface trace of the historic Cerro Prieto fault towards the northwest, it is found to pass about 13 km to the southwest of PFO, causing the model value of the near-radial NW-SE strain record to show extensional, or positive strain. The observed signal is, however, unmistakably compressional. This can only be true if the effective fault strike passes to the northeast of the observatory. Figure 4.7d makes this point more clearly. A modeled fault strike of -40.3 degrees would not show any radial strain at the observatory; only by rotating the fault clockwise from this azimuth may we account for the negative value of the NW-SE strain. The lack of any surficial manifestation of the Cerro Prieto fault immediately following the earthquake (Suarez et al., 1982) allows for this possibility but it seems unlikely that the whole fault should be twisted by this amount. Several alternatives are described in the Discussion section. Figure 4.12 presents the Chi**2 contours for this event, the only other earthquake for which we have all four measures of deformation.

4.4.4 Chihuahua Valley - 1978 (#3) and Homestead Valley - 1975 (#5) -

Both the Chihuahua Valley ML 4.4 and the Homestead Valley ML 5.2 earthquakes occurred well off the main trace of the major fault systems in southern California. The Chihuahua Valley event took place on June 5, 1978, about half way in between the Elsinore and San Jacinto Fault zones at a distance from PFO of 33 km; while the March 15, 1979, Homestead Valley earthquake sequence (ML 4.9, 5.2, 4.5, and 4.8) occurred on a fault system which roughly parallels the strike of the San Jacinto fault zone but is located some 20-40 km to the northeast of the San Andreas where it bends due westward. The distance to this event is 79 km, due north of the observatory. Because of the exceptional number of recordings of the Homestead Valley events several detailed descriptions are available. Hutton et al., (1980) report the focal mechanism for the largest earthquake in this brief sequence to be right-lateral slip on a near-vertical fault plane striking -4 degrees, some 15 degrees different (clockwise) from the strike of the mapped faults in the area. All four of the related events were aligned along an azimuth of roughly -12 degrees. Using a combination of both seismic and geodetic observations, Stein and Lisowski (1983) estimate the total moment for the sequence at 4.2 (+-.8) x 10**17 Nm, only 40 percent greater than the value given by Equation (3) for the dominant event based on its observed surface-wave magnitude (Ms 5.6). Because a fault plane solution was not available for the Chihuahua Valley earthquake it was assumed to have a mechanism in concert with the adjacent fault traces.

The resolution of the deformation from both the Chihuahua Valley and the main Homestead Valley events was very poor, particularly so for Chihuahua

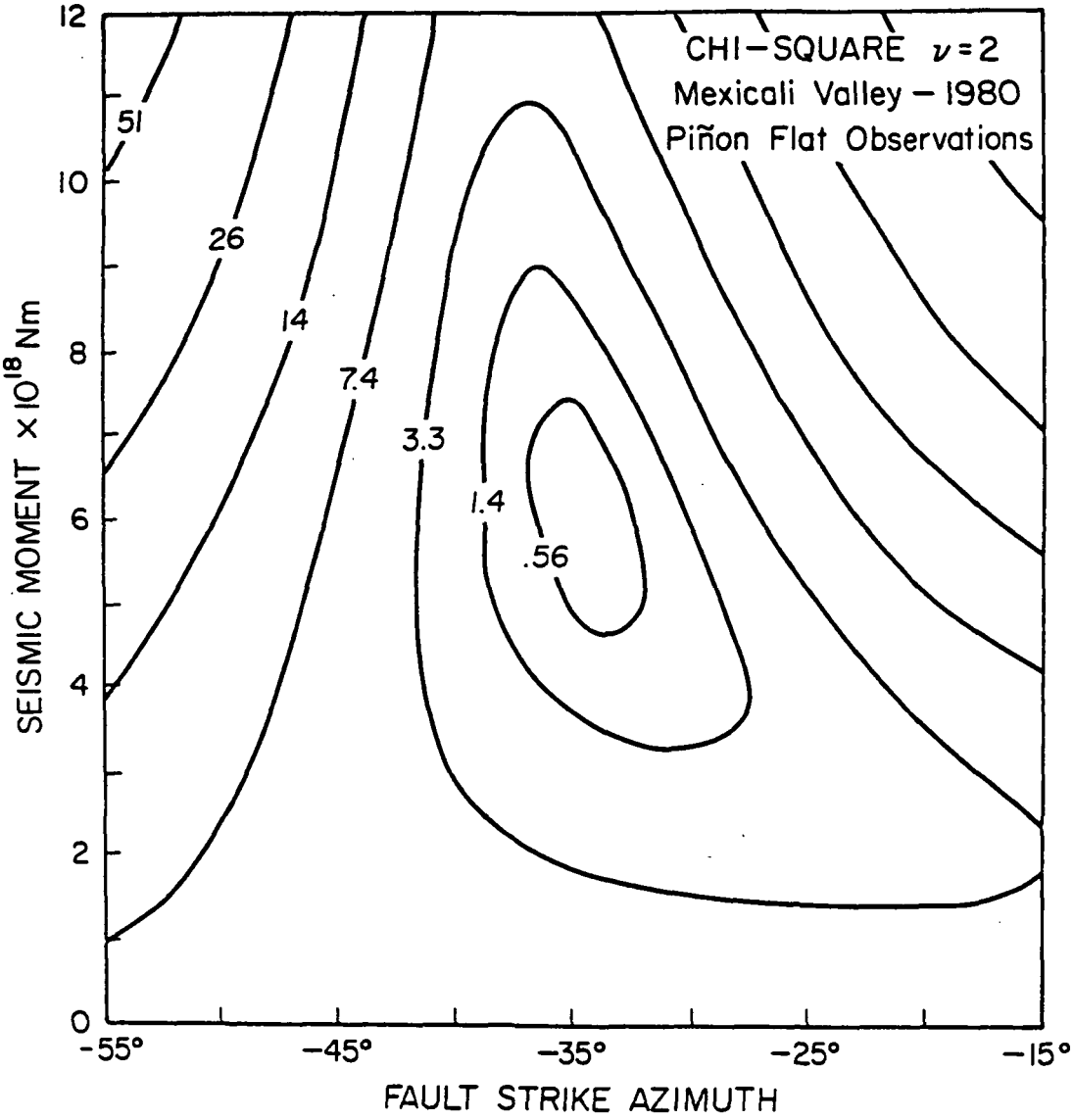

Figure 4.12. Chi-square contours of modeled strain values versus observations for the Mexicali Valley earthquake.

Valley. Even for the largest signal from this event (.4 ne) the uncertainty of the observation includes the possibility of zero deformation. Nevertheless, a simple model of the rupture as a .13 m right-lateral dislocation on a 1 km**2 surface, striking -52 degrees at a depth of 12 km, yields results practically identical to the observation (Table 4.2). The seismic moment for this imagined geometry is 3.3 x 10**15 Nm which compares favorably with its local magnitude of 4.4. Figure 4.7e indicates the sensitivity of the inferred parameters to the data.

Modeling of the Homestead Valley earthquake is even more speculative; while at least one component, the NS strainmeter, shows significant strain 2.0 (+-0.6) ne, the only other instrument in operation at the time (EW) does not. Ameliorating this situation somewhat is the far-field nature of the observations, here more than 10 fault lengths, which makes even a single observation valuable in understanding the source. A fault plane with moment 3.0 x 10**17 Nm (Mw 5.6) at an azimuth of -6 degrees is compatible with the two observations.

4.4.5 Lower Buck Ridge - 1976 (#2), SE Buck Ridge - 1979 (#4), and - Upper Buck Ridge - 1979 (#6)

Owing to their location the ML 4.3 Lower Buck Ridge earthquake of August 12, 1976, ML 4.2 SE Buck Ridge earthquake of February 12, 1979, and the ML 3.7 Upper Buck Ridge earthquake of July 2, 1979, are the smallest events to have caused measurable distortion at the site. At respective hypocentral spacing of only 21, 17, and 14 km these events are estimated to have caused accelerations of roughly 0.1 m/sec**2 at PFO, based on a modified form of Equation (5) which accounts for the high stress drop of the nearby earthquakes. Table 4.2 indicates that the short baselength instrument exhibited their, by now, expected unstable response to high accelerations. By comparison, the strainmeters signals are of the magnitude given by our RMS scaling law (4).

Because of their proximity, these events, like the three other earthquakes still to be described, are difficult to model. Their source areas are generally small and probably less regular than the larger and more distant events. Each of the six remaining earthquakes took place within 25 km of the observatory, typically with depth-to-epicental aspect ratios near unity. In this regime even slight variations in the fault strike or source depth can cause substantial changes in the calculated model values. While not considered for any of the observations it would be appropriate here to include yet another source parameter: the fault inclination (dip), for these events which are so nearly underfoot. The data, however, are inadequate for such an investigation.

Despite the disclaimer the observations from the SE Buck Ridge earthquake can be fit quite well (Table 4.2). This seems to be due to two

factors: the event was located at a depth of only 4 km (aspect ratio, .24) and it appears to be much smaller than stated in the seismic catalog. Figure 4.7f shows that the low resolution of the event places little restriction on the fault strike (choosen to be -52 degrees), but that the moment is clearly less than the 2 x 10**15 Nm associated with a ML 4.2 earthquake. Rather, the data demand a moment some five times smaller, 4 x 10**14 Nm, which corresponds to a magnitude of 3.7.

Coincidentally this is the same size as listed for the Upper Buck Ridge earthquake. Attempts to model this somewhat greater aspect ratio (.38) event were not successful. However, the size of the theoretical RMS strain-steps is just equal to the precision of the instrumentation (.4 ne). Similarly the one observation of the Lower Buck Ridge, 1976 earthquake is possibly insignificant (Table 4.2). With an aspect ratio of unity this early event (1978) caused two of the three laser strainmeters to fail by dislodging various unrestrained optical components.

4.4.6 Horse Canyon - 1975 (#1), Buck Ridge - 1980 (#9), and - Anza - 1982 (#12)

These final three events, Horse Canyon ML 4.8 of August 2, 1975, Buck Ridge ML 5.5 of February 25, 1980, and Anza ML 4.8 of June 15, 1982, are distinguished by their value toward understanding the tectonic stress at the southeast end of the Anza seismic gap and by the near complete failure of the instrumentation at PFO to record their deformation. Because of their significance they have been studied in depth by Hartzell and Brune (1979) and Frankel (1984). These reports provide an excellent opportunity to compare the near-field details of moderate size events as deduced by seismic and static means. However, the exceptional accelerations from the events cause both ill-resolved movement of the fiducial end-monuments and loss of optical alignment in the long baselength laser strainmeters.

From inception of PFO in 1971, the 1975 Horse Canyon earthquake (Delta = 13 km) was the first event with the potential to induce measurable deformation at the site. The calculated deformations of 11 ne (Table 4.2) are nearly equal to those recorded for the Imperial Valley earthquake. Of the four high resolution instruments which were in operation at that time, the three laser strainmeters and the superconducting gravimeter of Goodkind and Warburton (Goodkind, 1979), none of them survived the impact. Only the NS strainmeter returned to operation without realignment of the components. Even if all the strainmeters had functioned properly, interpretation of their records would have been difficult. Signals from the tiltmeters attached to the sides of the end-monuments showed tremendous tilts, in excess of 2 microradians (Table 4.2), and most likely underwent substantial lateral displacements. Without a proper estimate of this monument motion the change in distance recorded by a laser interferometer can not be corrected to deduce the earth's strain.

Hartzell and Brune (1979) were able to estimate many of the source parameters using a collection of near-field accelerometer records, recordings of aftershocks from a small portable seismometer array, and a more distant observation of the surface waves. One of the Caltech accelerometers, located at PFO, showed peak horizontal signals of nearly .8 m/s**2 (~8 percent g) and explains why the rather delicate sensors at the site did not operate continuously throughout the event. Analysis of the main shock, which occured at a depth of 13 km, and the distribution of aftershocks suggests that stress relief took place in two stages: first growing quickly over a 1 km**2 core region (the asperity) then progressing much more slowly (10 s) over a total area of 4 km**2. Only a small fraction (6.5 x 10**15 Nm) of the overall seismic moment is attributed to the initial rupturing of the high stress-drop (22.5 MPa) asperity. Hartzell and Brune conclude that the total moment was about 3 x 10**16 Nm, with an average dislocation of 25 cm and stress-drop of 9 MPa. Frankel (1984), using a more complete set of Love-wave recordings, determined the long-period moment to be 1.9 (+-.8) x 10**16 Nm. I have adopted this value for the calculated factors in Table 4.2.

Although the instruments at PFO did not produce any record of the coseismic deformation, their normal behavior immediately prior to the event supports the faulting model of Hartzell and Brune. They characterize the earthquake as having a body-wave moment estimate some 4-6 times smaller than the surface-wave value, indicating both a small high frequency generating region and a 4-6 times larger, slowly deforming, surface. Because of the small size of the source, this cannot be attributed to saturation of of the short-period waves which occurs when the source region exceeds ~10 km. The order of these events is important. It has been suggested for some deep earthquakes, (e.g., Kanamori and Cipar, 1974; Gilbert and Dziewonski, 1975; and Sacks et al., 1978) that the events are preceded by a very long-period deformation. The strain data at PFO demand the opposite relationship for this near-surface strike slip event. Sampled at a 2 s interval, none of the strainmeters show any unusual deformation greater than 10**-10 e in the minute before the earthquake, nor do they suggest any longer term precursor (Berger and Wyatt, 1978, Hartzell and Brune, 1979).

A total of only three useful deformation measurements were obtained for both the Buck Ridge earthquake, located 13 km south-southwest at a depth of 14 km, and the recent Anza event, situated 20 km to the west-southwest of PFO at a depth of 12 km. Again the high peak seismic accelerations, measured by the U.S. Geological Survey strong-motion accelerographs as 1.4 m/s**2 and .53 m/s**2, were the problem. For the Buck Ridge event, the end-monument tiltmeters alone indicate the need for strainmeter corrections which are more than an order of magnitude greater than the expected strains. Again, any simultaneous displacement which may have occured at the base of the columns adds noise to the strain measurements. Both the NS and EW strainmeters operated throughout the Buck Ridge earthquake, but implausibly large signals produced by the NS component indicate that it miscounted interference fringes sometime during the heavy ground shaking. Indeed even the alignment of the laser beam between the ends of the strainmeter which must be aligned within +-10**-5 radians is an issue for this event. The short fluid tiltmeter

record provides the only reliable constraint on the coseismic deformation. All three of the strainmeters, as well as the extended (535 m) fluid tiltmeter, produced records for the Anza 1980 event. However, in this case only the NW-SE strainmeter and the tiltmeter ran continuously. Temporarily both the NS and EW instruments misbehaved which, for measurements not based on an absolute length measurement, is catastrophic. Signals from the end-monument tiltmeters show little or no correction was needed for the stain measurements, in keeping with the lesser acceleration experienced at the site. Nevertheless the 12 short baselength tilt records for this event show signals ranging from 10 to 600 nrad (deltaepsilonRMS = 350 nrad), while the expected value is about 10 nrad.

Given (1983) finds the focal mechanism of the 1980 Buck Ridge earthquake to have a strike of -53 degrees on the steeply northeast dipping (~80 degrees) San Jacinto fault plane adjacent to PFO. Both this event and the coplanar 1975 Horse Canyon earthquake (~5 km distant) are characterized as high stress-drop events, with relatively few aftershocks occurring over a small area. Sanders and Kanamori (1984) report an aftershock zone some 3 km long and 6 km high, while Frankel (1984) estimates a source radius of 990 m, based on the displacement pulses recorded by near-field accelerometers, and a radius of 1250 m, based on the pattern of aftershocks. When compared with the source dimensions for other ML 5.5 southern California earthquakes (Thatcher and Hanks, 1973) both these estimates are found to be extraordinarily small. Similarly the seismic moment estimates are unusual. Using the displacement records, and a model of both the radiation pattern and surrounding medium, Frankel calculates the moment to be 2.5 +-.7 x 10**16 Nm. Matching synthetic far-field 30-40 s love waves to four other recordings of the event he finds the moment to be 5.6 +-2.6 x 10**16 Nm. This discrepancy is attributed to the heterogeneity along the rupture surface such that the 0.5-1.0 s, short-period, moment represents the seismic radiation from localized areas of high strength, whereas the long period energy is produced by the larger rupture surface. Nevertheless, even the bigger moment corresponds to only a ML 5.2 event (Equation 3). The single deformation recording at PFO suggests the overall static moment may be a factor of two larger (ML = 5.4). Accepting the source parameters as deduced from the seismic records, the theoretical deformation pattern for the tilt component at an azimuth of 95.6 degrees shows a broad lobe centered at PFO. Scaling the seismic moment to fit this observation gives a value of 1.1 x 10**17 Nm. Considering the uncertainty of the observation and model this estimate can not be given much credence but it does suggest slightly greater deformation than any of the other methods, more in keeping with the local magnitude of 5.5.

In contrast to the Buck Ridge earthquake, the two recordings of site deformation for the Anza 1982 earthquake show good agreement with the surface-wave estimate of the seismic moment. Frankel reports a moment of 1.1 x 10**16 Nm from the integrated strong-motion recordings and a long-period value of 2.3 x 10**16 Nm. C. Johnson (personal communication, 1982) found a well constrained source mechanism of right-lateral faulting on a nearly vertical surface trending -28 degrees at a depth of 12 km. The hypocenters

of the main shock and largest aftershocks indicate a similar fault strike of -26 degrees, much different from trend of -53 degrees for the overall San Jacinto fault zone in this area (Sanders and Kanamori, 1984). Most significantly the rupture did not take place along any mapped fault trace. Frankel gives the source radius as 780 m while Sanders and Kanamori found the aftershock regime to be limited to a volume 2.5 km long, 3 km high, and 1.5 km wide. They did not find any activity on the San Jacinto fault even though it was only 4 km distant. Using this information, model values of the NW-SE strain and the tilt at 107.3 degrees were calculated for PFO. The observed NW-SE deformation of 7.0 +-1.0 ne is well matched by the model value of 7.8 ne assuming a moment of 2.3 x 10**11 Nm and strike of -28 degrees; the tilt agreement is not as good at -3.2 +-1.0 nrad and -0.8 nrad theoretically. Because the NW-SE measurement is located in a lobe of uniform distortion while the tilt is very near a node, a simple 8 degree rotation of the fault strike brings the modeled tilt into alignment with the observation without adversely affecting the strain. Whether this average rupture orientation is correct or merely reflects the highly unstable nature of this underdetermined inversion problem cannot be resolved with only these two field observations. The strain measurement suggest the static moment is, for this event, no greater than the long-period surface-wave estimate.

Of the other signals recorded at PFO during the Anza earthquake, one is particularly interesting as it bears on the interpretation of water well observations. Figure 4.13 presents the well level record in borehole CIC around the time of the event (data provided by R. Moyle, USGS/WRD, 1982). Below the top trace are the record of the water height with the volumetric earth tides removed, the barometric correction, and finally the residual series showing the offset at the time of the event. The existence of the tidal signal in the well, which may be considered its response to changing bulk porosity of the rock near the borehole in the presence of tidal strains (Bredehoeft, 1967; Van Der Kamp and Gale, 1982; Bower, 1983); provides a means of calibrating the water well height in terms of volumetric or areal strain. Based on the tidal record of this well and the areal strain from the laser strainmeters (NS + EW) we find a sensitivity of -1.0 microe/m. Unfortunately better time resolution of the original graphic recordings is not possible so we can not isolate the strictly coseismic response of the well, but considering the total change of water level within 24 hours of the earthquake (+ .03 m) we calculate an equivalent areal strain of -30 ne. This value is an order of magnitude larger than the modeled areal strain of -1 ne and suggests that this particular well should be classified as a short-baselength instrument: subject to the influence of local site effects.

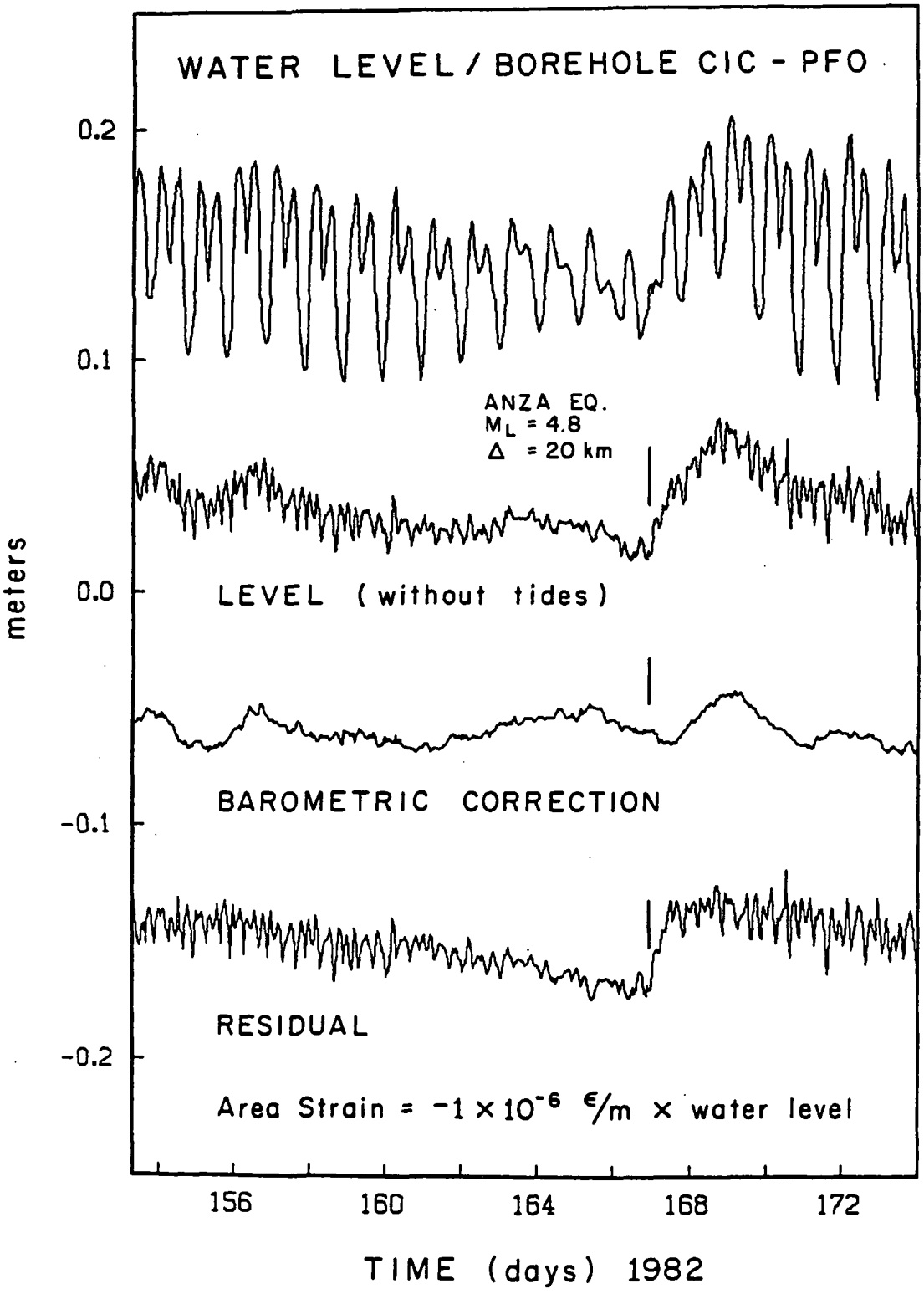

Figure 4.13. Water level records corrected for tidal response and barometric effects for a week before, and a few days after, the 1982 Anza earthquake (#12).

4.5 Discussion

4.5.1 Seismic vs. Static Moment -

Of the features common to the well-resolved earthquakes, most conspicuous is the tendency toward static moments greater than those determined by seismic means. Physically there are many possible explanations for this observation: poor seismic resolution of the very low frequency dislocations, subseismic deformation over a broad region (perhaps extending into the lithosphere and including pre- and post seismic slip), somewhat delayed sympathetic slip on adjacent fault systems, and low rigidity in the receiver region. The distinction between these first two items is blurred; only for the very largest events can the lowest-order mode of the earth (~3200 s) be used for inferring something of the source mechanism. For most moderate events the seismic signal vanishes into the background earth noise at periods of 500 s or less. Any deformation which occurs at periods longer than this may therefore be considered subseismic (i.e., not due to traveling waves). Of course there is one more reason why the deformation derived moment estimates might differ from the seismic values: an incorrect scale factor in our modeling (e.g., the R**-3 dependence in Equation 2). The overall scatter of the data, except for the bigger events, suggests otherwise. Fortunately for two of these events we have geodetic evidence indicating yet greater moments. Starting with the Imperial Valley earthquake, we shall address each of these points in the context of the larger events and then proceed to a more general discussion of the observations from PFO.

Reminiscent of the frequency imposed limitations of various seismic magnitude scales (Kanamori, 1983), estimates of the moment tend to increase as the modeled radiation frequency decreases. Generally speaking, seismic energy at a given period is related to the source behavior at that same period. To learn all we might wish about the static (zero-frequency) moment would require the examination of very long periods signals indeed. Practically, consistent results are obtained from periods that greatly exceed the nominal rupturing time (~source length/shear velocity). Initially, Kanamori and Regan (1982) reported a seismic moment of 6 x 10**18 Nm for the Imperial Valley earthquake based on long-period Love and Rayleigh waves (~120 s). This was ammended to 7 x 10**18 Nm using 200-250 s Rayleigh-wave phases, with an indication of larger moments at the lowest frequencies resolved (9 x 10**18 Nm at 256 s, H. Kanamori, personal communication, 1981). They also discussed the rather unusual circumstance, for large California earthquakes, of the local magnitude being roughly equal to the moment magnitude. Typically it is smaller, as ML is an earthquake measure at high frequencies and tends to underestimate the earthquake size for magnitudes greater than 6. Using strong-motion data Archuleta (1984) was able to construct a rupture model which fit these short-period observations with a moment of 6.7 x 10**18 Nm, similar to the value reported by Hartzell and Heaton (1983).

Surprisingly, an inverse theory approach yielded a moment of 9.13 x10**18 Nm for this same data set (Olson and Apsel, 1982). In view of these refined estimates there is little cause to question the value deduced from the strain data (9 x 10**18 Nm), unless the NS strain observation, because of its position in the deformation pattern, is preferentially choosen as the best indicator of the moment; scaling the moment to fit this observation gives 1.0 (+-.1) x 10**19 Nm.

Figure 4.14 shows why we might expect the static moment to be greater. Removing from 10 days of observations the coseismic offsets for both the Imperial Valley and Brawley earthquakes, along with the tidal signals, yields a very noisy record showing apparent accelerated postseismic deformation (Figure 4.14, lower half). A roughly exponential decay, with a time constant of only 14 hours, is evident in the residual NS strain, while the NW-SE is much noisier and hence less suggestive. Supporting the supposition that they are real is the fact that the exponentials are in the same sense and relative proportion (~30 percent) as the coseismic offsets. (Estimates of the amplitudes are given in Table 4.2.) It seems quite possible that these signals are an expression of accomodation in the lower crust (below 10 km) caused by the dislocation in the material above. If so, some fraction of this would occur throughout the seismic event and would be better resolved by the strainmeters. The cumulative strains suggest that the overall moment for the Imperial Valley earthquake, within one day of the event, may be as large as 1.2 x 10**19 Nm. Over periods of months Snay et al., (1982) use geodetic data to determine the dislocation on the Imperial Fault for a hypothetical fault plane extending from the surface to 100 km. They obtain values of roughly .4 m over the entire surface, sufficient to explain a moment of 6 x 10**19 Nm, although they point to the discussion of Prescott and Nur (1981) in suggesting that the deeper deformation is unlikely to occur as slip along well defined fault planes below a depth of 20 km in California.

Because of the size of these exponential strain signals, they cannot alone be explained by the postseismic logarithmic slip (U = .11 m, tau = 1.75 days) found by Langbein et al., (1983) at the north end of the Imperial fault--slip which appears to be limited to the upper 5 km. The displacement, fault plane area, and presumed rigidity of this zone are too small and too slow to have caused detectable deformation at PFO. Using a set of observations very similar to those employed by Langbein et al., Smith and Wyss (1968) reported a corresponding logarthmic decay of surface slip following the 1966 Parkfield, California, earthquake. Based on an assumption of only .103 m of coseismic fault displacement between depths of .5 to 14 km, they concluded that the cumulative surface displacement, .21 m after one year, meant that at least half of the postseismic deformation was aseismic fault slippage. However, more recent studies by Archuleta and Day (1980) credit the initial dislocation as ~.43 m of offset on a fault in the depth interval of 3 to 9 km. In this case all of the observed surface displacement for the Parkfield event may be attributed to stress-induced viscous shearing, or viscoelastic deformation, in the shallow low-strength crust--a model that fits the Imperial Valley data equally well.

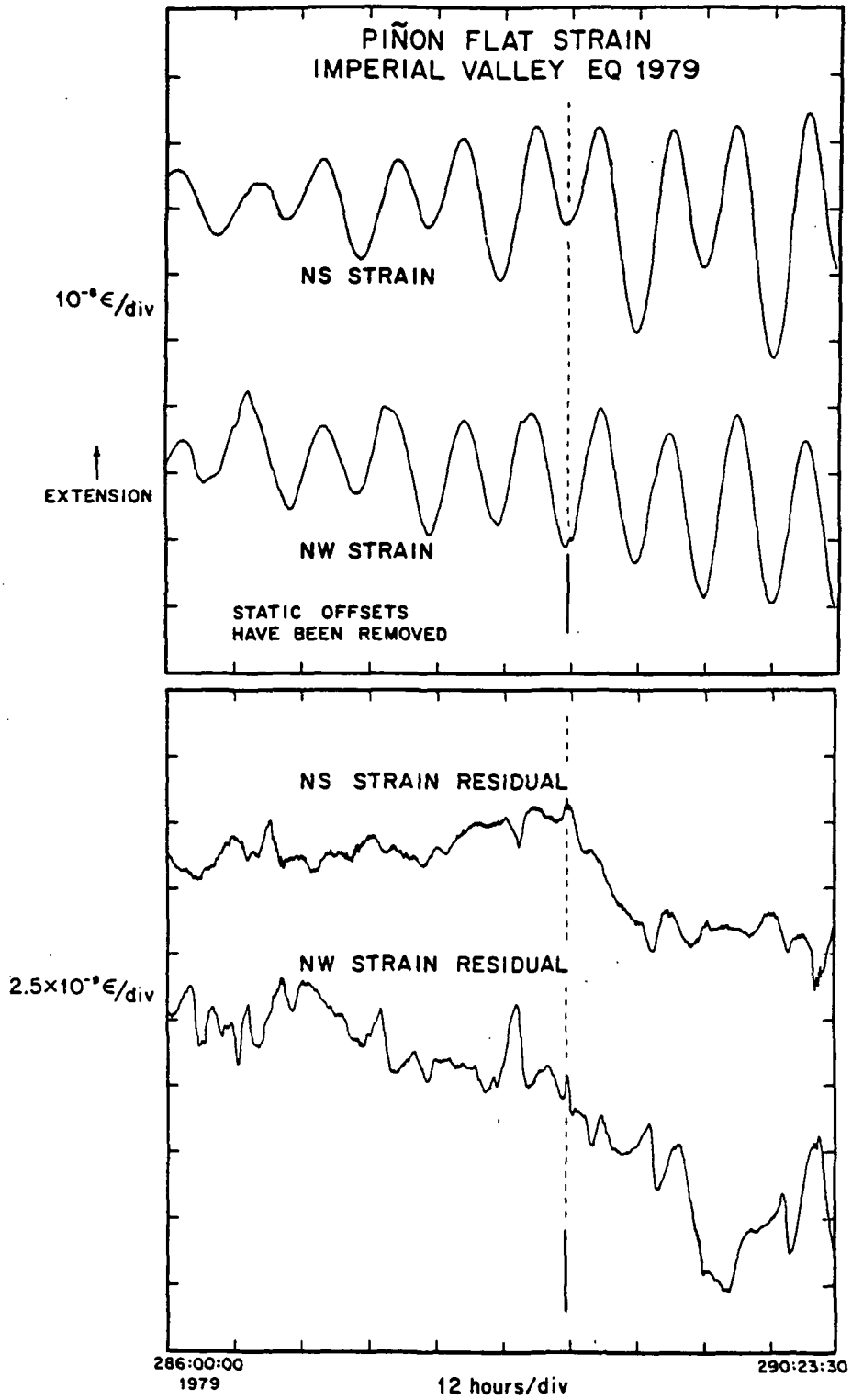

Figure 4.14. Strain records and residual strain signals (with both the tidal and coseismic offsets signals removed) for several days before and after the 1979 Imperial Valley earthquake. A suggestion of postseismic deformation is evident.

Coseismic slip, or creep, on adjacent faults is another mechanism which could lead to an increased static moment. Triggered slip was reported on 20 km-long stretches of both the Superstition Hills fault, approximately 20 km NW of the Imperial fault (Fuis et al., 1982), and the southern end of the San Andreas fault more than 90 km to the NNW (Sieh, 1982). Because the average displacements for both of these amounted to only 5 mm, and the evidence suggests that were limited to the surface layers (~< 100 m depth) the effective moment for these events may be estimated to be 3 x 10**14 Nm. Using Equation 3, along with their respective distances to PFO of 95 and 55 km, gives strains a factor of 300 and 50 smaller than can be resolved. Unless the triggered slip on the much closer San Andreas fault actually extended beyond 5 km, the observed slip could not have produced deformations of order .4 ne at PFO. Such extensive aseismic deformation seems unlikely, but Sieh (1982) discusses the possibility in light of the similar surface behavior following the 1968 ML 6.4 Borrego Mountain earthquake.

Although properly part of the main event, we have not yet considered the substantial dislocation which took place on the Brawley fault at the time of the Imperial Valley earthquake. The justification for this is that its contribution to the overall moment and the strain field at PFO was small. Archuleta (1984) estimates the length of this NS trending fault as 10 km, with depth 8 km, and moment 2.7 x 10**17 Nm. Located at roughly the same distance to PFO as the Imperial fault, this moment, which is only 4 percent of the total, is calculated to cause only 4 percent changes in the theoretical strains. It is because these signals were calculated to be no larger than the uncertainty of the measurements at the observatory (~1 ne) that this dislocation was not included in the original modeling.

The final consideration, that of low receiver rigidity as a cause of amplified distortion at PFO, may be ruled out on several accounts. Geologically, the site is situated on competent crystalline rock, part of the southern California Batholith of late Mesozoic age (Parcel, 1981). On the time scale of millions of years this material has been transported comparatively unscathed, indicating its relative strength. This is to be contrasted with the sedimentary layers and metasedimentary basement in the Imperial Valley (Fuis, 1984), the site of the larger earthquakes during this period. On a historic scale the pattern of seismicity too suggests that PFO, and indeed all of the San Jacinto and Santa Rosa mountains, as well as the northwest part of the Imperial Valley, behave as a cohesive structural block. There are very few events internal to this unit, in sharp contrast to the scatter-plot character of the earthquake locations in the surrounding area (Allen, 1981). Further, the distribution of geodetic distortion across this area is consistent with a simple model of slip at depth along both the San Jacinto and San Andreas faults, with a minimum of deformation in between (King and Savage, 1983). All this is not meant to infer that the block is completely rigid; rather the best evidence indicates a nearly homogeneous elastic crust. Tidal analyses (Agnew, 1979), and indeed the coseismic deformation data itself, indicate the excellent agreement between our theoretical notions and the observations. What little geologic and topographic alteration there is (~10 percent, Berger and Beaumont, 1976)

suggests that the observed deformations should be sligthly less than the regional strain; interpretation of the coseismic strains at PFO should yield a lower bound on the true moment.

Though situated nearly 200 km from PFO the Mexicali Valley earthquake of 1980 caused measurable strains at the site. This could not have been true if the local magnitude (6.1) were indicative of its true size. Anderson and Simons (1982) report a surface-wave magnitude of 6.4 more in-line with events such as the 1940 Imperial Valley earthquake where the 6.7 local magnitude was substantially less than the surface-wave magnitude of 7.1 (Richter, 1958). Both the surface-wave value and the work of Munguia-Orozco (1983) give a moment of 4.5 x 10**18 Nm; the strain data imply 6.1 (+-1.5) 10**18 Nm. While not excluding the seismic estimate the PFO observations suggest a moment some 35 percent larger, an excess nearly equal to that obtained for the Imperial Valley earthquake of 1979 (~30 percent). The similarity of the tectonic setting of these two events, and the potential for accelerated slip in the approximately 5 km of sedimentary material above the modeled fault plane are both good reasons to believe the greater value. As mentioned earlier for the larger events, without a high dynamic-range filter (or very fast sampling) we must wait for the passage of the seismic coda to establish the static offset. This delay, amounting to nearly 1200 s here, allows post-seismic slip to be a significant component of the moment estimate. There was very little evidence of sympathetic slip on adjacent faults in the locale. Indeed a thorough reconnaissance did not turn-up any tectonic features which could be related to the main trace of the Cerro Prieto fault (Suarez et al., 1982).

Geodetic observations from the Westmorland earthquake provide the best evidence to support the generally larger moment estimates from the strain data, while the Brawley earthquake shows a similar relationship. Resorting to Equation (3) the local magnitude of the Westmorland event (5.7) gives an equivalent moment of 3.5 x 10**17 Nm, about 30 percent less than deduced from the strain observations. For Brawley we have 1.8 x 10**17 Nm (ML 5.5) compared to the strain derived moment of 2.3 x 10**17 Nm. Unfortunately a search of the recent literature did not yield surface-wave estimates for either of these events. Without the more comparable values, at issue here is not only the difference between static and seismic methods but the applicablility of Equation (3), as seismic events approach local magnitude 6. The question of whether there was unaccounted subseismic deformation therefore divides between the very high frequencies used for determining ML (~> 1. Hz) and all lower ones. Because the fault sizes are thought to be about 10 km and the shear-wave (maximum rupture) velocity in the Imperial Valley only 1.8-3.2 km/sec (Archuleta, 1982b), we should expect greater moment estimates from any technique which relies on lower frequencies. J. Savage (personal communication, 1982) reports just such a value for the Westmorland earthquake. Using changes in the geodetic line-lengths which cross the conjugate fault zone at the north end of the Imperial fault, he determines a moment of 1.3 x 10**18 Nm, on a fault plane taken to be 10 km long, between depths of 3 to 10 km, and striking 54 degrees. The left-lateral slip on this surface is calculated to be 0.6 (+-0.1) m. This

static moment estimate is more than a factor of two greater than the PFO coseismic reckoning (5.3 x 10**17 Nm). Salient to our discussion, the geodetic measurements were recorded more than 80 days before, and 10 days after, the earthquake and might easily include longer-term deformation on both this fault and ones nearby. Interestingly, the most sensitive strain record for this event (NW) shows, in Figure 4.9, an indication of continued deformation in the 4-6 hours after the earthquake.

Sharp et al., (1982a) found right-lateral triggered slip on sections of both the Imperial and Superstition Hills faults in response to the Westmorland earthquake. While they did not locate any clear evidence of surface rupturing in the epicentral region the maximum horizontal displacements on the triggered faults were 8 and 14 mm respectively, over fault lengths of roughly 16 km. The overall pattern of movement was similar to that which has occurred several times in the last two decades. Because these dislocations were located some 20 km to southeast and southwest of the Westmorland main event they are slightly more distant from the observatory, and thus less likely to produce detectable deformation for the same size moment. Assuming for each a fault area roughly equal to that given for the earthquake (70 km**2), an average slip equal to the maximum observed, and ignoring the difference in distances, the maximum moment is calculated to be 3 x 10**16 Nm and the deformation at PFO only .06 of the total observed. Because this contribution is less than could be resolved, triggered slip does not appear to be adequate to explain the difference between the seismic and static moments for the Westmorland event.

Details of the Brawley event are harder to unscramble. Following so closely in the wake of the Imperial Valley earthquake (8 hours) evidence of possible subseismic deformation or after-slip on adjacent faults has already been discussed as part of the much larger event. Indeed Heaton et al., (1983) were unable to establish a cause-and-effect relationship between this event and the extensive nearby ground failure. There seems to be little doubt that this earthquake was smaller than the comparable Westmorland event. Adopting the lower of the two reported local magnitudes (5.5), this earthquake too shows a static moment about 30 percent larger than magnitude-based value.

For all four events located the the Imperial/Mexicali Valley province we arrive at static moment estimates which indicate greater deformation than communicated by seismic energy. What little evidence we have for the next smaller earthquakes, Homestead Valley 1979 and Buck Ridge 1980, shows the same association in a setting antithetic to the spreading-center environment. For Homestead Valley we find the surface-wave magnitude greatly exceeds the local magnitude and gives a moment of 3 x 10**17 Nm which can be fit by the strain data, though a larger moment would do slightly better. Situated in highly stressed granitic material, the static moment of the very close-by Buck Ridge event is crudely calculated to be 1.1 x 10**17 Nm while the surface-wave value is 5.6 x 10**16 Nm (Frankel, 1984). This same pattern is often reported in studies of coseismic deformation (Mavko, 1981; or, for example, Kanamori, 1973; King et al., 1981; Sacks et al., 1981; and Stein

and Lisowski, 1983). Although, as Mikumo (1973) points out for the exceptionally well recorded Central Gifu, Japan, earthquake of 1969, the suseptibility of observatory-based recordings to a number of local effects makes their interpretation difficult. Canitez and Toksoz (1972) for the 1971 San Fernando earthquake and Dunbar et al., (1980) for the 1952 Kern County event found static moment values nearly identical to the surface-wave estimates.

4.5.2 deltaepsilonRMS vs Distance and Moment -

Because all of these strain data are at one epicentral distance for a given earthquake they are inadequate to either prove or disprove the strong radial dependence given by Equations (3) and (4)--where only a 15 percent error in the epicentral distance translates to a 50 percent error in the moment. They are, however, substantially within the stated uncertainty of a factor of two. Where they do disagree substantially there is often sufficient reason to question the reported magnitude of the event. Indeed the entire preceeding section is an example of such an excercise. Fortunately there have been two excellent data sets (Japanese Network of Crustal Movement Observatories, 1970, and Mc Garr et al., 1982) which substantiate our suposition. And, significantly, the twelve events described here are the only ones for which the properly-functioning long-base instruments at PFO have shown deformation.

On the other hand, if our coseismic modeling were in error we should expect to see a systematic variation in the ratio of the observed-to-theoretical RMS deformation as a function of distance. Plotted in Figure 4.2, as a function of both reported moment magnitude and distance, are those events recorded at PFO by at least two instruments. Near each point is the event number and its ratio of the RMS strain observations to the value given by (4). Viewed from the perspective of the distance axis, there is a suggestion of radial dependence. This is especially so if the Mw 5.6 (#5), 5.1 (#9), and 4.8 (#12) events, for which there are only two field measurements, are removed. However, these remaining ratios may equally well be interpreted as a function of the seismic moment. Based on the evidence of substantial subseismic deformation for the larger events this latter effect is considered more likely and it seems unnecessary to postulate other than R**-3 dependence. Moreover, all seven of the twelve events for which there are three or more observatory measurements agree with Equation (4) within its uncertainty. Recalling that the RMS relationship was developed assuming five independent measurements of deformation, the agreement here tends to substantiate the validity of the equation.

4.5.3 Pattern of Deformation -

The least ambiguous feature of the strain measurements at PFO is their pattern: meaning their relative magnitude and sign. It was this consistency that first motivated a thorough review of the observations. Much of the modeling described in the Observations section is based on resolving the azimuthal relationship of the fault strike to the observatory using the pattern of the observations.

In a coordinate system tied to the fault strike, a gradual rotation of the earthquake has the effect not only of changing the position of the observatory, but also the effective azimuth of a particular observation. For example, the contours of Figure 4.6 represent the theoretical strain at a fixed absolute azimuth throughout the quadrant, with the fault azimuth fixed as well. Selecting a different fault strike requires identifying the new observatory location and recalculating this figure for the (apparently) new orientation of the sensor. Fortunately this latter effect is not a major factor for small rotations as can be realized by considering how little a strain change would be expected for a few degree twist of the sensor.

By chance, the contour diagrams for the choosen fault strike of the 1980 Mexicali Valley earthquake (-35 degrees) looks nearly identical to those presented in Figure 4.6 for the Imperial Valley event. This choice disagrees considerably from the accepted orientation of this fault, - 44 degrees, at its southern end near the Gulf of California (Biehler, 1964). Referring to Figure 4.6, we can see that a very minor anti-clockwise rotation of the fault, back towards its historic axis, will cause the theoretical NW-SE strain (at 135 degrees) to show expansional (positive) strain, in contradiction with the observation. Yet the geometrical relationship of the fault and observatory demands that the site be situated in the positive-strain quadrant.

This observation, the pattern of aftershocks, and the conspicuous similarity of the Imperial and Cerro Prieto fault zones, leads to the postulation of a secondary north-south trending fault near the northwest end of the Cerro Prieto fault. As reported by Wong and Frez (1982), the aftershocks of the Mexicali Valley earthquake appear to occupy two regions: one, a clustering of events about 12 km northwest of the focal point along the accepted fault strike, and second, a spread-out sequence heading roughly north from about this location toward the end of the Imperial fault. It is unfortunate that due to instrumental uncertainties they could not establish the focal mechanisms for these events. In parallel with the Imperial Valley aftershocks, these events tended to become shallower toward the northwest end of the fault. The existence of a north-south-going fault, along the line of the aftershocks in the Mexicali Valley, with a moment approaching a fourth of the total, would satisfy the data from PFO and mimic the tectonic role of the Brawley fault in the Imperial Valley. Not only the congruous details of the en-echelon fault systems but the historic record suggests the similar nature of these regimes at the northwest ends of the Imperial and Cerro Prieto faults. Where Imperial Valley had its 1940 event (Ms 7.1) with several

meters of surficial fault dislocation (Richter, 1958) followed by the lesser 1979 event (Mw 6.5) to the northwest, the Cerro Prieto fault had the 1934 Colorado Delta earthquake (ML 7.1) with a recorded surface rupture near its entry into the Gulf of California (Allen et al., 1965) succeeded by the 1980 Mexicali Valley event (Mw 6.4) again to the northwest.

A distribution of right-stepping faults mapped northward along the line of aftershocks will not produce the observed pattern of strain at PFO. By linear superposition each of these elements, aligned parallel to the main fault trace, will cause the same sign deformation at the observatory until they are approximately 13 km offset to the northeast of the original trace. At this distance, which is, by coincidence, the location of the southeast end of the Imperial fault, the observatory effectively passes into the correct quadrant. This suggests two obvious alternatives to our previous idea: triggered slip on the Imperial fault, or a series of north-south aligned fractures, along the main Cerro Prieto fault. For the former, not only is the Imperial fault trace offset from the Cerro Prieto but its strike is more favorable, at -37 degrees. Indeed there is evidence to support the possibility of remote deformation. Sharp (1982) reports a maximum of .16 m of right-lateral displacement along a very short (1 km) and punctuated, surface rupture near the town of Ejido Saltillo, Mexico. This feature, striking -10 degrees to -15 degrees is located about 8 km to the southeast of the documented rupture for the 1940 Imperial Valley event. Sharp notes the similarity between these surface cracks and those observed along the Brawley fault zone which broke in 1975 and 1979. The rational for ascribing this dislocation to slip on the Imperial fault rather than an expression of the supposed north-south branch of the Cerro Prieto is its location about 5 km to the east of the zone of aftershocks. For the second alternative we may again draw a parallel with the Imperial fault. As reviewed by Hartzell and Heaton (1983), well located epicenters along the Imperial fault tend to cluster on the northeast side, suggesting a fault plane dipping 75 degrees to the northeast. However, Johnson (1979) determined that many of these events are actually off the fault on a set of north-south-trending subfaults situated near the main dislocation surface. A collection of these faults, associated with the Cerro Prieto system would have the proper characteristics to explain the data. Whatever the exact mechanism, the records from PFO suggest substantial deformation occurred off the main trace of the Cerro Prieto fault: only a small portion, if we accept an auxiliary north-south fault, or considerably more if the deformation is limited to motion on the nearby Imperial fault or to distributed slip on a set of skewed subfaults.

Although poorly resolved, the 1979 Homestead Valley earthquake (ML 5.2) is another example of where the observations require a particular fault strike. Because the rupture took place due north of the observatory at a azimuth very close to north-south, both of the observed strain measurements (NS and EW) lie very near a nodal line in the deformation pattern. Even a small variation in the assumed fault strike of say, 5 degrees, changes the magnitude of the theoretical values by 100 percent; a 10 degree change reverses the sign of the signals. Only by accepting a fault strike of -6

degrees can the model be brought into agreement with the data. This result is similar to the excellent modeling presented by Stein and Lisowski (1983).

4.5.4 Acceleration and Instrument Baselength -

It is generally accepted that the surface of the earth is a noisy place. However, the spatial character of that noise, as recorded by various baselength deformation monitors, is still not well known. Worse yet, the ground may be expected to behave differently at different depths and different frequencies, to a variety of external agents; so there is much to be learned. Because most of the sensors at PFO are installed at the surface, with baselengths either greater than 500 m or less than 1 m, we may address here only a small piece of the spatio-temporal noise spectrum. In particular, our observations of coseismic strain-steps are useful in quantifying the magnitude of very localized deformation in response to ground shaking.

The nature of the near-surface material at PFO has been discussed by Wyatt (1982). For the most part, both the long and short baselength instruments are attached to competent, but extremely weathered, rock at a depth of 3-4 m. It is at this depth that conventional construction equipment fails to make headway in the friable rock. The end-monuments for the long-base instruments were cemented along their bottom fourth into ~1 m diameter holes, while the short baselength tiltmeters were constrained in much narrower boreholes by sand which was compacted around the sensors (Wyatt and Berger, 1980). This latter technique, as described by Allen et al., (1972), is remarkably good both at low and high frequencies. Over long periods of time the azimuthal sense of the secular signal is maintained despite removing and reinstalling a particular sensor; likewise an instrument can be installed so as not to show any abnormal response to striking the nearby ground. The extraordinary coseismic steps seen on these short baselength instruments are therefore considered to be real deformation of the surrounding earth.

The other short baselength tilt measurements are the tiltmeters attached to the end-monuments of the extended instruments. These signals are used primarily to correct for lateral translation at the top of the monuments, but are useful in their own right. Not surprisingly, in view of their precarious attachment to the ground, it is usually one of these measurements which heads the list of exagerated coseismic tilts (e.g., Table 4.3). With the upper three quarters of the end-monuments unconstrained laterally, they often respond rather poorly to large horizontal acceleration. (This configuration was made by choice, in order to isolate the strainmeter monuments from the less competent rock nearer the ground surface; the tilt record is then crucial to correct for tilting, assuming the base of the monument is stable.) Because of the differences in baselengths a large end-monument tilt of, say, 10**-6 rad, introduces only a small length error in the 731 m strainmeter measurement, of 3.7 x 10**-6 m, corresponding to 5 * 10***-9 e. As it turns

out, only one of the strain records given in Table 4.2 required correction. While end-monument tilts of order 10**-6 rad were observed for four of the events, they nearly always coincided with those instruments which failed.

The four biaxial shallow borehole tiltmeters produced coseismic signals just as large, though they were generally less than those from end-monument sensors. Table 4.2 presents the RMS of all six measurements in both the NS and EW directions, while their combined RMS deformation is displayed in Table 4.1 for comparison with the theoretical value. Without question most of these records are dominated by local ground adjustment, imparting very little information about the true deformation field. For the most distant earthquakes, the low gain of the sensors limits their RMS measures to about 2 least-counts of the digitizer (20 ne). Because of their inherent noise it is unlikely that operating them at a higher gain or sampling faster would yield useful results even for the more remote events. Evident in the component values is a pattern of either roughly equal NS and EW magnitudes or EW tilt far in excess of the other. To some degree this is an artifact of the more dominant end-monument tilts, but the trend generally holds throughout the signals for a given event, suggesting preferential shaking in the EW direction for a number of the earthquakes.

Figure 4.15 shows the relationship between the nominal horizontal accelerations at PFO and the signals produced by the short baselength tiltmeters. To account for the atypically high accelerations observed at PFO, a modified form of Espinosa's (1979) empirical relationship (Equation 5) was used for all events within 100 km:

$$Ah = 2.08*10^{-28}\ 10^{ML}\ DELTA^{(11.94-1.56\ \log\ DELTA)} \qquad (6)$$

Because none of the recorded signals were sensibly related to the theoretical ground deformation, the RMS tilts are presented in the figure rather than their ratio to the calculated distortion. The effect of seismic accelerations is obvious. Only as the accelerations approach the lower end of the range, .05 m/s**2, do the near-surface short-baselength instruments remain stable. For those events the RMS magnitude is limited to 20 nrad by the electronics. As the acceleration increases, so does the degree of local adjustment. In fact, the correlation is so good that the random disturbance of these sensors could almost be used to quantify the earthquake magnitude. Certainly they are inadequate to define the true crustal deformation.

Of course the same comment could be made about the longer instruments. At acceleration levels of .5 m/s**2 we may expect these sensors to show erroneous signals. But their cause for failure stems from two reasons: first, the delicate nature of the particular sensors and, second, the induced movement of the end-monuments. An absolute distance measurement scheme, as employed, for example, in the fluid tiltmeter, avoids the first problem; continuous recording throughout the event is then unnecessary. The second point, which is evident at accelerations of 1.0 m/sec**2, seems to represent

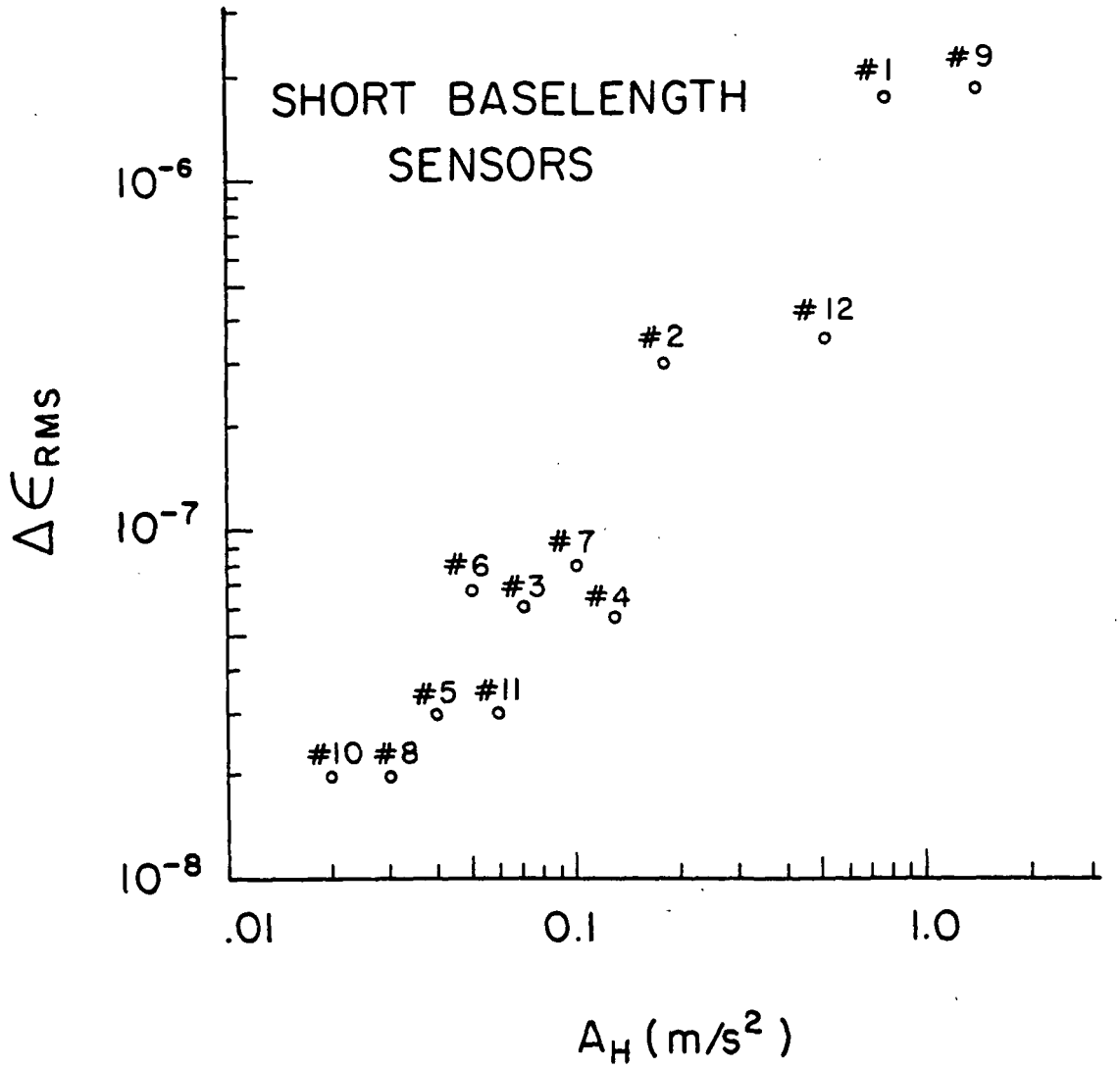

Figure 4.15. Strains recorded by short baselength tiltmeters for a range of peak horizontal accelerations. The local surface distortion, measured over base-lines of ~ 1 m, is clearly related to acceleration and uncorrelated with the theoretical deformation, referenced by event number.

the fundamental bound on near-surface observatory-based instrumentation. An attempt to circumvent this problem by optically anchoring the end-monuments to shallow depth (Wyatt et al., 1982b) has been made and future earthquakes will testify to its success or failure.

4.5.5 Measurement Uncertainty -

Without doubt, the error bounds on the observations given in Table 4.2 are excessive: meant to include all sources of instrumental inaccuracy, as well as the underlying limitations of the recorded data set. For the closer earthquakes it is the subjective accessment which dominates the estimate, whereas for the more distant, and consequently larger events, the uncertainty becomes a calculable value. Following a technique outlined by D. C. Agnew (personal communication, 1982) we may determine the resolving power of the data from PFO.

Even the best records from the observatory are noisy. At the high frequencies (.01-1 Hz) the source of the incoherent background noise is recognizable as coming from the instrumentation, at the much lower frequencies (~1 micro Hz) it is not. But across the entire spectrum it is often easily described by a single number (Agnew, 1984). Because the power spectrum of the noise from high-quality deformation sensors has the general form:

$$P(\omega) = Pr/\omega^{**2} \qquad (7)$$

where the frequency, omega, is in radians/second, we need only specify the constant Pr. Judged by its units, Pr ((e/s)**2/Hz) may be called the strain-rate power spectral density. Working with a quantity whose value is frequency independent has many advantages over the spectrum given by Equation (7). Most statistical tests presuppose independent errors, but if the signal is actually a random walk (i.e., power proportional to omega**-2) all parts of it are correlated with one another and the normal tests are not valid. Only one refinement is still needed to this simple mathematical model before applying it to our problem. We have taken the deformation rate spectrum to be constant, but we cannot treat it as white-noise over an infinite bandwidth, for such a series has infinite variance. Indeed, to record such a signal properly would require an infinitely fast data logger, capable of resolving the limitless high frequencies. Real recorders sample somewhat slower and their sampling interval, combined with the fact that they are actually recording the deformation signal and not its rate, allows us to consider the deformation rate spectrum as band limited to frequencies less than the Nyquist frequency, fny = 1/(2 deltaT). The variance of the resulting spectrum is:

$$\sigma^2 = \int_0^{fny} \cdot Pr \; df$$

$$= Pr/(2 \; deltaT)$$

and the square root of this is the standard deviation for a single sample.

The detection of a coseismic step is now remarkably easy. When an instantaneous change in the strain occurs (deltaepsilon), it will appear in the rate series as a single spike of amplitude deltaepsilon/deltaT. For it to be significant at the 95 percent confidence level, its value must exceed 1.96 sigma:

deltaepsilon/deltaT > 1.96 sigma

or

deltaepsilon > 1.4 (Pr deltaT)**.5

For a representative value of Pr, 4 x 10**-22 (e/s)**2/Hz, and a time difference set not by the recorder, but rather by the time delay between identifiable strain levels before and after the event, say deltaT = 1200 s, we obtain a theoretical limit of 1 ne. In Table 4.2, uncertainties of roughly twice this limiting value have been assigned to comparable earthquakes. Although the dependence of the uncertainties on effective sample interval is not a rapid function of time, at least one motivation for proper recording of the full seismic signal is clear; with suitable filtering, the seismic coda can be reduced and the underlying strain-step quantified with greater precision.

4.6 Conclusions

Given sufficient spatial averaging, it is clear that the surface of the earth will yield useful information about its internal deformation. While this has long been accepted for geodetic measurements, made over baselengths of several kilometers, there have been only a handful of convincing reports from observatory-based systems (sensor lengths < 1 km) such as those used here. To large measure the success which has been achieved in modeling coseismic signals is because the short-term response of the earth is so nearly elastic (Mavko, 1981). Evidentally, this simple response extends out to quite short spatial wavelengths. The marked difference between the records from short baselength instruments and longer ones at PFO argues that the spatial spectrum of coseismic surface displacement noise is well behaved and probably flat between these two wavelengths. Despite our original doubts, quite plausible records are obtained even for those events whose deformation just equals the resolution of the long-base sensors. This pattern holds throughout the range of earthquakes and site accelerations

until they are so great as to jeopardize the operation of the equipment (0.1 m/s**2). Of course the most interesting events are the larger ones and it is those which tend to cause the existing instrumentation to fail--so there is more to be done.

High-resolution continuously-recording strainmeters and tiltmeters provide the means for monitoring deformations which might otherwise go unresolved: namely, any pre-, post-, or interseismic adjustments. Too slow for the generation of seismic energy (e.g., Bonafede et al., 1983) and too fast for surveying techniques, these signals should tell us much about the character of the source region. For two of the recent events in southern California (Imperial Valley, 1979; Westmorland, 1981), the records seem to show postseismic deformation about 25 percent the size of the coseismic signal, occurring over a time span of a few hours. This suggestive pattern is, however, not repeated for any of the other earthquakes in this period. But perhaps more important, from the point of view of earthquake warning, there is no evidence of immediate preseismic deformation down to the resolution of the sensors. At longer periods, the noise of the observations limits our ability to recognize anomalous strains, but for the existing instruments, an unexpected change of order 2 ne (consistent among the long baselength sensors) should be easily recognizable over intervals of several hours. Again, we have not found any such signals.

Related to the search for precursory phenomena is the possibility of earth tidal-triggering of seismic events (e.g., Heaton, 1982). The strain- and tiltmeters are well suited to resolve the periods in the day when the conditions at the site are most favorable for strike-slip movement in a given orientation. Because the crust nearby should be undergoing roughly the same distortion, such direct measurements of the earth tide are more reliable indicators than most theoretical models, which are often in error by ~30 percent near the coastline of continents (Agnew, 1984). Unfortunately, records around the time of the most likely candidate for tidal-triggering, the Imperial Valley earthquake, are not encouraging. While the strain normal to the axis of the fault was near its daily maximum (i.e., extensional), the shear-strain along the axis was left-lateral, in opposition to the eventual dislocation.

Perhaps the most significant result is the evidence of coseismic deformation in excess of the seismically determined value. In his pivotal work on the relationship of seismic moment to rates of fault slip, Brune (1968) recognized the disparity between the geodetically determined slip rates and that attributable to historic earthquakes in southern California. He suggested that either the regional deformation rate was much less (~40 percent) than accepted, that potential slip for a large earthquake is accumulating rapidly, or that a great deal of creep is occurring without associated earthquakes (equivalent to a narrower fault zone than supposed). Considering all the evidence, Mavko (1981) concludes that a seismic event is often just a fraction of a larger episode of strain release. Indeed the observation that fault displacements, for large earthquakes (Length > 2 * fault width) scale as the length of the faulting, argues that the lower edge

of these fault planes must extend into regions of stress-relieved material (Scholz, 1982). Perhaps a large portion of the missing moment is occurring as suggested by the records presented here, in the form of nearly coseismic deformation. As in the case of the Horse Canyon earthquake (Hartzell and Brune, 1979), the initial rupture may represent only the adjustment of a small highly-stressed area of the fault (an asperity), with more gradual deformation over a larger area once the locked portion is freed. It is possible that, upon close examination, many of the strike-slip earthquakes in southern California will be recognized as multi-stage events where the motion of one area allows accelerated, but aseismic, deformation on another. The recognition of those areas which are relieved, and consequently the identification of those which are not, will be an important step in our understanding of the earthquake process.

References

Agnew, D.C. (1979). Strain tides at Piñon Flat: analysis and interpretation, Ph.D. Thesis, University of California, San Diego, 84 pp.

Agnew, D.C. (1984). Tiltmeters and Strainmeters, Methods in Experimental Physics, (in preparation).

Aki, K. (1966). Generation and propagation of G-waves from the Niigata earthquake on June 16, 1964, 2., Estimation of earthquake moment, released energy, and stress-strain drop from G-waves spectrum, Bull. Earthquake Res. Inst., Tokyo Univ., 44, 73-78.

Alewine, R.W.III and T.H. Heaton (1973). Tilts associated with the Pt. Mugu earthquake, in Proc. of the Conf. on Tectonic Problems of the San Andreas Fault System, R.L. Kovach and A. Nur, Editors, Stanford University Publications, Geological Sciences, XIII, Stanford, California.

Allen, C.R., P. St. Amand, C.F. Richter, and J.M. Nordquist (1965). Relationship between seismicity and geologic structure in the southern California region, Bull. Seism. Soc. Am., 55, 753-797.

Allen, C.R., (1981). The Modern San Andreas Fault, in The Geotectonic Development of California, W.G. Ernst, ed., Prentice-Hall, New Jersey.

Allen, R.V., M.D. Wood, and C.E. Mortensen (1973). Some instruments and techniques for measurement of tidal tilt, Phil. Trans. R. Soc. Lond. A., 274, 219-222.

Allen, R.V. (1978). Tiltmeter observations near a large earthquake, Bull. Seis. Soc. Am., 68, 855-857.

Anderson, J.G. and R.S. Simons (1982). Introduction, in the Mexicali Valley Earthquake of 9 June 1980, J.G. Anderson and R.S. Simons, eds., Earthquake Eng. Res. Inst. Newsletter, 16, 73-105.

Archuleta, R.J. (1982a). Hypocenter for the 1979 Imperial Valley, California, earthquake, Geophys. Res. Lttrs., 9, 625-628.

Archuleta, R.J. (1982b). Analysis of near-source static and dynamic measurements from the 1979 Imperial Valley Earthquake, Bull. Seism. Soc. Am., 72, 1927-1956.

Archuleta, R.J. (1984). A faulting model for the 1979 Imperial Valley

Earthquake, J. Geophys. Res., (in press).

Archuleta, R.J. and S.M. Day (1980). Dynamic rupture in a layered medium: the 1966 Parkfield earthquake, Bull. Seism. Soc. Am., 70, 671-689.

Ben-Menahem, A., S.J. Singh, and F. Solomon (1970). Deformation of an homogeneous earth model by finite dislocations, Rev. Geophys. Space Phys., 8, 591-632.

Berger, J. and R.H. Lovberg (1970). Earth strain measurements with a laser interferometer, Science, 170, 296-303.

Berger, J. and C. Beaumont (1976). An analysis of tidal strain observations from the United States of America: II. The inhomogeneous tide, Bull. Seism. Soc. Am., 66, 1821-1846.

Berger, J. and F. Wyatt (1978). Some remarks on the base length of tilt and strain measurements, in Proceedings of Conference VII, Stress and Strain Measurements Related to Earthquake Prediction, Open-file Rep. 79-370, U.S. Geological Survey, Menlo Park, 3-32.

Berger, J., J.N. Brune, J. Goodkind, F. Wyatt, D.C. Agnew, and C. Beaumont (1981). The seismotectonics of plate boundaries, Final Report, National Aeronautics and Space Administration, NGR 05-009-246, pp 84.

Biehler, S., R.L. Kovach, and C.R. Allen (1964). Geophysical framework of northern end of Gulf of California structural province, Am. Assoc. Petr. Geol. Memoir 3, 126-143.

Bonafede, M., E. Boschi, and M. Dragoni (1983). Viscoelastic stress relaxation on deep fault sections as a possible source of very long period elastic waves, J. Geophys. Res., 88, 2251-2260.

Bower, D., (1983). Bedrock fracture parameters from the interpretation of well tides, J. Geophys. Res., 88, 5025-5035.

Bredehoeft, J.D. (1967). Response of well-aquifer systems to earth tides, J. Geophys, Res., 72, 3075-3087.

Brune, J.N. (1968). Seismic moment, seismicity, and rate of slip along major fault zones, J. Geophys. Res., 73, 777-784.

Canitez, N. and M. N. Toksoz (1972). Static and dynamic study of earthquake source mechanism: San Fernando earthquake, J. Geophys. Res., 77, 2583-2594.

Chinnery, M.A. (1961). The deformation of the ground around surface faults, Bull. Seism. Soc. Am., 51, 355-372.

Cohen, S.C. (1980). Postseismic viscoelastic deformation and stress, 2., Stress theory and computation; dependence of displacment, strain, and stress on fault parameters, J. Geophys. Res., 85, 3151-3158.

Darby, D., J.J. Gonzalez, and P. Lesage, (1984). Geodetic studies in Baja California, Mexico, and the evaluation of short-range data from 1974 to 1982, J. Geophys. Res., 89, 2478-2490.

Dunbar, W.S., D.M. Boone, and W. Thatcher (1980). Pre-, co-, and postseismic strain changes associated with the 1952 ML = 7.2 Kern County, California, earthquake, Bull. Seism. Soc. Am., 70, 1893-1905.

Espinosa, A.F. (1979). An empirical relation for attenuation of peak horizontal accelertions as a functin of ML, Earthquake Notes, 50, 14.

Evans, K. and F. Wyatt (1984). Water table effects on the measurement of earth strain, Tectonophysics, 108 (in press).

Frankel, A. (1984). Source parameters of two ML ~=5 earthquakes near Anza, California, and a comparison with an Imperial Valley aftershock. Bull. Seism. Soc. Am., (submitted).

Frez, J. (1982). Main shock locaction and fault mechanics, in the Mexicali Velley earthquake of 9 June 1980, J.G. Anderson and R.J. Simons, eds., Earthquake Eng. Res. Inst. Newsletter, 16, 73-105.

Fuis, G.S. (1982). Displacement on the Superstition Hills fault triggered by the earthquake, in the Imperial Valley, California, earthquake of October 15, 1979, U.S. Geol. Surv. Prof. Pap., 145-154.

Fuis., G.S., W.D. Mooney, J.H. Healy, G.A. McMechan, and W.J. Lutter (1984). A seismic refraction survey of the Imperial Valley region, California, J. Geophys. Res., 89, 1165-1189.

Geological Survey Professional Paper 1254 (1982). The Imperial Valley, California, earthquake of October 15, 1979, United States Department of the Interior, Geological Survey.

Gilbert, F. and A.M. Dziewonski (1975). An application of normal mode theory to the retrieval of structural parameters and source mechanism from seismic spectra, Phil. Trans. Roy. Soc. Lond., Ser. A., 278, 187-269.

Given, D. (1983). Seismicity and structure of the trifurcation in the San Jacinto fault zone, southern California, Master's thesis, California State University, Los Angeles, 73 pp.

Gladwin, M. (1984). High precision multi-component borehole deformation

monitoring, Rev. Sci, Inst., (in press).

Goodkind, J.M. (1979). Continuous measurements with the superconducting gravimeter, Tectonophysics, 52, 99-105.

Hanks, T.C. and H. Kanamori (1979). A moment magnitude scale, J. Geophys. Res., 84, 2348-2350.

Harsh, P.W. (1982). Distribution of afterslip along the Imperial fault, in the Imperial Valley, California, earthquake of October 15, 1979, U.S. Geol. Surv. Prof. Pap., 193-203.

Hartzell, S.H. and J.N. Brune (1979). The Horse Canyon earthquake of August 2, 1975 -- Two stage stress release process in a strike-slip earthquake, Bull. Seism. Soc. Am., 69, 1161-1173.

Hartzell, S. and D. Helmberger (1982). Strong motion modeling of the Imperial Valley earthquake of 1979, Bull. Seis. Soc. Am., 72, 571-596.

Hartzell, S.H. and T.H. Heaton (1983). Inversion of strong motion and teleseismic waveform data for the fault rupture history of the 1979 Imperial Valley, California, earthquake, Bull. Seism. Soc. Am., 73, 1553-1583.

Heaton, T.H. (1982). Tidal triggering of earthquakes, Bull. Seism. Soc. Am., 72, 2182-2200.

Heaton, T.H., J.G. Anderson, and P.T. German (1983). Ground failure along the New River caused by the October 1979 Imperial Valley earthquake sequence, Bull. Seism. Soc. Am., 73, 1161-1171.

Hutton, L.K., C.E. Johnson, J.C. Pechmann, J.E. Ebel, T.W. Given, D.M. Cole, and P.T. German (1980). Epicentral locations for the Homestead Valley earthquake sequences, March 15, 1979, Calif. Geol., 33, 110-114.

Iwasaki, T. and R. Sato (1979). Strain field in a semi-infinite medium due to an inclined rectangular fault, J. Phys. Earth, 27, 285-314.

Japanese Network of Crustal Movement Observatories (1970). Spatial distribution of strain-steps associated with the earthquake of the central part of Gifu, Prefecture, September 9, 1969, Bull. Earthq. Res. Inst., 48, 1217-1333.

Johnson, C.E. (1979). I. CEDAR--An approach to the computer automation of short-period local seismic networks, II. Seismotectonics of the Imperial Valley of Southern California, Ph.D. thesis, California Institute of Technology, Pasadena.

Johnson, C.E. and L.K. Hutton (1982). Aftershocks and preearthquake seismicity, in the Imperial Valley, California, earthquake of October 15, 1979, U.S. Geol. Surv. Prof. Pap. 1254, 59-76.

Jordan, T.H. and J.B. Minster (1978). Present-day plate motions, J. Geophys. Res., 83, 5331-5354.

Jovanovich, D.B. (1975). An inversion method for estimating the source parameters of seismic and aseismic events from static strain data, Geophys. J. R. astr. Soc., 43, 347-365.

Jovanovich, D.B., M.I. Husseini, and M.A. Chinnery (1974). Elastic dislocations in a layered half-space -- II: Point Source, Geophys. J. R. astro. Soc., 39, 219-239.

Kanamori, H. (1973). Mode of strain release associated with major earthquakes in Japan, Annu. Rev. Earth Planet. Sci, 1, 212-239.

Kanamori, H. (1977). The energy release in great earthquakes, J. Geophys. Res., 82, 2981-2987.

Kanamori, H. (1983). Magnitude scale and quantification of earthquakes, Tectonophysics, 93, 185-199.

Kanamori, H. and J.J. Cipar (1974). Focal process of the great Chilean earthquake, May 22, 1960, Phys. Earth Planet. Inter., 9, 128-136.

Kanamori, H. and J. Regan (1981). Long period seismic waves, in The Imperial Valley, California Earthquake of October 15, 1979, U.S. Geol. Surv. Prof. Pap., 1254, 55-58.

King, N.E. J. C. Savage, M. Lisowski, and W.H. Prescott (1981). Preseismic and coseismic deformation associated with the Coyote Lake, California, earthquake, J. Geophys. Res., 86, 892-898.

King, N.E. and J.C. Savage (1983). Strain-rate profile across the Elsinore, San Jacinto, and San Andreas Faults near Palm Springs, California, 1973-81, Geophys. Res. Lttrs., 10, 55-57.

Langbein, J., A. McGarr, M.J.S. Johnston, and P.W. Harsh (1983). Geodetic measurements of postseismic crustal deformation following the 1979 Imperial Valley earthquake, California, Bull. Seism. Soc. Am., 73, 1203-1224.

Linde, A.T., I.S. Sachs, M. Johnston, F. Wyatt, and D. Agnew (1982). The borehole strainmeter program in California -- installation and preliminary results, Carnegie Inst. Wash. Year Book 81, 517-520.

Liu, H-S. and E.S. Chang (1979). On the selection of station sites for observing strain steps and earthquake forerunners in California, Bull.

Seism. Soc. Am., 69, 1989-1994.

Mansinha, L. and D.E. Smylie (1971). The displacement field of inclined faults, Bull. Seism. Soc. Am., 61, 1433-1440.

Maruyama, T. (1964). Statical elastic dislocations in an infinite and seim-infinite medium, Bull. Earthquake Res. Inst., Tokyo Univ., 42, 289-368.

Mavko, G.M. (1981). Mechanics of motion on major faults, Annu. Rev. Earth Planet. Sci, 9, 81-112.

McGarr, A., I.S. Sacks, A.T. Linde, S.M. Spottiswoode, and R.W.E. Green (1982). Coseismic and other short-term strain changes recorded with Sacks-Evertson strainmeters in a deep mine, South Africa, Geophys. J. R. astro. Soc., 70, 717-740.

McHugh, S. and M.J.S. Johston (1977). An analysis of coseismic tilt changes from an array in Central California, J. Geophys. Res., 82, 5692-5698.

Mikumo, T. (1973). Faulting mechanisms of the Gifu earthquake of September 9, 1969, and some related problems, J. Phys. Earth., 21, 191-212.

Munguia-Orozco, L. (1983). Strong ground motion and source mechanism studies for earthquakes in the northern Baja California - southern California region, University of California, San Diego, Ph.D. thesis, 152 p.

National Academy of Sciences (1981). Geodetic Monitoring of Tectonic Deformation - Towards a Strategy, NAS Committee on Geodesy, Washington, D.C.

Olson, A.H. and R.J. Apsel (1982). Finite faults and inverse theory with applications to the 1979 Imperial Valley earthquake, Bull. Seism. Soc. Am., 72, 1969-2001.

Parcel, R.F. (1981). Structure and petrology of the Santa Rosa shear zone in the Pinyon Flat area, Riverside County, California, in Geology of the San Jacinto Mountains, Annual Field Trip Guidebook No. 9, A.R. Brown and R.W. Ruff, eds., South Coast Geological Society, Santa Ana, Ca.

Pfluke, J.H. and R.M. Stewart (1973). Aleutian strain events: observations and interpretation, Geophy. J.R. astro. Soc., 35, 229-241.

Prescott, W.H., J.C. Savage, and W.T. Kinoshita (1979). Strain accumulation rates in western United States between 1970 and 1978, J.

Geophys. Res., 84, 5423-5435.

Prescott, W.H. and A. Nur (1981). The accomodation of relative motion at depth on the San Andreas fault system in California, J. Geophys. Res., 86, 999-1004.

Press, F. (1965). Displacements, strains, and tilts at teleseismic distances, J. Geophys. Res., 70, 2395-2412.

Raleigh, C.B., K. Sieh, L.R. Sykes, and D.L. Anderson (1982). Forecasting southern California earthquakes, Science, 217, 1097-1104.

Richter, C.F. (1958). Elementary seismology, W.H. Freeman, San Francisco, 768 pp.

Sacks, I.S., S. Suyehiro, D.W. Evertson, and Y. Yamagishi (1971). Sacks-Evertson strainmeter, its installation in Japan and some preliminary results concerning strain steps, Pap. Meteor. Geophys., 22, 195-208.

Sacks, I.S., S. Suyehiro, A.T. Linde, and J.A. Snoke (1978). Slow earthquakes and stress redistribution, Nature, 275, 599-602.

Sacks, I.S., A.T. Linde, J.A. Snoke, and S. Suyehiro (1981). A slow earthquake following the Izu-Oshima earthquake of 1978, in Earthquake Prediction - An International Review, Maurice Ewing Series 4, American Geophysical Union.

Sanders, C., K. McNally, and H. Kanamori (1981). The state of stress near the Anza seismic gap, San Jacinto fault zone, in Geology of the San Jacinto Mountains, Annual Field Trip Guidebk., 9, A.R. Brown and R.W. Ruff, eds., South Coast Geol. Soc., Santa Ana, Calif., 61-67.

Sanders, C.O. and H. Kanamori (1984). A seismotectonic analysis of the Anza seismic gap, San Jacinto fault zone, Southern California, J. Geophys. Res., (in press).

Savage, J.E. and L.M. Hastie (1966). Surface deformation associated with dip-slip faulting, J. Geophys, Res. 70, 2395-2412.

Savage, J.C., W.H. Prescott, M. Lisowski, and N.E. King (1981a). Strain on the San Andreas Fault near Palmdale, California: Rapid aseismic change, Science, 211, 56-58.

Savage, J.C., W.H. Prescott, M. and N.E. King (1981b). Strain accumulation in southern California, 1973-1980, J. Geophys. Res., 86, 6991-7002.

Scholz, C.H. (1982). Scaling laws for large earthquakes: consequences for physical models, Bull. Seis. Soc. Am., 72, 1-14.

Sharp, R.V. (1967). San Jacinto Fault zone in the Peninsular Ranges of Southern California, Geol. Soc. Amer. Bull., 78, 705-730.

Sharp, R.V. (1981). Variable rates of late Quaternary strike slip on the San Jacinto fault zone, southern California, J. Geophys. Res., 86, 1752-1754.

Sharp, R.V. (1982). Surface ruptures observed at Ejido Saltillo, Baja California after the Mexicali Valley Earthquake of June 9, 1980, in The Mexicali Valley Earthquake of 9 June 1980, J.G. Anderson and R.S. Simons, eds., Earthquake Eng. Res. Inst. Newsletter, 16, 94-99.

Sharp, R.V., J.J. Lienkaemper, and M.J. Rymer (1982a). Surface displacements on the Imperial and Superstition Hills faults triggered by the 26 April 1981 Westmorland, California, earthquake, Earthquake Notes, 53, 12.

Sharp, R.V., J.J. Lienkaemper, M.G. Bonilla, D.B. Burke, B.F. Fox, D.G. Herd, D.M. Miller, D.M. Morton, D.J. Ponti, M.J. Rymer, J.C. Tinsley, J.C. Yount, J.E. Kahle, E.W. Hart, and K. Sieh (1982b). Surface faulting in the central Imperial Valley, in The Imperial Valley, California, Earthquake of October 15, 1979, U.S. Geol. Surv. Prof. Pap. 1254, 119-143.

Sieh, K. (1978). Slip along the San Andreas fault associated with the great 1857 earthquake, Bull. Seism. Soc. Am., 68, 1421-1448.

Sieh, K.E. (1981). Seismic potential of the dormant southern 200 km of the San Andreas Fault, abstract, EOS, 62, 1048.

Sieh, K.E. (1982). Slip along the San Andreas fault associated with the earthquake, in The Imperial Valley, California, earthquake of October 15, 1979, U.S. Geol. Surv. Prof. Pap. 1254, 155-160.

Smith, S.W. and M. Wyss (1968). Displacement on the San Andrea subsequent to the 1966 Parkfield Earthquake, Bull. Seism. Soc. Am, 58, 1955-1973.

Snay, R.A., M.W. Cline, and E.L. Timmerman (1982). Horizontal deformation in the Imperial Valley, California, between 1934 and 1980, J. Geophys. Res, 87, 3959-3968.

Stacey, F.D. and J.M.W. Rynn (1970). Spurious local effects associated with teleseismic tilts and strains, in Earthquake Displacement Fields and the Rotation of the Earth, L. Mansinha, D.E. Smylie and A.E. Beck, eds., D. Reidel Publishing Co., Doydrecht, Holland.

Stein, R.S. and M. Lisowski (1983). The 1979 Homestead Valley earthquake sequence, California: control of aftershocks and postseismic deformation, J. Geophys, Res., 88, 6477-6490.

Suarez V., F., K.E. Sieh, and W.E. Elders (1982). A review of geological effects and damage distribution of the June 9, 1980, Mexicali Valley earthquake, in The Mexicali Valley Earthquake of 9 June 1980, J.G. Anderson and R.S. Simons, eds., Earthquake Eng. Res. Inst. Newsletter, 16, 73-105.

Takemoto, S. (1970). Strain steps and the dislocation fault model, Bull. Disas. Prev. Inst., Kyoto Univ., 20, 1-15.

Thatcher, W. and T.C. Hanks (1973). Source parameters of Southern California earthquakes, J. Geophys. Res., 78, 8547-8576.

Thatcher, W., J.A. Hileman, and T.C. Hanks (1975). Seismic slip distribution along the San Jacinto Fault zone, Southern California, and its implications, Geol. Soc. Amer. Bull., 86, 1140-1146.

Van der Kamp, G. and J.E. Gale (1983). Theory of earth tide and barometric effects in porous formations with compressible grains, Water Resour. Res., 19, 538-544.

Wideman, C.J. and M.W. Major (1967). Strain steps associated with earthquakes, Bull. Seism. Soc. Amer., 57, 1429-1444.

Wilson, M.E. and S.H. Wood (1980). Tectonic tilt rates derived from lake-level measurements, Salton Sea, California, Science, 207, 183-186.

Wong, V. and J. Frez (1982). Aftershock locations and fault mechanisms, in The Mexicali Valley Earthquake of 9 June 1980, J.G. Anderson and R.S. Simons, eds., Earthquake Eng. Res. Inst. Newsletter, 16, 73-105.

Wyatt, F. (1982). Displacements of surface monuments - Horizontal motion, J. Geophys. Res., 87, 979-989.

Wyatt, F. and J. Berger (1980). Investigations of tilt measurements using shallow borehole tiltmeters, J. Geophys. Res., 85, 4351-4362.

Wyatt, F., G. Cabaniss, and D.C. Agnew (1982a). A comparison of tiltmeters at tidal frequencies, Geophys. Res. Lttrs., 9, 743-746.

Wyatt, F., K. Beckstrom, and J. Berger (1982b). The optical anchor - A geophysical strainmeter, Bull. Seismol. Soc Amer., 72, 1701-1715.

Wyatt, F., D.C. Agnew, A. Linde, and I.S. Sacks (1983). Borehole strainmeter studies at Piñon Flat Observatory, Carnegie Inst. Wash. Year Book 82, 533-538.